NUMERICAL SIMULATION OF FLOW AROUND SHIP HULL CONSIDERING RUDDER-PROPELLER INTERACTION

MASTER OF SCIENCE

in

NAVAL ARCHITECTURE AND MARINE ENGINEERING

Nabila Naz

Student No.: 1014122002 P

Session: October 2014

DEPARTMENT OF

NAVAL ARCHITECTURE AND MARINE ENGINEERING

BANGLADESH UNIVERSITY OF ENGINEERING AND TECHNOLOGY

DHAKA-1000

28th January, 2017

NUMERICAL SIMULATION OF FLOW AROUND SHIP HULL CONSIDERING RUDDER-PROPELLER INTERACTION

By

Nabila Naz

Student No.: 1014122002 P

Session: October 2014

A thesis submitted to the

Department of Naval Architecture and Marine Engineering

in partial fulfillment of the requirements for the degree of

MASTER OF SCIENCE

in

NAVAL ARCHITECTURE AND MARINE ENGINEERING

DEPARTMENT OF NAVAL ARCHITECTURE AND MARINE ENGINEERING

BANGLADESH UNIVERSITY OF ENGINEERING AND TECHNOLOGY

DHAKA-1000

28th January, 2017

Certificate of Approval

The thesis entitled **NUMERICAL SIMULATIONOF FLOWAROUNDSHIP HULL CONSIDERING RUDDER-PROPELLERINTERACTION** submitted by **Nabila Naz**, Student No.: 1014122002P, Session: October, 2014 to the Department of Naval Architecture and Marine Engineering, Bangladesh University of Engineering and Technology (BUET), Dhaka-1000, Bangladesh has been acceptedas satisfactory in partial fulfillment of the requirements for the degree of **Masterof Science** in **Naval Architecture and Marine Engineering** on 28th January, 2017.

Board of Examiners

1. **Dr. Md. MashudKarim** — Chairman (Supervisor)
Professor
Department of NAME, BUET, Dhaka-1000.

2. **Dr. Goutam Kumar Saha** — Member (Ex-Officio)
Professor and Head
Department of NAME, BUET, Dhaka-1000.

3. **Dr. Md. RefayetUllah** — Member
Professor
Department of NAME, BUET, Dhaka-1000.

4. **Dr. M. Rafiqul Islam** — Member
Professor
Department of NAME, BUET, Dhaka-1000.

5. **Prof. Dr. Md. Quamrul Islam** — Member (External)
House No. 48/3B
BUET Teacher's Quarter
Dhakeshwari (R/A), Dhaka-1000.

Certificate of Research

This is to certify that the candidate has done this work and it was not submitted elsewhere for the award of any degree or diploma.

28.01.2017

Supervisor

Dr. Md. Mashud Karim

Professor

Department of Naval Architecture and Marine Engineering (NAME)

Bangladesh University of Engineering and Technology (BUET)

Dhaka-1000, Bangladesh

Declaration

I do hereby declare that I, the candidate, have done this work and it was not submitted elsewhere for the award of any degree or diploma.

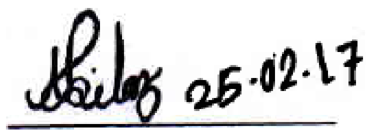

Candidate

Nabila Naz

PG Student No: 1014122002P

Department of Naval Architecture and Marine Engineering (NAME)

Bangladesh University of Engineering and Technology (BUET)

Dhaka-1000, Bangladesh

Acknowledgment

At first, I would like to acknowledge the blessings of almighty Allah, The Beneficent, and The Merciful for His divine help in completing this thesis successfully.

Then I would like to express my profound gratitude to my thesis supervisor, Dr. Md. Mashud Karim, Professor of the department of Naval Architecture and Marine Engineering, BUET, for his heartiest cooperation throughout the preparation of the thesis. During my graduation period there was not a single moment that I could not ask him for advice or ask to make some time to discuss my work. The work was mostly conducted at the high configurated computers of him. I am extremenly thankful and indebted to him for providing me all necessary technical supports to perform my thesis work efficiency. Without his guidance, wise suggestions, encouragement, great assistance and all the given amenities this thesis may not be completed.

Besides, I would like to mention (CP#2084) project of Higher Education Quality Enhancement Program (HEQEP), UGC, Ministry of Education, Govt. of Bangladesh for providing necessary research facilities during the thesis work.

In addition to my supervisor, I would like to thank all the members of board of examiners: Prof. Dr. Md. Quamrul Islam, Prof Dr. Md. Refayet Ullah, Prof Dr. M. Rafiqul Islam, Prof. Dr. Goutam Kumar Saha for their insightful comments and encouragement which certainly improve this thesis. I would like to gratefully acknowledge my teachers and colleagues of Department of Naval Architecture and Marine Engineering for their help during my period of study and staffs for their support and kindness.

My sincere appreciation goes to all the developers of the Shipflow CFD code, other open source softwares used in this thesis including but not limited to MATLAB, OpenProp, and Origin.

Last but not least, I would like to acknowledge my gratitude to my mother, belated father, and younger brother who have always encouraged me and provided all necessary facilities to elevate my knowledge up to this level, and without their support and guidance, it would be impossible for me to carry out the thesis work properly.

Nabila Naz

28th January, 2017

Dedicated to my

Beloved Parents

and Respected Teachers

Contents

List of Figures

List of Tables

Abstract

Flow around ship hull considering rudder-propeller interaction has always been a subject of great concern both for naval architects and shipyards in order to ensure that a ship can operate efficiently and economically at a desired speed. Although extensive researches concerning the flow around bare ship hull have been carried out in the past decades, the hull-propeller-rudder interaction is very much important for accurate prediction of flow specially at stern region of ship. In this research, the flow around ship hull is numerically simulated considering the hull-propeller-rudder interaction. The effect of rudder positions on propeller efficiency is also determined for different longitudinal distances from propeller.

Firstly, the flow around the bare ship hull is computed using 'Zonal Approach'. In this approach, 'potential flow solver' is used in the region outside the boundary layer and wake whereas 'boundary layer solver' is used in thin boundary layer region near the forward half of the hull. On the other hand, viscous flow solver is used in the stern/wake region. Three dimensional Rankine source panel method with non-linear free-surface boundary condition is used to capture free-surface potential flow around ship hull. The results of potential flow solver are provided as an input to boundary layer solver to predict transition and boundary layer parameters on the forward half of the ship. In the stern region where the viscous effects are predominant, RANS (Reynolds-Averaged Navier-Stokes) solver is used to analyze the flow incorporating k-ω SST turbulence model. Propeller open water characteristics are determined utilizing an open source code OpenProp based on Lifting Line theory. The computed open water characteristics are given as input for determining self propulsion characteristics.

To analyze the flow physics and validate computed results, two cases of simulations are carried out with KRISO Container Ship (KCS) and Japan Bulk Carrier (JBC). Free-surface wave pattern, wave elevation and wave making resistance coeffieicent are obtained from potential flow solution. Frictional resistance coefficients are obtained from boundary layer and viscous flow solver respectively. A Verification and Validation (V&V) study for resistance coefficients has also been carried out using ITTC recommended procedure.

To determine open water and self propulsion characteristics, KP 505 and DTMB 4119 propellers are used for KCS and JBC hull respectively. The computed results of propeller open water characteristics show good agreement with the available experiemental results. Semi balanced horn type rudder is used for both hulls to compare self propulsion characteristics at varying rudder positions.

Finally, the flow around ship hull considering rudder-propeller interaction has been computed using RANS solver coupled with Lifting Line theory. All the above mentioned simulations are implemented using commercial Computational Fluid Dynamics (CFD) software 'Shipflow' developed by Chalmers University of Technology. It is revealed that CFD can be successfully applied to determine the preliminary resistance and power in maritime industry.

Nomenclature

Acronyms

Symbol	Description
ADI	Alternating Direction Implicit
C F D	Computational Fluid Dynamics
D N S	Direct Numerical Simulation
E E D I	Energy Efficiency Design Index
E F D	Experimental Fluid Dynamics
FVM	Finite Volume Method
GCI	Grid Convergence Index
I M O	International Maritime Organisation
I T T C	International Towing Tank Conference
K C S	KRISO Container Ship
J B C	JAPAN Bulk Carrier
LE S	Large Eddy Simulation
LL	Lifting Line
N AC A	National Advisory Committee for Aeronautics
N M R I	National Maritime Research Institute
P O W	Propeller Open Water
R AN S	Reynolds Averaged Navier-Stokes
R E	Richardson Extrapolation
V &V	Verification and Validation
VOF	Volume of Fluid

Roman Symbols

Symbol	Description
C_B	Block coefficient
C_F	Frictional resistance coefficient
C_M	Midship section coefficient
C_P	Pressure coefficient
Ct	Total resistance coefficient
C_V	Viscous resistance coefficient
C_w	Wave making resistance coefficient
F_i	Body force
F_n	Froude number
g	Gravitational constant
H	Free surface location estimate
h	Free surface location perturbation
J	Advance coefficient
u_i	Velocity at x-direction
k	Turbulent Kinetic Energy
T	Thrust
Q	Torque
n_s	Shaft revolution rate

p	Pressure
p_a	Atmospheric pressure
p_v	Vapor pressure
P_D	Delivered power
P_T	Thrust power
P_E	Effective power
Q	Torque
R	Radius of curvature of the free surface
R_{ji}	Reynolds stress
R_n	Reynolds number
R_w	Wave resistance
R_T	Total resistance
S	Wetted surface area
t	Thrust deduction
$E\%D$	Percentage of error relative to EFD results
U_D	Data uncertainty
U_G	Grid discretization uncertainty
U_{SN}	Numerical uncertainty
U_∞	Free-stream velocity
V	Ship velocity
U_i	Mean velocity
$u_i^{'}$	Fluctuating velocity
V_A	Advance velocity
V_W	Effective wake velocity
W	Wake fraction
y^+	Nondimensional wall distance
P/D	Pitch/Diameter
C/D	Chord/Diameter
fo/C	Chamber/Chord
to/D	Thickness/Diameter

Greek Symbols

Symbol	Description
η_O	Propeller efficiency
μ	Dynamic viscosity
∇	Gradient operator
ρ	Density
Φ	Velocity potential estimate
φ	Velocity potential
ϕ	Velocity potential perturbation
$\bar{\sigma}_{ji}$	Average stress vector
γ	Coefficient of surface tension

Chapter 1

Introduction

1.1 Motivation

Determination of resistance and propulsive characteristics of ship has always been biggest concern at all stages of a design both for naval architects and ship yards. The main target of shipbuilding in this century is to design ships with more fuel efficiency and less pollutant and green-house gas emission which will ultimately reduce the cost of transportation without harming the environment. Due to great deal of emphasis on economical and environmental efficiency gained, designers are forced to optimize the existing solutions and search for new designs. To design a more fuel efficient ship, the naval architects or ship designers need to predict the amount of power required. The power requirement of ships in turn depends on how much resistance they have to overcome in a seaway. In order to achieve these tasks, the features of the flow around the ship hull must be well-understood and measured accurately in a way that designers can try many hulls and propulsion arrangements without spending too much time, effort and resources.

Hence, the hydrodynamic performance of ships with rudder-propeller interaction needs to be investigated by the ship designers. Estimation of bare hull resistance is the first step towards knowing the performance of the ship in a seaway which can be computed efficiently with wide number of numerical methods. The propeller open water characteristics can be successfully determined by various computational methods such as vortex lattice method or boundary element method. But simulation of self-propulsion test has not been fully established yet due to the difficulty of calculating the effective wake. The effective wake resulted from the interaction between propeller and ship hull as shown in Figure 1.1.

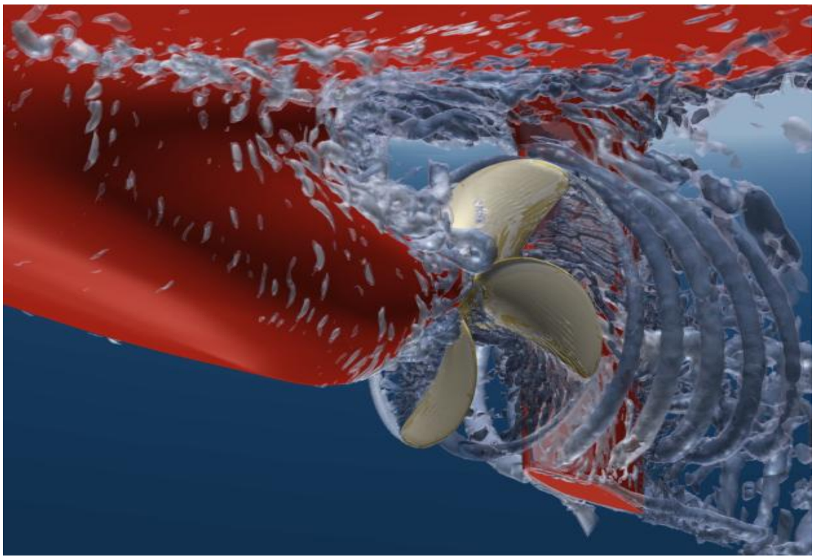

Figure 1.1: Effective wake resulted from the interaction between propeller and ship hull [1]

Presence of rudder affects the wake generated by ship and propeller performance can be increased or decreased depending on various rudder positions. Effective wake with presence of rudder is shown in Figure 1.2.

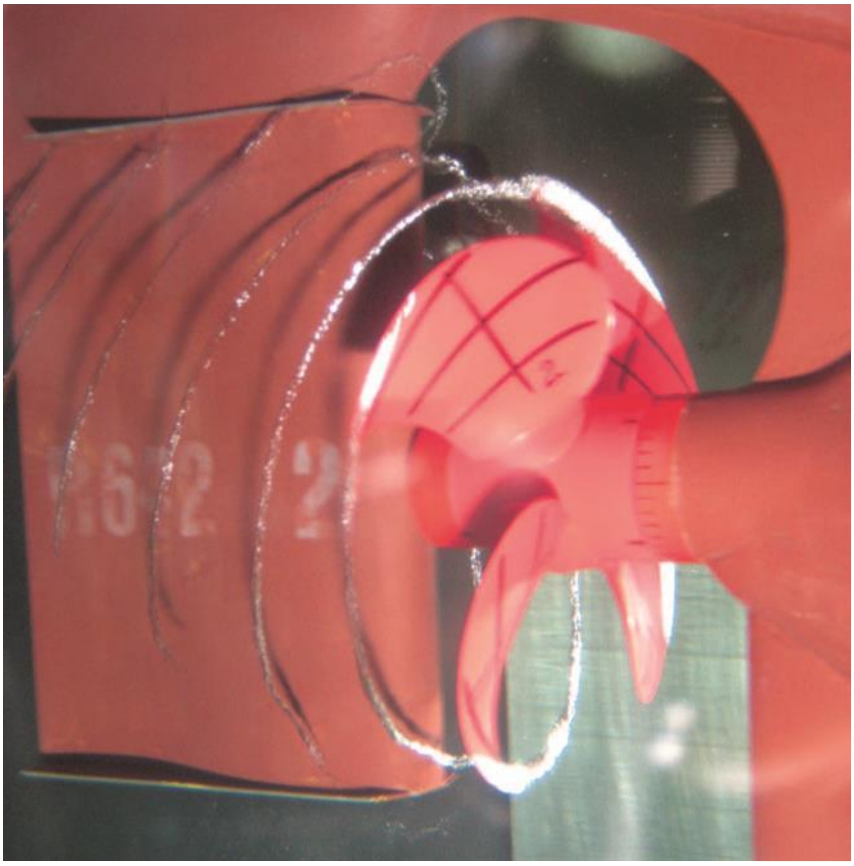

Figure 1.2: Effective wake with presence of rudder [2]

Based on the present emphasis on increased ship speeds, the flow around ship hull considering rudder-propeller interaction has attracted researchers for the improvement of ship’s performance. There are mainly three different ways to predict resistance and propulsive factors. They are empirical methods, physical experiments and numerical methods.

1.1.1 Empirical Methods

Simplest and fastest among them is empirical methods [3] which can be used only at the earliest design stage, when main dimensions and hull coefficients often vary due to lack of accuracy. The empirical approach combines systematic model testing on a handful of basic hull shapes, with standardized series of propeller and regression analysis. Only certain parameters of ships and propeller in general such as length, breadth, propeller diameteretc are considered in this approach. It does not account for the varying shape of the ships and propeller that are of similar dimensions and types. But the frictional resistance, which is one of the principal components of total ship resistance, depends significantly upon the shape of the hull and wake generated by propeller. So, undoubtedly, empirical formulas for ship resistance and propeller open water characteristics do not necessarily give an accurate result to the ship designers.

1.1.2 Physical Experiments: Towing Tank and Cavitation Tunnel Test

The most reliable and accurate method for predicting hull resistance is model testing. In this method a small model of the actual ship is built and tested in a long basin in calm water or waves to estimate the ship hull resistance as shown in Figure 1.3. The model resistance is then converted to actual ship hull resistance by Froude's Law or other methods [4]. Using model testing facility for the prediction of calm water and wave resistance of ships is very costly, time consuming and problematic when it comes to scaling from model scale to full scale, because model tests carried out at Froude similarity while Reynolds similarity cannot be fulfilled.

Figure 1.3: Towing tank at Gdansk University of Technology, Poland [5]

Experimentally propeller open water characteristics can be obtained using a cavitation tunnel. This is a vertical water circuit with large diameter pipes. At the top, it carries the measuring facilities. A parallel inflow is established. With or without a ship model, the propeller, attached to a dynamometer, is brought into the inflow, and its thrust and torque is measured at different ratios of propeller speed (number of revolutions) to inflow velocity. Though cavitation tunnel [6] / water tunnel experiments of marine propeller provide most accurate results of propeller open water characteristics it is very costly and time consuming when several propeller models need to be tested.

A propeller in a water tunnel experiment is shown in Figures 1.4.

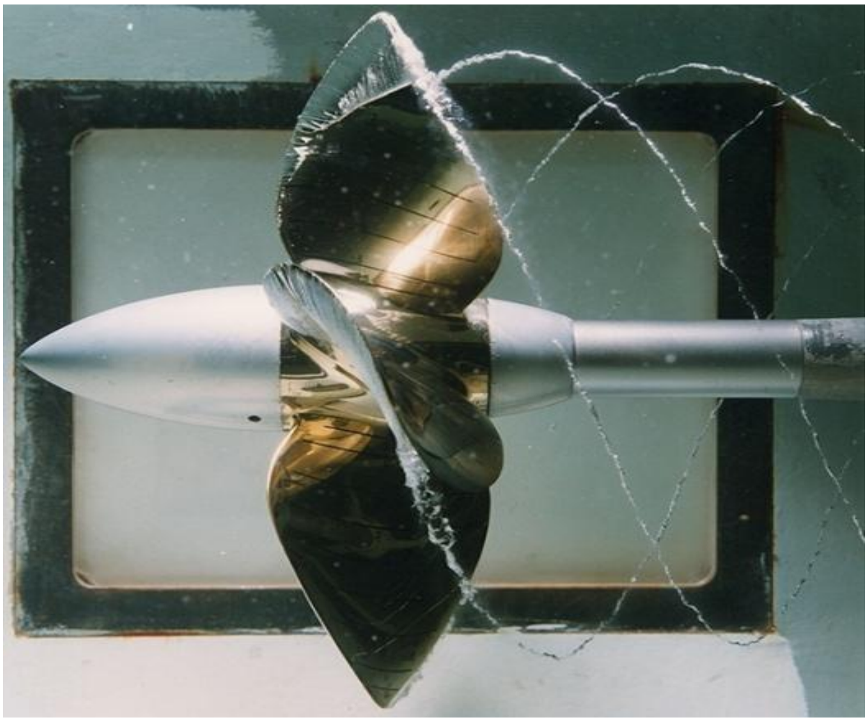

Figure 1.4: Cavitating propeller in a water tunnel at the David Taylor Model Basin [7]

1.1.3 Numerical Methods: Computational Fluid Dynamics

The rapid growth of computer capacities during the past decades has opened new horizons for marine hydrodynamics. The development of Computational Fluid Dynamics (CFD) technique has made it possible to predict the fluid velocity distribution by solving the fundamental equations of motion using numerical methods. The benefits of CFD compared to traditional model tests are many, with the major ones being listed below [8]:

- Simulation cost is relatively low compared to physical experiments.
- CFD simulations can be carried out faster than physical experiments. In addition, changes to the original design can be made quickly.
- Comprehensive data can be extracted from CFD, whereas a physical test case can only provide data from a limited number of locations. In addition, there is no testing apparatus interacting with the flow.
- Greater control of the set-up of the experiment. Conditions which would be difficult or impossible to achieve in a towing tank can be easily created in numerical tank.

As described by Lars Larsson and Hoyte C. Raven [9] CFD simulation starts with building the conceptual model. At this stage physical phenomena behind the specified problem are identified. A conceptual mathematical model, which consists of sets of differential or integral equations, is formed. In order to solve these equations numerically, they have to be discretized first and then solved by numerical methods. Iterative approach is used by most of the numerical methods. When convergence criterion is satisfied, iterative solver stops and the solution is supposed to be calculated.

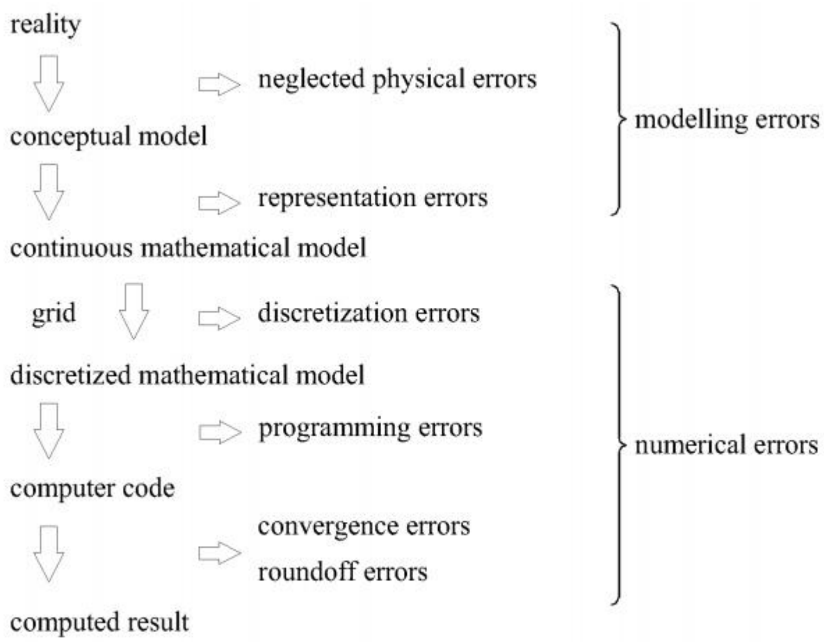

Figure 1.5: Sources of errors in computed results [9]

However, as shown in Figure 1.5 each step introduces errors to the solution. Modeling errors occur due to assumptions needed to construct the conceptual model and approximations in equations such as linearization or usage of empirical data. Numerical errors are discretization errors, convergence errors and roundoff errors which is introduced due to internal representation of numbers.

Due to the errors described, there is no guarantee that computed results will match with the physical reality. Therefore a systematic approach should be used in order to determine the quality of method. Comparing the result of a computation with an experimental result can be thought of simple or straight forward way to do it. More thorough understanding of the effects of numerical errors and modeling errors on computed results can be achieved if they are considered separately.

Discretization errors are dependent on the numerical scheme and grid quality which is limited by the cell aspect ratio, smooth distribution of cell sizes, deviation from orthogonality, refinement in regions of high gradients, alignment of grid lines with flow directions, etc. When the step size of the grid is reduced substantially, discretization errors must die out in a flawless numerical method. The effect of the numerical errors can be determined by checking the solutions of grids with different step-sizes. This method is called verification. After this step, validation of computed results against experimental data takes places. If the comparison of experimental data and grid independent computation shows conflicting results, continuous mathematical model is to be blamed as a result of modeling errors. Therefore a rigorous Verification and Validation method is needed for determining the errors and uncertainties.

The main advantage of CFD comes from its ability to fulfill both Froude and Reynolds similarities meaning that model-scale results and full-scale results can be directly calculated while providing a great deal of detail about the flow [10]. However the absolute accuracy of

CFD is still under concern and final decisions about the predictions of resistance and propulsive factors are still made by model tests.

1.2 Literature Review

In recent years, due to the increased computers capacity as well as to the reduced time spent on running the practical calculation of the flow around a ship, the interaction between the ship hull and its propeller seems to be a very interesting topic. Previously studies have focused upon reducing hull resistance while neglecting the effects of the propeller and the interaction between the ship hull and the propeller. Nowadays, the interaction between the propeller and ship stern flow became the subject of many investigations. Extensive research and investigations into the complex flow phenomena that exist between the propeller and rudder have been performed.

Initially, it was carried out based on a set of empirical methods [3], model testing [11] and wind tunnel [12] experiments. Among them model testing is considered as the most reliable and accurate method for performance prediction of a ship. The works of Oyan [13] and Kayano*et. al.* [14] are among recent experimental investigations to determine ship's propulsive performance. In these investigations, they predicted speed and powering of ships based on model testing using the load varying self propulsion method. However, this method is very costly and time consuming.

At present Computational Fluid Dynamic (CFD) methods developed to a stage, where they become interesting not only from a financial but also from a performance point of view. Fundamental studies of CFD techniques were based on the potential flow theory due to low memory power of computers. Moraes, *et.al.* [15] used slender body theory of Michell [3] and CFD based 3D potential panel method to determine wave resistance of catamarans. After maturing itself in time, potential flow solvers also allowed the inclusion of free surface into the problem. With the developments in computer science, RANSE solvers were started to be used widespread which allowed solving for the viscous flows around ships. As the computer capabilities were extended, appendages like propeller/ rudder were also included in the solutions.

Some previous studies focused on observing the propeller action under fully wetted condition, in order to compare the pressures on the hull with and without propeller effects, but this is mainly limited by the high demand of accuracy in the CFD codes and by the large computational effort. It is very important to know how to investigate, locate and even eliminate the influence of the possible errors, such as turbulence modeling errors, integral and interpolation errors, flow limiter errors, grid and geometry errors, iterative errors and other errors yet unnoticed. Therefore, a careful analysis and validation is required for CFD.

Molland and Turnock [16] conducted wind tunnel investigations on the influence of propeller loadings on a series of rudder geometries. The tests highlighted the distribution of loading over rudder through measurements of rudder forces, moments and pressure distribution. Simonsen [17] investigated the flow field around a propeller-rudder and hull combination using Reynolds Averaged Navier-Stokes (RANS) simulations. Bertram

[18] investigated the problem of the propeller-induced perturbation on the rudder. The study aimed at providing insights on the key mechanisms governing the complex interaction between the propeller wake structures and the rudder. Important flow features distinguishing flow field around a rudder operating in the race of a propeller were highlighted, examples of which are the complex dynamics of propeller tip vortices and the restoring mechanism of the tip vortex downstream of the rudder. Phillips *et al.* [19] also investigated the interaction between the propeller and rudder using a commercial RANS code; the influence of the propeller on the flow was modeled using three body force propeller models. They developed an iterative meshing approach which allows good capture of extents of propeller race downstream of the rudder and the vortical structures.

There are mainly two methods to compute the flow around a ship with a rotating propeller. One method is RANS-BEM method in which the viscous flow around the hull is solved by a RANS code and the flow around the propeller is solved with a BEM. The coupling between the two codes is done through a two-way coupling: interpolation of the propeller induced velocities from BEM in RANS and imposing the total wake field from RANS in the BEM method. Second method is a full RANS method in which the flow around both ship and propeller are solved in a RANS code. This is accomplished using sliding interfaces: the connection between the rotating grid block around the propeller, and the ship-fixed grid around the hull.

Depending on the goal of the calculation a choice can be made between these two methods. A RANS-BEM solves the propeller flow in an inviscid way. Advantages are the lower calculation time and the resulting effective wake field which can be very useful in propeller design studies. A full RANS method makes no assumptions with respect to the propeller vortex system, time-averaging, etc. It is therefore slower, but it includes physics which can be very important in studies like: cavitation in behind condition, effect of rudders on propulsion, post-swirl energy saving devices, etc.

Kim*et. al.* [20], Krasilnikov [21] and Rijpkema *et. al.* [22] used hybrid RANS and potential based numerical simulation for self-propulsion performance of ships. Very recently, Sakamoto and Kume [23] and Kawabuchi *et. al.* [24] used unsteady RANS based CFD simulation with sliding grid technique to determine hull-propeller interaction. Though this method guarantees accuracy, time required to calculate the interaction at a single speed is too long and it is only possible using high performance super computer. Moreover, the effect of changing position of rudder on propulsive characteristics of ship has not been considered in their works.

As it is stated a V&V method is needed for determining the errors and uncertainties. Thus, there has been many studies for developing a standard V&V methodology such as: Several constructive V&V methods based on Richardson Extrapolation (RE) have been put forward in the past decade. Roache [25] introduced a Grid Convergence Index (GCI) with a safety factor for numerical uncertainty estimation; the ITTC [26] recommended an uncertainty assessment methodology based on the approach by Stern *et al.* [27] in which the error and uncertainty are estimated with a correction factor taking the closeness to asymptotic range into consideration: Eca and Hoekstra [28-30] developed a method on basis of RE and GCI, but with a Least Squares Root approach to take the numerical scatter into account.

In order to extend the applications of V&V methods and highlight its importance in CFD, workshops have been organized. However an application on ship hydrodynamics is still very limited. For the purpose of filling this gap and assessing the state of art in numerical hydrodynamics, the series of international Workshops on CFD in Ship Hydrodynamics was introduced [31]. Test cases, conditions and EFD data are provided by the organizers and based on a questionnaire; participants submit the results of computations together with the V&V results. In 2015 NMRI [32] organized 7th of the Workshop series at Japan with 3 hulls; JAPAN Bulk Carrier (JBC), KRISO Container Ship (KCS) and ONR Tumblehome Ship (ONRT).

1.3 Objective

Although a significant number of numerical codes were developed for the prediction of bare hull ship resistance and propeller open water characteristics. The numerical simulation of flow around ship hull considering rudder-propeller interaction has not fully established yet due to the difficulty of capturing the complex flow interacting hull-propeller-rudder. Therefore, in this thesis an attempt is made to demonstrate that ship powering requirements can be reduced by optimizing the interaction between a ship's rudder and propeller.

The major objectives of this study are as follows:

- Detail investigation of a numerical model to determine the flow around two modern benchmark ships hull considering rudder-propeller interaction.
- Utilization of a computer code to determine propeller open water characteristics for different propeller geometry.
- Analysis of hydrodynamic characteristics of ship and propeller at varying speeds.
- A Verification and Validation (V&V) study for bare hull resistance.
- Comparing resistance characteristics of ships with/without rudder-propeller.
- Determination of Self-Propulsion characteristics at varying rudder positions.
- Analysis of effective wake and axial velocity at varying rudder positions.
- Validation of the computational results with the available published results.

1.4 Outline of Methodology

In this study, flow around two modern bench-mark ships hull namely KCS [32] and JBC [32] will be computed with self propulsion characteristics of KP505 [32] and DTMB 4119 [33] propellers respectively. Semi balanced horn type rudder at varying positions will be modelled to determine its effect on propulsive characteristics.

To compute the flow around a ship in an efficient way, numerical study is performed around bare hull first using 'Zonal Approach' incorporating 'Potential Flow', 'Thin Boundary Layer Flow' and 'Viscous Flow Solver' successively. For computing waves, wave resistance, free-surface wave profile 'Potential Flow Solver' has been used for various Froude numbers. This potential solving module provided also the input to a boundary layer method, which predicts transition and boundary layer parameters on the forward half of the ship. For predicting the viscous flow in the stern region, a Reynolds-Averaged-Navier-Stokes (RANS) code with boundary conditions defined by the potential flow results and the boundary layer parameters with and without propeller effects is used. The free surface is obtained as potential-flow solution and is kept fixed for the solution of the RANS equations.

The geometry of the ship hull will be represented by a single block structured H-O type grid. Additional grids for the propeller and the rudder will be fitted with hull by overlapping grid generation technique. For turbulence modeling, k-ω SST model without wall functions [34] will be used by the RANS solver. Finite Volume Method (FVM) will be used to discretize the governing equations which will be solved iteratively with ADI (Alternating Direction Implicit) solver using computer software 'Shipflow' [34].

The RANS computations include the propeller action by applying the body force method. The method considers the thrust and the torque of propeller as a field of forces which can be added to the body force terms in the RANS equations. The propeller forces will be calculated with a simple theory called Lifting Line Theory [35]. A computer program based on this theory will be utilized using OpenProp MATLAB code to determine propeller open water characteristics. These open water performance curves of OpenProp will be used for self-propulsion simulation with Shipflow results. Moreover, different longitudinal rudder positions will be investigated and compared to each other in order to improve propulsive performance. Finally, computed results from numerical solutions will be compared with the available published results.

Verification and validation studies for resistance coefficients have also been carried out using ITTC [26] recommended procedure. This analysis will lead to ensure the applicability of the numerical codes for accurate and reliable prediction of hydrodynamic behavior of ships in calm water with rudder-propeller interaction.

1.5 Thesis Framework

For complete understanding of the work, the thesis is divided into a number of chapters describing its different topics.

Chapter 1 first discusses the motivation and literature review for the origin of the problem and possible approaches to solve it. From these discussions it is clear that a number of research works have been done to determine the hydrodynamic performance of ships with propeller and rudder effect using empirical, experimental and numerical approaches. The objectives and outline of the methodology are given in details in later part of the chapter.

Chapter 2 presents fundamental numerical methods and theory to determine flow around ship hull considering rudder-propeller effect. This chapter also provides detail description of numerical methods, mesh generation; grid generation technique used by Shipflow and also discusses propeller theory used by OpenProp for the present analysis. A brief description of Verification and Validation (V&V) study is also presented here. The formulation of the governing equations and numerical schemes are explained in details to depict a deeper insight into the underlying theory and principles behind the simulation.

In chapter 3, geometry and test conditions of ship's hull, propellers and rudder used for the present study are provided.

In chapter 4, a detail description of results and discussions for the present analysis are presented.

In chapter 5, the conclusions of the findings with future recommendations for further study related to this analysis are discussed.

In Appendices A1 and A2 sample input and output files of KCS hull for the present computation are included.

Chapter 2

Numerical Method and Theory

The purpose of numerical methods is to solve the basic equations governing fluid flow, namely the continuity equation and the Navier-Stokes equations.

At the first part of this chapter the equations that govern the three regions namely potential flow region, thin boundary layer flow region and viscous flow region are discussed. The theory that is used to analyze propeller open water characteristics are described with rudder-propeller interaction.

In the second part, the detail description of the numerical methods which are used by CFD software Shipflow to simulate flow around ship hull considering rudder-propeller interaction is provided.

Finally, a brief description of the Verification and Validation (V&V) study is provided.

2.1 Governing Equations

The equations which govern any flow are the so called Navier-Stokes equations. These equations are the result of applying Newton's second law on a fluid element. The equations govern the flow of air as well as the flow of the water. The flow of air is neglected here because there is only a small interaction between the air and water.

2.1.1 Conservation Laws

There are three basic conservation equations: conservation of mass, conservation of momentum and conservation of energy. The conservation of energy is excluded here because the flow around a ship hull is a low speed, incompressible fluid flow and the temperature difference between body and fluid is assumed to be small. Conservation of mass is described by the continuity equation-

$$\frac{D\rho}{Dt} + \rho divV = 0 \tag{2.1}$$

In which $\frac{D}{Dt} = \frac{\partial}{\partial t} + u\frac{\partial}{\partial x} + v\frac{\partial}{\partial y} + z\frac{\partial}{\partial z}$ (2.2)

$$divV = \frac{\partial u}{\partial x} + \frac{\partial v}{\partial y} + \frac{\partial w}{\partial z} \tag{2.3}$$

For an incompressible fluid $\rho = const.$ This simplifies the continuity Equation (2.1) as-

$$divV = 0 \tag{2.4}$$

The conservation of momentum equation is acquired when Newton's second law is applied to a fluid particle. A continuous, isotropic and linear viscous fluid is assumed. The so called Navier Stokes (NS) equation is written here using indicial notation-

$$\rho \frac{Du_i}{Dt} = \rho g_i - \frac{\partial p}{\partial x_i} + \frac{\partial}{\partial x_j}\left[\mu\left(\frac{\partial u_i}{\partial x_j} + \frac{\partial u_j}{\partial x_i} \right) + \delta_{ij}\lambda div V \right] \tag{2.5}$$

Water is incompressible and the continuity equation for an incompressible fluid can be used to simplify the NS equation. When the viscosity of the water is assumed to be constant the NS equation is further simplified to the Navier-Stokes equation for incompressible, constant viscosity flow as follows:

$$\rho \frac{Du_i}{Dt} = \rho g_i - \frac{\partial p}{\partial x_i} + \frac{\partial}{\partial x_j} \mu\left(\frac{\partial u_i}{\partial x_j} + \frac{\partial u_j}{\partial x_i} \right) \tag{2.6}$$

The viscosity of liquids, like water, is temperature dependent but the temperature differences in the fluid are assumed to be small so the assumption of constant viscosity is justified.

2.1.2 Boundary Conditions for Potential Flow Solution

At the upstream or at inlet boundary, the values of the velocity (V) and the pressure (p) must be known.

$$V = V_o \;\; p = p_o \tag{2.7}$$

The far field boundary conditions can be split into two parts: the boundary to the side of the ship and the boundary behind the ship. The disturbances to the side will disappear and the boundary conditions are the same as the upstream conditions (2.7). The disturbances (waves) behind the ship will not disappear and this leads to a different boundary condition. In practice, Neumann boundary conditions (2.8 and 2.9) are used at the downstream boundary-

$$\frac{\partial V}{\partial x} = 0 \tag{2.8}$$

$$\frac{\partial p}{\partial x} = 0 \tag{2.9}$$

The no-slip boundary condition is applied for the velocity at the solid surface which is:

$$V = 0 \tag{2.10}$$

At the free surface there has to be kinematic equivalence between liquid and gas which means that the velocity of the flow at the free surface has to be tangent to the free surface.

$$w(x, y, \eta) = \frac{D\eta}{Dt} = \frac{\partial \eta}{\partial t} + u\frac{\partial \eta}{\partial x} + v\frac{\partial \eta}{\partial y} + z\frac{\partial \eta}{\partial z} \tag{2.11}$$

In which η(x, y, t) is the equation which describes the location of the free surface. There also has to be pressure equilibrium at the free surface.

$$p(x,y,\eta) = p_a - \gamma\left(\frac{1}{R_x} - \frac{1}{R_y}\right) \tag{2.12}$$

Where γ is the coefficient of surface tension and R_x and R_y are the radii of curvature of the free surface. In a wave trough $p < p_a$ and in a wave crest $p > p_a$.

2.2 Potential Flow

The principal assumptions in potential flow are: inviscid, irrotational, incompressible, and steady flow. These assumptions are valid for the flow around a ship because the Reynolds number is relatively high and the effect of viscosity will be limited to a thin layer close to the hull and the wake. The large scale flow features such as the wave pattern are not affected much and this justifies the use of the potential flow assumption to model this large scale flow features.

The potential flow assumptions are used to simplify the Navier Stokes Equation (2.6) which lead to the following equation:

$$\frac{1}{2}\nabla V^2 = \rho g - \nabla p \tag{2.13}$$

The continuity equation remains the same, i.e.,

$$divV = 0 \tag{2.14}$$

The velocity vector can be written as the gradient of a scalar. This scalar is called the velocity potential-

$$V = \nabla\phi \tag{2.15}$$

This is substituted in the Bernoulli and continuity equations which lead to:

$$p + \rho gz + \frac{1}{2}(\nabla\phi.\nabla\phi) = const. \tag{2.16}$$

$$\nabla^2\phi = 0 \tag{2.17}$$

The continuity Equation (2.4) transforms into the Laplace Equation (2.17) which is linear and homogeneous. This allows the superposition of different solutions. The pressure and velocity are decoupled which makes it possible to solve the Laplace equation first and compute the pressure later.

The no-slip boundary condition (2.10) at the body changes to the tangential flow boundary condition. The simplifications introduced by the potential flow assumptions have decreased the degrees of freedom which make it impossible to maintain the no-slip condition.
The tangential flow condition means that the fluid cannot flow through the body that means:

$$\phi_n = 0 \tag{2.18}$$

The velocity potential is substituted in the kinematic boundary condition at the free surface (2.11) and the time dependent terms are dropped because of the steady flow assumption. The location of the free surface is described by the single valued function η(x, y) which makes it impossible to calculate overturning (breaking) waves and spray. These effects are considered to have a small influence on the global wave pattern and thus are this single valued free surface approach allowed. Two boundary conditions exist at the free surface. The velocity vector at the free surface is tangential to the free surface.

$$\phi_x \eta_x + \phi_y \eta_y - \phi_z = 0 \text{ at } z = \eta(x, y) \tag{2.19}$$

and the pressure in the water at the free surface has to be equal to the atmospheric pressure.

$$p_a + \rho g z + \frac{1}{2}(\nabla\phi . \nabla\phi) = const. \text{ at } z = \eta(x, y) \tag{2.20}$$

which can be rewritten as –

$$g\eta + \frac{1}{2}\left[(\phi_x)^2 + (\phi_y)^2 + (\phi_z)^2 - U_\infty^2 \right] = 0 \tag{2.21}$$

By reducing the Navier-Stokes equations to the potential flow equations a lot of information is lost. This leads to the situation that the solution of the potential flow equations is no longer unique and more than one solution exist. This can give non-physical solutions such as waves upstream of the bow. An extra condition is added to avoid non-physical solutions: the radiation condition. The radiation condition states that free surface waves generated by a ship cannot travel in the upstream direction.

2.2.1 Linearization of the Free Surface Boundary Conditions

The free surface conditions are nonlinear and this makes it difficult to solve them. To overcome this problem the boundary conditions are linearized. This is done by dividing the potential, ϕ in two parts: an estimated flow or base flow, Φ and a perturbation φ. A good estimate will result in a small perturbation which justifies the linearization.

$$\nabla\phi = \nabla\Phi + \nabla\varphi \tag{2.22}$$

$$\eta = H + h \tag{2.23}$$

This can then be substituted into the free surface boundary conditions (2.19) and (2.21) which leads to:

$$\Phi_x\eta_x + \Phi_y\eta_y + \varphi_x H_x + \varphi_y H_y - \Phi_z - \varphi_z = 0 \tag{2.24}$$

$$\eta = \frac{1}{2g}(U_\infty^2 - \Phi_x^2 - \Phi_y^2 - \Phi_z^2 - 2\Phi_x\varphi_y - 2\Phi_y\varphi_y - 2\Phi_z\varphi_z) \tag{2.25}$$

These equations have to be satisfied at the free surface. The location of this free surface is unknown and therefore these equations need to be transferred to the estimated surface, $z = h$.

$$\nabla\phi_{(z=\eta)} \approx \nabla\Phi_{(z=H)} + \nabla\varphi_{(z=H)} + h\frac{\partial\nabla\Phi}{\partial z} \tag{2.26}$$

Dawson proposed to neglect the transfer term $h\frac{\partial\nabla\Phi}{\partial z}$ and the higher order terms which leads to the combined linear free surface boundary condition on the known surface $z = H$:

$$\begin{aligned}&-\frac{1}{2g}\Phi_x\frac{\partial}{\partial x}(\Phi_x^2 + \Phi_y^2 + \Phi_z^2 + 2\Phi_x\varphi_x + 2\Phi_y\varphi_y + 2\Phi_z\varphi_z)\\ &-\frac{1}{2g}\Phi_y\frac{\partial}{\partial y}(\Phi_x^2 + \Phi_y^2 + \Phi_z^2 + 2\Phi_x\varphi_x + 2\Phi_y\varphi_y + 2\Phi_z\varphi_z)\\ &+\varphi_x H_x + \varphi_y H_y - \Phi_z - \varphi_z = 0\end{aligned} \tag{2.27}$$

Wave making resistance is obtained by solving the potential flow solution. Pressure on the hull surface by Bernoulli's equation as follows:

$$p - p_\infty = \frac{1}{2}\rho(U^2 - \nabla\Phi.\nabla\Phi) - \rho g z \tag{2.28}$$

Hydrodynamic force, R_W and wave making resistance coefficient, C_W:

$$R_W = -\int_S (p - p_\infty) n_x ds \tag{2.29}$$

$$C_W = \frac{R_W}{0.5\rho S V^2} \tag{2.30}$$

2.3 Thin Boundary Layer Flow

Thin boundary layer near the forward half of the hull is computed with Boundary Layer solver of Shipflow [34] using the momentum integral equation:

$$\frac{d\theta}{dx} + \frac{\theta}{u}.(H+2)\frac{dU}{dx} = \frac{C_f}{2} \tag{2.31}$$

where θ, H, C_f denote momentum thickness, shape factor and friction coefficient respectively.

2.4 Turbulent Flow Simulation: RANS Method

A turbulent flow field is characterized by velocity fluctuations in all directions and has an infinite number of scales (degrees of freedom). Solving the Navier-Stokes equations for a turbulent flow is impossible because the equations are elliptic, non-linear, coupled (pressure-velocity, temperature-velocity). The flow is three dimensional, chaotic, diffusive, dissipative, and intermittent. The most important characteristic of a turbulent flow is the infinite number of scales so that a full numerical resolution of the flow requires the construction of a grid with very large number of nodes.

There are different types of methods to compute the turbulent flow depending on the approximation or modeling the turbulence. Direct Numerical Simulation (DNS) method is based on the instantaneous continuity and Navier–Stokes equations (2.4), (2.5) and developes a transient solution on a sufficiently fine spatial mesh with sufficiently small time steps to resolve even the smallest turbulent eddies and the fastest fluctuations [36]. According to Zou[37] this conditions for ship hydrodynamics however are extremely expensive in terms of computational power since full scale ships are mostly order of 100 m on the other hand smallest scale eddies are down to 0.1 mm. Large Eddy Simulation (LES) resolves the large scale turbulent motions in order to model the small scale eddies using sub-grid scale models. Reynolds Averaged Navier-Stokes (RANS) method solves the mean flow by time-averaging the Navier-Stokes equation and models the turbulence. Due to the limited computational resources, Zou[37] indicates that RANS method is the most widely used CFD technique in practice.

The incompressible Navier-Stokes equations in conservation form are:

$$\frac{\partial u_i}{\partial x_i} = 0 \tag{2.32}$$

$$\rho \frac{\partial u_i}{\partial t} + \rho \frac{\partial}{\partial x_j}\left(u_j u_i\right) = -\frac{\partial p}{\partial x_i} + \frac{\partial}{\partial x_j}\left(2\mu s_{ij}\right) \tag{2.33}$$

where the strain-rate tensor s_{ij} is given by:

$$s_{ij} = \frac{1}{2}\left(\frac{\partial u_i}{\partial x_j} + \frac{\partial u_j}{\partial x_i}\right) \tag{2.34}$$

By the application of equation (2.32), the equations of motion can be written as follows:

$$\rho \frac{\partial u_i}{\partial t} + \rho u_j \frac{\partial u_i}{\partial x_j} = -\frac{\partial p}{\partial x_i} + \mu \frac{\partial^2 u_i}{\partial x_i x_j} \tag{2.35}$$

In turbulent flows, the field properties become random functions of space and time. Hence, the field variables u_i and p must be expressed as the sum of mean and fluctuating parts as:

$$u_i = U_i + u_i^{'} \; p = P + p^{'} \tag{2.36}$$

where the mean and fluctuating parts satisfy the following:

$$\overline{u}_i = U_i, \quad \overline{u}_i^{'} = 0 \tag{2.37}$$

$$\overline{p} = P, \quad \overline{p}_i^{'} = 0 \tag{2.38}$$

with the bar denoting the time average.

Inserting Equation (2.36) into Equations (2.32) and (2.33) and taking the time average to obtain the Reynolds Averaged Navier-Stokes (RANS) equations as follows:

$$\frac{\partial U_i}{\partial x_i} = 0 \tag{2.39}$$

$$\rho \frac{\partial U_i}{\partial t} + \rho \frac{\partial}{\partial x_j}\left(U_i U_j\right) = -\frac{\partial P}{\partial x_i} + \frac{\partial}{\partial x_j}\left(2\mu S_{ij} - \rho \overline{u_i^{'} u_j^{'}}\right) \tag{2.40}$$

where S_{ij} is the mean strain-rate tensor:

$$S_{ij} = \frac{1}{2}\left(\frac{\partial U_i}{\partial x_j} + \frac{\partial U_j}{\partial x_i}\right) \tag{2.41}$$

The quantity $\tau_{ij} = \overline{u_i^{'} u_j^{'}}$ is known as the Reynolds stress tensor which is symmetric and thus has six components. By the application of Equation (2.39), Equation (2.40) can then be expressed as:

$$\frac{\partial U_i}{\partial t} + U_j \frac{\partial U_i}{\partial x_j} = -\frac{\partial P}{\partial x_i} + \upsilon \frac{\partial^2 U_i}{\partial x_i \partial x_j} - \frac{\partial \overline{u_i^{'} u_j^{'}}_i}{\partial x_j} \tag{2.42}$$

where $\upsilon = \dfrac{\mu}{\rho}$ (2.43)

By decomposing the instantaneous properties into mean and fluctuating parts, 3 unknown quantities are introduced. Unfortunately, no additional equations are gained. This means that the system is not yet closed. To close the system, enough equations must be found to solve for the unknowns. Therefore, turbulence models are needed to determine these variables in terms of known quantities.

2.4.1 Turbulence Modeling

A turbulence model is a computational procedure to close the system of mean flow equations. For most engineering applications it is unnecessary to resolve the details of the turbulent fluctuations. Turbulence models allow the calculation of the mean flow without first calculating the full time-dependent flow field. It is necessary to know how turbulence affected the mean flow. There are several turbulence models for solving the RANS equations.

Common turbulence models are:

- Zero equation model: mixing length model.
- One equation model: Spalart-Almaras.
- Two equation model: $k-\varepsilon$ models
  - Standard $k-\varepsilon$ model
  - Renormalization-group (RNG) $k-\varepsilon$ model
  - Realizable $k-\varepsilon$ model
- Two equation model: $k-\omega$ models
  - Standard $k-\omega$ model
  - Shear-Stress Transport (SST) $k-\omega$ model
- Seven equations model: Reynolds stress model (RSM)

Here the number of equations denotes the number of additional PDEs that are being solved.

2.4. 2 Selection of Turbulence Modeling

It is an unfortunate fact that no single turbulence model is universally accepted as being superior for all classes of problems. The choice of turbulence model will depend on considerations such as the physics encompassed in the flow, the established practice for a specific class of problem, the level of accuracy required, the available computational resources, and the amount of time available for the simulation. To make the most appropriate choice of model for required application, one needs to understand the capabilities and limitations of the various options.

For a turbulence model to be useful it must have the following characteristics:

- must have wide applicability,
- be accurate,
- simple,and
- economical to run.

In this thesis Shear-Stress Transport (SST) $k-\omega$ model will be used for modeling the turbulence flow.

2.4. 3 Shear-Stress Transport (SST) $k-\omega$ model

This model was developed by Menter [38] to effectively blend the robust and accurate formulation of the $k-\omega$ model in the near-wall region with the free-stream independence of the $k-\varepsilon$ model in the far field. To achieve this, the $k-\varepsilon$ model is converted into a $k-\omega$ formulation.

SST $k-\omega$ model is similar to the standard $k-\omega$ model, but includes the following refinements:

- The standard $k-\omega$ model and the transformed $k-\varepsilon$ model are both multiplied by a blending function and both models are added together. The blending function is designed to be one in the near wall region, which activates the standard $k-\omega$ model, and zero away from the surface, which activates the transformed $k-\varepsilon$ model.
- The SST model incorporates a damped cross-diffusion derivative term in the ω equation.
- The definition of the turbulent viscosity is modified to account for the transport of the turbulent shear stress.
- The modeling constants are different.

These features make the SST $k-\omega$ model more accurate and reliable for a wider class of flows (e.g., adverse pressure gradient flows, airfoils, transonic shock waves) than the standard $k-\omega$ model.

2.4. 3.1 Transport Equations of $k-\omega$ SST model

The turbulence kinetic energy, k and the specific dissipation rate, ω are obtained from the following transport equations:

$$\frac{\partial}{\partial t}(\rho k)+\frac{\partial}{\partial x_i}(\rho k u_i)=\frac{\partial}{\partial x_j}\left(\Gamma_k \frac{\partial k}{\partial x_j}\right)+G_k-Y_k+S_k \tag{2.44}$$

$$\frac{\partial}{\partial t}(\rho \omega)+\frac{\partial}{\partial x_i}(\rho \omega u_i)=\frac{\partial}{\partial x_j}\left(\Gamma_\omega \frac{\partial \omega}{\partial x_j}\right)+G_\omega-Y_\omega+S_\omega \tag{2.45}$$

In these equations, G_k represents the generation of turbulence kinetic energy due to mean velocity gradients, G_ω represents the generation of specific dissipation rate, ω. Γ_k and Γ_ω represent the effective diffusivity of k and ω respectively. Y_k and Y_ω represent the dissipation of k and ω due to turbulence.

2.5 Wall Functions vs. Near-Wall Model

Traditionally, there are two approaches to modeling the near-wall region**.** In one approach, the viscosity-affected inner region (viscous sublayer and buffer layer) is not resolved. Instead, semi-empirical formulas called “wall functions” are used to bridge the viscosity-affected region between the wall and the fully-turbulent region. The use of wall functions obviates the need to modify the turbulence models to account for the presence of the wall.

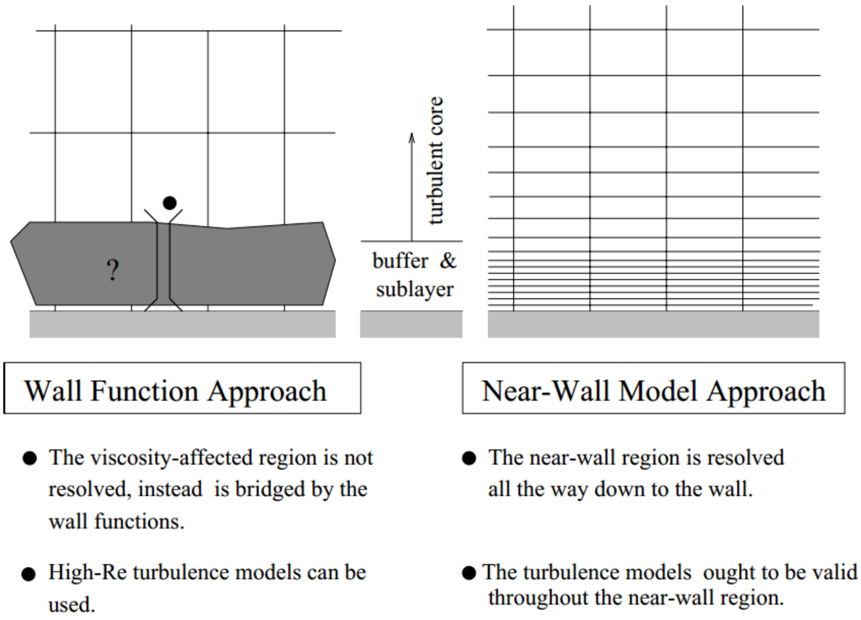

Figure 2.1: Wall functions vs. near-wall model [39]

In another approach, the turbulence models are modified to enable the viscosity-affected region to be resolved with a mesh all the way to the wall, including the viscous sublayer. This approach is known as "near-wall modeling approach". These two approaches are depicted schematically in Figure 2.1.

In SST $k-\omega$ model, the flow is resolved up to the wall. Therefore near-wall model approach is used instead of wall function for the treatment of boundary layer region.

2.6 Propeller Theory

Typical propeller characteristics that play an important role in designing propellers are advance coefficient J, thrust coefficient K_t and torque coefficient K_q. The definitions of these characteristics are:

$$J = \frac{V_A}{nD} \tag{2.46}$$

$$K_t = \frac{T}{\rho n^2 D^4} \tag{2.47}$$

$$K_q = \frac{Q}{\rho n^2 D^5} \tag{2.48}$$

The power generated by engine delivered to the propeller, P_D is defined by:

$$P_D = 2\pi n Q_n \tag{2.49}$$

where V_A is advance velocity, T is thrust and Q_n is the generated torque and D is the propeller diameter.

The open water efficiency η_o is the efficiency of propeller working in a homogeneous flow without any ship hull. It is defined as thrust power P_T divided shaft power P_D.

$$\eta_o = \frac{TV_A}{P_D} = \frac{JK_T}{2\pi K_Q} \tag{2.50}$$

Propulsive efficiency η_D is equal to effective power P_E divided to shaft power P_D .

$$P_E = R_T V_S \tag{2.51}$$

$$P_D = 2\pi n_S Q_S \tag{2.52}$$

$$Q_s = 2\pi\rho n^2 D^5 K_q \tag{2.53}$$

$$\eta_D = \frac{P_E}{P_D} \tag{2.54}$$

In these equations R_T is total ship resistance, V_S is ship speed, n_s and Q_s are shaft revolution rate and applied torque to the shaft respectively.

By towing a ship hull, at the stern a high-pressure region is observed which affects the total resistance of the ship. During the self propulsion test, high-pressure area located at the aft part of the ship is affected by a working propeller. Therefore magnitude of pressure in this high pressure region is reduced. Consequently, there is an increase in resistance due to existence of propeller. For propelling the ship at a specific speed V_S , produced thrust T by the propeller should be larger than total resistance of the ship hull, R_T . Thrust deduction t is the normalized form of difference between T and R_T and is defined as in equation

$$t = \frac{T - R_T}{T} = 1 - \frac{R_T}{T} \tag{2.55}$$

Because of the friction wake at the aft part of the ship where the propeller is working, the velocity of water, V_w at the propeller plane is less than the speed V of the ship.

The direction V_w is in the same direction of ship movement. Meanwhile, the propeller is accelerating the water flow with the speed of V_A in the opposite direction of the ship's speed.

V_w is called effective wake velocity at the propeller which is obtained by subtracting ship's speed V from propeller advance velocity V_A

$$V_W = V - V_A \tag{2.56}$$

Wake fraction is a dimensionless form of effective wake velocity and is defined as:

$$W = \frac{V_W}{V} = \frac{V - V_A}{V} \tag{2.57}$$

2.6.1 Causes of Wake

Flow around a propeller is affected by the presence of a hull. Average speed of the water through the propeller plane is usually less than the hull speed. Potential and viscous nature of the boundary layer contributes to the development of the wake which causes formation of potential and frictional/viscous wake.

Some factors such as shape of ship hull, size and position of propeller, affect the wake fraction and therefore the propeller efficiency. Propeller accelerates the flow which decreases the wake and it may also decrease or prevent the flow separation.

2.6.1.1 Potential Wake

When streamline flow pasts the hull it increases the pressure around the stern and decreases the velocity of the water past the hull causes potential wake at stern of the ship as shown in Figure 2.2.

2.6.1.2 Frictional/ Viscous Wake

At the stern of the ship boundary layer decelerates the flow. Due to strong flow deceleration results in strong frictional/ viscous wake at the stern as shown in Figure 2.3.

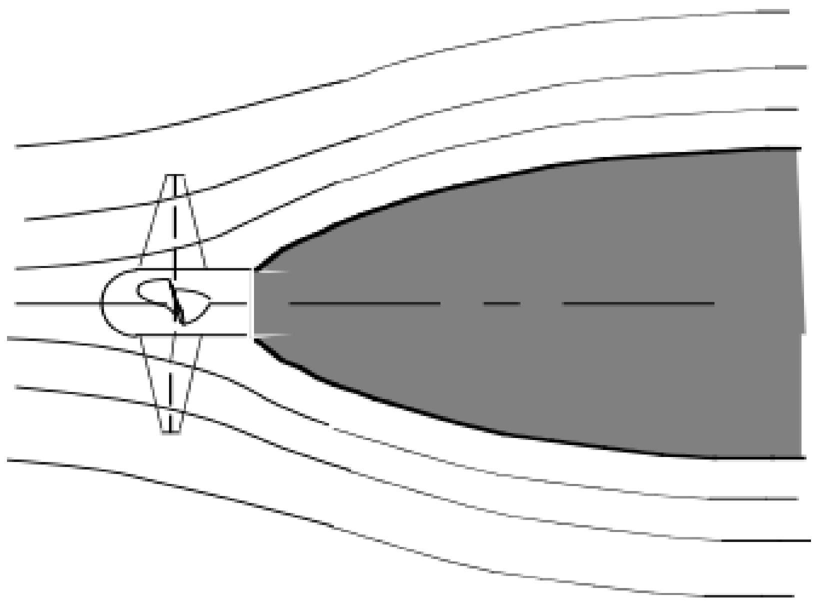

Figure 2.2: Potentialwake formations at stern [40]

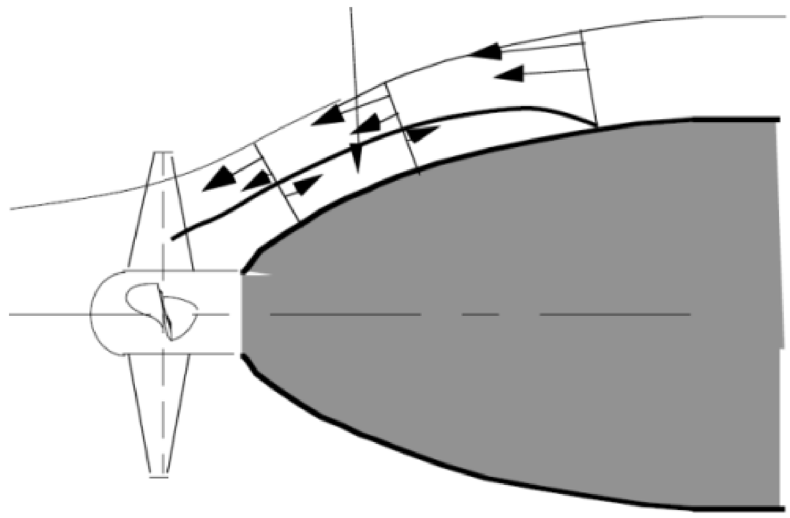

Figure 2.3: Viscous wake formations at stern [40]

2.6.2 Propeller Lifting Line Formulation

The lifting line method is a mathematical rather plain approach to compute the lift of a wing. It is based on the classical lifting line theory [35], which is adapted to the marine propeller problem in Lerbs analysis method for moderately loaded propeller [35]. The method assumes the propeller blade sections to be replaced by a single line vortex that varies in strength from section to section. The line, about which the vortices act, is a continuous in radial direction. Figure 2.4 shows the discretisation of the propeller geometry by a lifting line. This figure shows also the free vortices shed from the each bound (lifting) vortex along the lifting line, to satisfy the Helmholtz's theorem of the principles of inviscid vortex behaviour.

Lifting line is a method to calculate the propellers characteristics which was proposed by H.W. Lerbs in 1952. In this method a propeller with finite number of blade, B, blade is modeled with a vortex system including hub vortex, bound vortex and helical free vortex. The vortex system is created as: hub vortex is generated along the X axis, bound vortex lines are generated corresponding every blade and helical free trailing vortex line tracing the propeller slipstream at specific radius. This vortex system is shown in Figures 2.4 and 2.5.

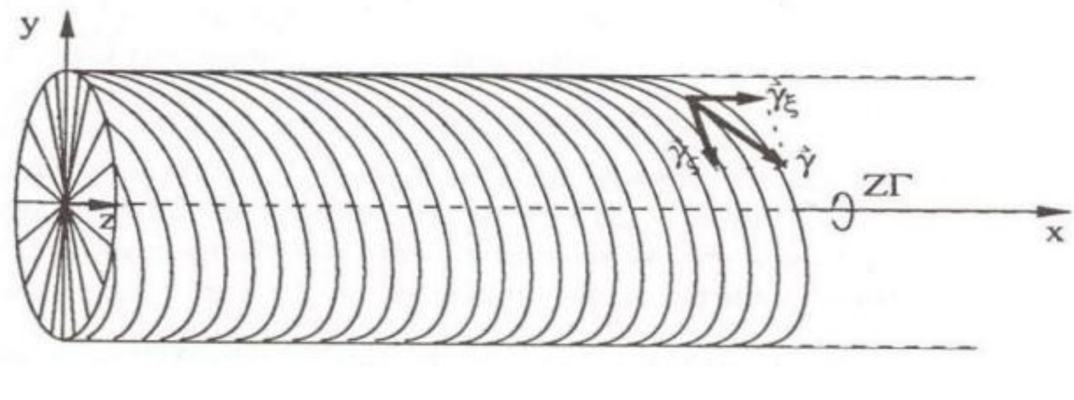

a) infinite number of blade

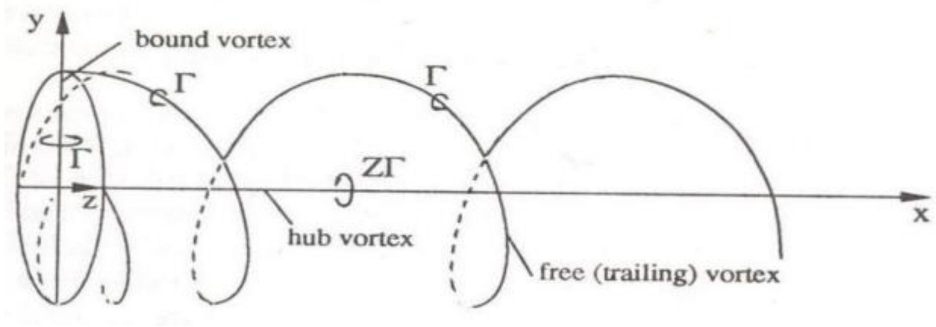

b) Z blade number

Figure 2.4: Lifting line vortex system of propeller; a)infinite number of blade, b) Z blade number [42].

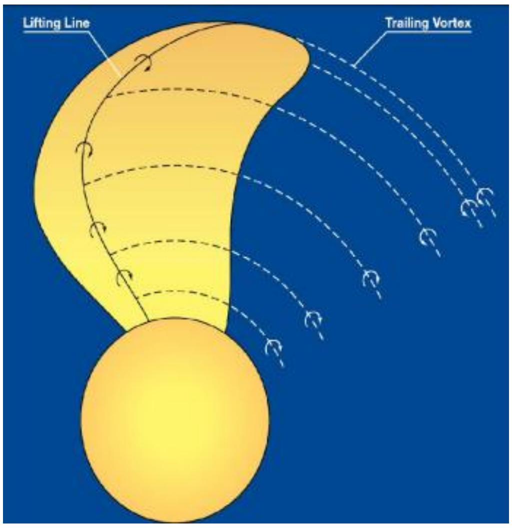

Figure 2.5: Lifting line vortex system of propeller [43].

Induced velocity by the propeller is divided into two different parts regarding the time dependency point of view. The steady part forms the major part of the induced flow which is not dependent to the time, and the time dependent part. An infinite-bladed propeller is utilized, in order to simplify the estimation of time independent part of the induced flow. In the case of the infinite-bladed propeller, the vortex system is applied by executing a sequence of bound vortex and helical vortex lines which are distributed between the propeller hub with the radius and propeller tip with the radius R. An assumption about helical vortexes is made which implies that the radius and pitch of all helical vortices are constant in the axial direction [42].

2.6.3 Rudder-Propeller Interaction

For approaching better maneuverability in ships, rudders are installed behind the propellers where they are faced by high-energy propeller slip streams. These slipstreams contain axial and tangential induced velocity created by the propeller. The flow properties and hydrodynamic performance are different when either rudder or propeller is working alone in aft part of the ship hull. A rudder which is situated in these high-energy slipstreams is facing different axial forces such as:

- Tangential velocity induced by propeller applies a thrust force on the rudder. In addition it can be mentioned that, the rudder recovers rotational energy of rotational slipstreams caused by the propeller. This recovery happens when the rudder also induces tangential velocity in opposite direction of the propeller slipstreams flow which cancel out a fraction of propeller induced tangential velocity.

- Due to induced axial velocity by the propeller in onset flow, the viscous drag force on the rudder is increased.

- The flow which has been accelerated by the propeller increases the pressure drag on the rudder.

Furthermore, as it is shown in Figure 2.6, the streams coming out of the propeller get blocked and diverted by the rudder which results in decreasing the total axial and tangential velocity. Thrust and torque will therefore be partly higher when a rudder is included. Consequently higher propulsive efficiency might be obtained from propeller/rudder combination as a propulsion system [44].

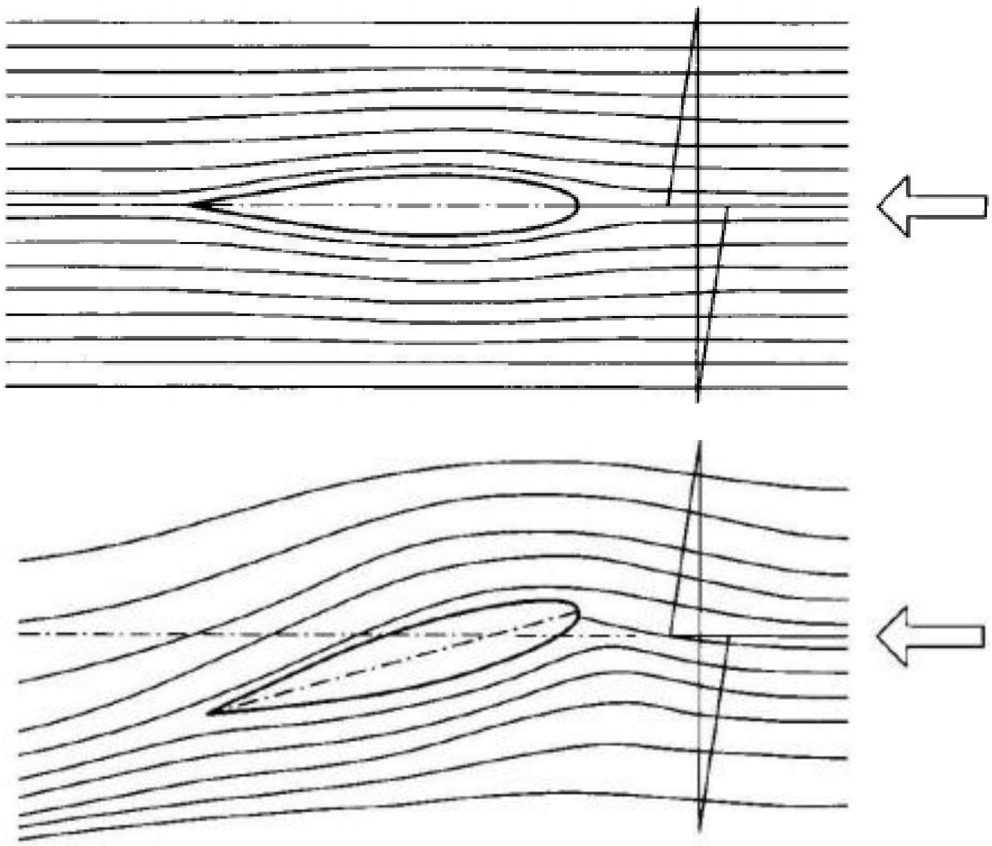

Figure 2.6: Blocked and diverted flow by rudder [44].

2.7 Numerical Methods in Shipflow

The CFD code implemented in this thesis is Shipflow which has been developed by FLOWTECH International AB with close cooperation of Shipping and Marine Technology Department at Chalmers University of Technology and SSPA. The code is specially optimised for ship hydrodynamics and all outputs of resistance and propulsion are presented in the naval architects way. The numerical methods used by this CFD code to analyse flow around ship hull with rudder and propeller effect are described in this section.

2.7.1 Co-ordinate System

The coordinate system (x, y, z) is defined as origin is located in the undisturbed free surface at fore perpendicular (F.P) of the hull so that the undisturbed incident flow with a constant speed U appears to be a streaming in the positive-x direction with y axis extends to the starboard side and z- axis upwards as shown in Figure 2.7.

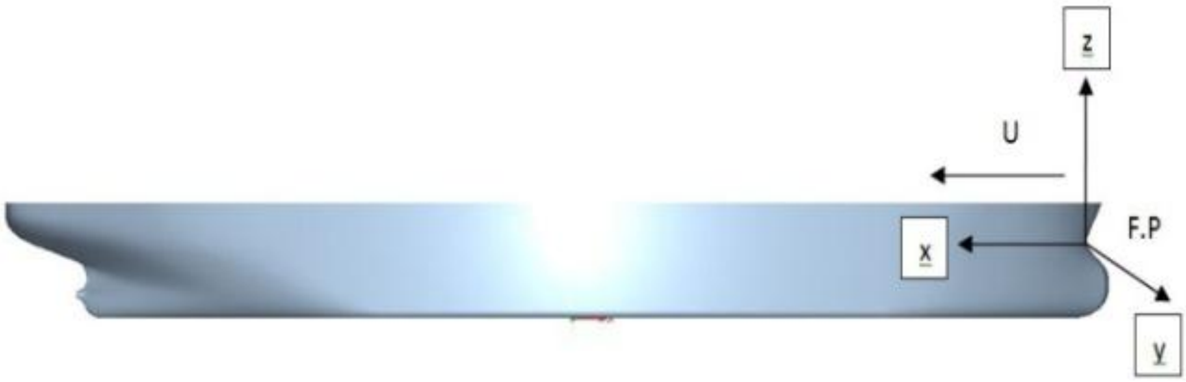

Figure 2.7: Cartesian coordinate system in Shipflow

2.7.2 Computational Method

To compute the flow around a ship in an efficient way, zonal approach is used as shown in Figure 2.8 which divides the flow around a ship into three different zones with different solution methods.

Region outside the boundary layer and wake is considered to be incompressible, inviscid and irrotational. Therefore, in the outer flow (zone 1), the potential flow theory is employed. The inner flow is divided into the thin boundary layer (zone 2) and stern/wake region (zone 3).

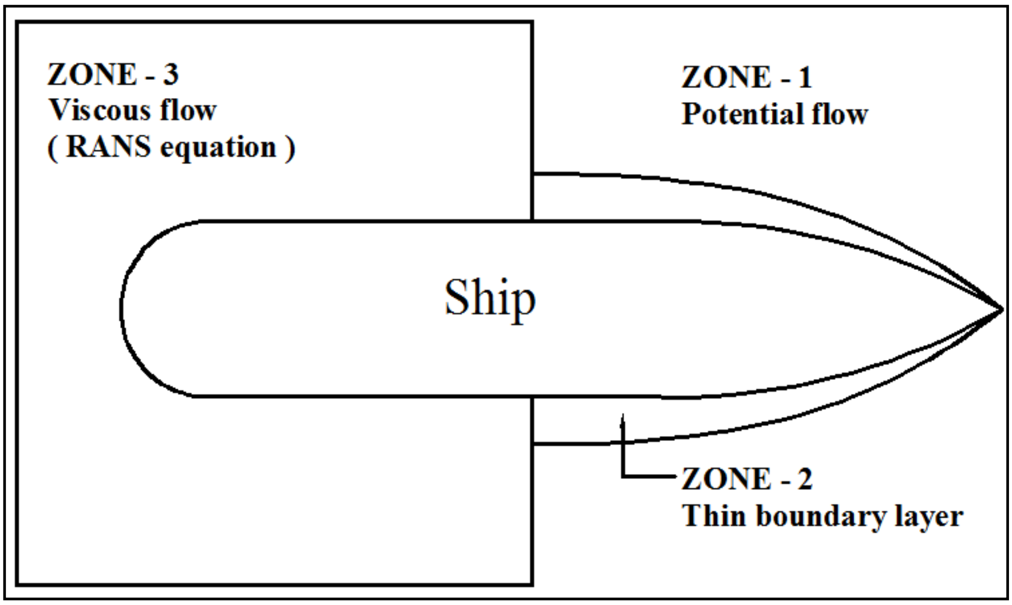

Figure 2.8: Shipflow zonal approach

2.8 Computational Method for Potential Flow

There are a lot of different ways to solve the Laplace equation for the velocity potential. Raven [45] compares the advantages and disadvantages of the possible solution strategies and his conclusion is that a panel method using Rankine sources on the hull and free surface will probably be the most efficient. A Rankine source is a point source which potential can be described as $\Phi = -\frac{\sigma}{4\pi r}$ such that it satisfies the Laplace equation $\nabla^2\Phi = 0$. The Laplace equation is homogeneous which makes it possible to add different solutions to create a new solution by the superposition principle. Since a Rankine source satisfies the Laplace equation, a combination of different Rankine sources can be used to represent a body in a potential flow. A more detailed description of the basics of panel methods can be found in [46].

Lifting surfaces can easily be included in a panel method and are needed to model appendages such as keels and rudders. A detailed explanation about lifting surfaces in free surface flows can be found in [47].

Potential flow solver of Shipflow can deal with both linear and nonlinear methods for the free surface.

2.8.1 Linear Free Surface Potential Flow

The linear case starts with the calculation of the estimate or base flow. For this base flow the slow ship approximation is used which means that no free surface waves are present (the free surface is flat). It is possible to calculate this base flow by meshing both the hull and free surface but it is more efficient to make use of symmetry by mirroring the underwater part of the hull in the water plane. This eliminates the need to mesh the free surface which saves computing time. The flow around this so called ”double body” is calculated and the slow ship approximation at the free surface is immediately satisfied.

To determine the perturbation both hull and free surface are meshed. The result of the double body flow calculation is used as an estimate and then the perturbation can be calculated using the equations from section 2.2.1.The resulting perturbation is added to the base flow which gives the linear free surface potential flow solution.

A problem of the linear method is that it does not take into account the shape of the hull above the still waterline. This is an important drawback because in most cases it will create problems and will influence on the flow around the hull.

2.8.2 Nonlinear Free Surface Potential Flow

The nonlinear solution method is an extension of the linear case. After the linear solution has been calculated this result is used as a new estimate. The hull and free surface panels are moved and the perturbation is calculated again. These steps are repeated until a converged solution is achieved. Convergence is achieved when the change in wave height for two consecutive iterations is below a set tolerance [47].

The first advantage of the nonlinear solution method is that it gives a solution of the system of equations and is no longer an approximation as in the linear case. The second advantage of the nonlinear solution is that when the panels are moved they are adjusted to fit the new intersection between the hull and free surface. This way the shape of the hull above the waterline is taken into account.

2.8.3 Special Features of the Solution Method

The radiation condition (section 2.2.1) is satisfied by using an upwind approximation for the second derivatives of the potential in the longitudinal direction at the free surface. This upwind discretization eliminates the formation of upstream waves. A central scheme is used for the second derivatives of the potential in the transverse direction.

The stability and convergence of the solution method is improved by using raised panels on the free surface. This means that the panels are raised above the free surface but the collocation points are on the actual free surface. Solutions using this raised panels showed point to point oscillations in the calculated source strength. An effective way to avoid this is to use a forward shift in the collocation point location. The phase and amplitude of the calculated waves show a dependency on the distance that the panels are raised and the forward shift of the collocation point. The two dimensional case of the nonlinear free surface potential flow has been studied in detail in [47] and also in [48] and the conclusion is that each upwind scheme has its own optimal raised distance. In general a forward shift of 25 to 30% of the panel length and a raised distance of more than 1 panel length lead to accurate results in the two dimensional case. For the three dimensional case the raised distance has some influence on the condition of the system of equations. This leads to a decrease in the raised distance when the Froude number increases: approximately 70% of the panel length for Fn 0.25 to approximately 30% of the panel length for Fn 0.55.

The nonlinear free surface potential flow can be calculated using a fixed location of the hull or a hull which is free to trim and sink. In case the hull is free to trim and sink an extra set of equations is added to the solver. The weight distribution of the hull has to be in equilibrium with the hydrodynamic forces. After each iteration the trim and sink are adjusted to maintain the equilibrium. This gives two extra convergence criteria: the change of the trim angle and the sink should be within a given tolerance.

Free-surface wave pattern, wave elevation and wave resistance are obtained from the Potential Flow solver of Shipflow CFD code.

2.8.4 Determination of the Wave Resistance

There are two ways to determine the wave resistance of ship: pressure integration and wave cut analysis both of which will be described here.

2.8.4.1 Pressure Integration

The pressure integration method determines the wave resistance by integrating the pressure on the hull panels. The pressure on the hull consists of the hydrostatic and the hydrodynamic pressure. For the linear solution the hydrostatic pressure sums to zero and this makes it possible to integrate only the dynamic pressure to get the wave resistance. For the nonlinear solutions the hydrostatic pressure does not cancel and thus both pressures need to be integrated. The magnitude of the hydrostatic pressure is often larger than that of the hydrodynamic pressure and this can cause some problems concerning the accuracy of the pressure integration method. The solution to this problem is to use a sufficient number of panels on the hull surface.

2.8.4.2 Wave Cut Analysis

The wave cut analysis technique determines the wave resistance by analyzing the wave pattern. Longitudinal or transverse wave cuts can be used but the transverse method is preferred because it puts less demands on the size of the free surface. The method determines the wave elevation in a number of transverse wave cuts behind the ship. The first requirement with respect to the location of the wave cuts is that the wave cuts need to be in a region where the wave pattern is relatively smooth. This means that the first wave cut cannot be too close to the stern of the ship. In Shipflow a minimum distance of 40% of the ship length is used. The second requirement is that the wave cuts cover at least one wavelength and the distribution of the wave cuts cannot be equidistant.

The wave cut method approximates the wave elevation in each wave cut by the sum of a series of elemental waves. The wave resistance is determined with the result of this approximation. A detailed description of the method can be found in [48]. The advantage of the wave cut analysis is that it is less dependent on the number of panels on the hull. This will make the wave cut method more robust than the pressure integration method for hulls with a complicated geometry (high curvature areas).

2.9 Numerical Methods in Viscous Flow Solver

Viscous Flow Solver solves the Reynolds Averaged Navier-Stokes equations with a finite volume code. Two turbulence models namely Explicit Algebraic Stress Model (EASM) and k −ω SST model are available in Shipflow [41].

In EASM the algebraic equations themselves are not very stable, however, and computer time is significantly more than with the standard and k −ω SST turbulence models. Therefore in this thesis k −ω SST turbulence models without wall functions has been used. The convective terms are discretized with a Roe scheme which is only first order accurate. Therefore in order to increase the accuracy a flux correction is applied explicitly. Two different second order schemes are applied. A MinMod limiter selects which scheme will be applied. The diffusion terms are discretized with central differences and a finite difference way with central differences. Alternating Direction Implicit (ADI) is used for solving the equations. The tri-diagonal systems are solved for the first order convective terms and the second order diffusion terms. A local artificial time-step is calculated for each ADI sweep based on CFL and von Neumann numbers in all directions except the implicit one [41].

2.9.1Determination of Free-Surface with Viscous Flow Solver

The viscous effects are very important for the stern flow around a ship. With Viscous flow solver the free-surface is modeled with Volume of Fluid (VOF) model. The VOF model is a surface-tracking technique designed for two or more immiscible fluids where the position of the interface between the fluids is of interest.

The VOF formulation relies on the fact that two or more fluids (or phases) are not interpenetrating. For each additional phase that is added to the model, a variable is introduced which is the volume fraction of the phase in the computational cell. In each control volume, the volume fractions of all phases sum to unity. The fields for all variables and properties are shared by the phases and represent volume-averaged values, as long as the volume fraction of each of the phases is known at each location. Thus the variables and properties in any given cell are either purely representative of one of the phases, or representative of a mixture of the phases, depending upon the volume fraction values. In other words, if the q^{th} fluid's volume fraction in the cell is denoted as α_q, then the following three conditions are possible:

- $\alpha_q = 0$: the cell is empty (of the q^{th} fluid)
- $\alpha_q = 1$: the cell is full (of the q^{th} fluid)
- $0 < \alpha_q < 1$: the cell contains the interface between the q^{th} fluid and one or more other fluids.

Based on the local values of α_q, the appropriate properties and variables will be assigned to each control volume within the domain.

The tracking of the interface between the phases is accomplished by the solution of a continuity equation for the volume fraction of one of the phases. For the q^{th}phase, this equation has the following form:

$$\frac{1}{\rho_q}\left[\frac{\delta}{\delta t}\left(\alpha_q\rho_q\right)+\nabla.\left(\alpha_q\rho_q\vec{v}_q\right)=S_{\alpha_q}+\sum_{p=1}^{n}\left(m_{pq}-m_{qp}\right)\right] \tag{2.58}$$

where m_{pq} is the mass transfer from phase p to phase q and m_{qp} is the mass transfer from phase q to phase p. S_{α_q} is the source term which is defined as zero.

The volume fraction equation will not be solved for the primary phase; the primary phase volume fraction will be computed based on the following constraint:

$$\sum_{q=1}^{n}\alpha_q=1 \tag{2.59}$$

2.9.2 Boundary Condition for Viscous Flow Solution

In order to solve the partial differential equations, boundary conditions are defined in the computational domain. Two layers of ghost cells are used in Viscous Flow Solver [41]. Two boundary conditions are used; Dirichlet and Neumann conditions. Boundary types employed in Viscous Flow Solver are no-slip, slip, inflow, outflow and interior as shown in Figure 2.9. Summary of the boundary conditions for computational domain is shown in Table 2.1.

No–slip boundary condition implies zero velocity components, a Neumann condition for the pressure, and a Dirichlet condition for k and ω:

$$u_i=0,\ \frac{\partial p}{\partial\xi_b}=0, \omega= f(\tau). \tag{2.60}$$

Since there are no wall-functions are used in Viscous Flow Solver, cell density near the hull and appendages should be fine enough. Therefore y+ values are to be kept smaller than one.

Slip condition simulates a symmetry condition by setting the normal velocity and normal gradient of other variables to zero as follows:

$$u_i n_i=0,\ \frac{\partial u_i}{\partial\xi_b}=0, \frac{\partial p}{\partial\xi_b}=0, \frac{\partial k}{\partial\xi_b}=0, \frac{\partial\omega}{\partial\xi_b}=0. \tag{2.61}$$

Inflow boundary condition sets a fixed uniform velocity inlet, estimated turbulent quantities (k , ω) and a zero pressure gradient normal to the inlet boundary. Which implies k , ω and the velocity is supposed to be constant whereas the pressure is extrapolated with zero-gradient.

$$u_i = const, \quad \frac{\partial p}{\partial \xi_b} = 0, k = const, \omega = const. \tag{2.62}$$

Outflow condition only consists of Neumann boundary condition that sets the gradient of velocity, k and pressure to zero, normal to the outflow plane.

$$\frac{\partial u_i}{\partial \xi_b} = 0, \; p = 0, \frac{\partial k}{\partial \xi_b} = 0, \frac{\partial \omega}{\partial \xi_b} = 0 \tag{2.63}$$

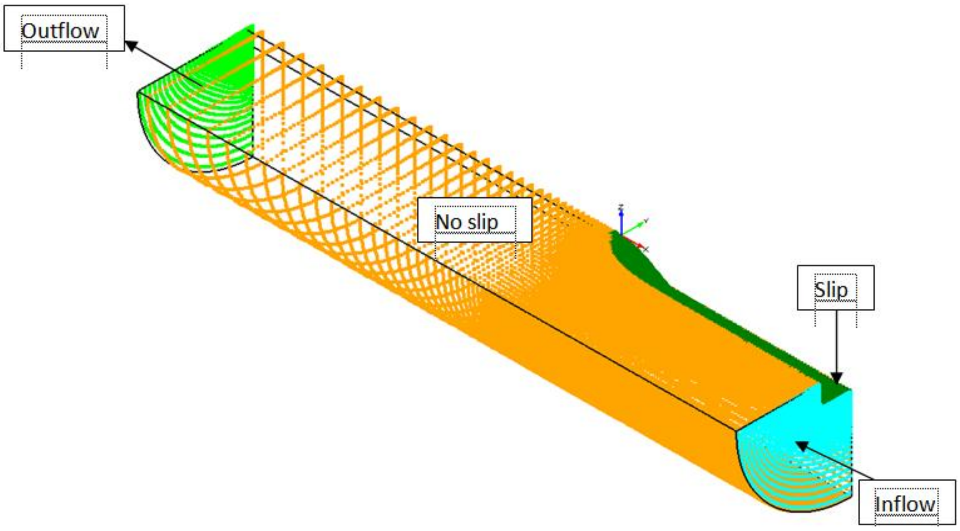

Figure 2.9: Boundary conditions for computational domain

Table 2.1: Boundary conditions for computational domain

Description	u	p	k	ω
No slip	$u_i = 0$	$\frac{\partial p}{\partial \xi_b} = 0$	$k = 0$	$\omega = f(u_\tau)$
Slip	$u_i n_i = 0$ $\frac{\partial u_i}{\partial \xi_b} = 0$	$\frac{\partial p}{\partial \xi_b} = 0$	$\frac{\partial k}{\partial \xi_b} = 0$	$\frac{\partial \omega}{\partial \xi_b} = 0$
Inflow	$u_i = const.$	$\frac{\partial p}{\partial \xi_b} = 0$	$k = const.$	$\omega = const.$
Outflow	$\frac{\partial u_i}{\partial \xi_b} = 0$	$p = 0$	$\frac{\partial k}{\partial \xi_b} = 0$	$\frac{\partial \omega}{\partial \xi_b} = 0$

2.9.3 Grid Generation

Finite volume method requires grid cells in order to discretize the partial differential equations and approximate algebraic equations. In Viscous Flow module only structured grids are used. A simple geometry such as bare hull can be represented by a single block structured grid while more complex geometries such as hull with appendixes can be expressed by the multi-block structured grid and overlapping grid. Three grid topologies used are H-H, H-O and O-O types. Figure 2.10 presents examples of grids with very coarse grid densities for clarity. Although it is possible to import grids from externally generated structured grids, all grids in this research work is created by in-house modules of grid generation.

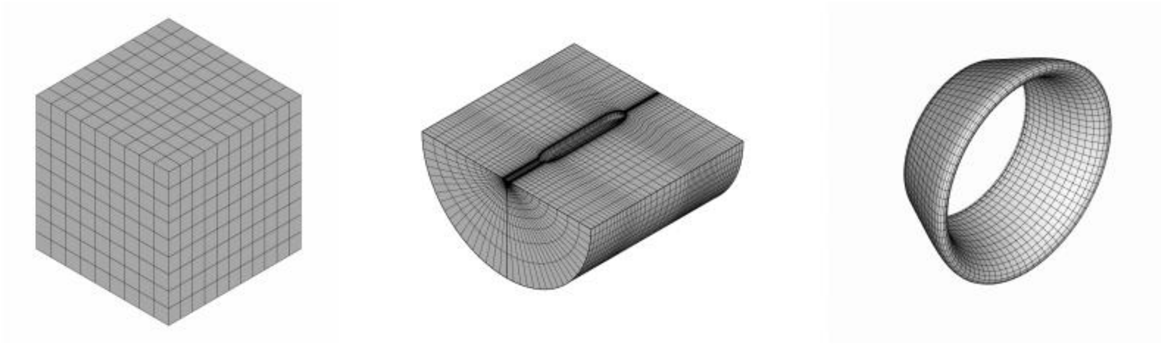

(a) H-H grid topology (b) H-O grid topology (c) O-O grid topology

Figure 2.10: Grid topologies [49]

2.9.4 Overlapping Grid

Overlapping grids were introduced to Viscous Solver in order to compute the flow around more complicated geometries (rudders, shafts, brackets, or fins) than a single block of structured grids [49]. Overlapping grid technique is powerful because it mostly offers the generality of unstructured grids while most of the advantages of structured grids is retained. One more advantage of overlapping grids is that they are not depending on the use of structured component grids even though all component grids are structured in Shipflow. It is very useful in ship hydrodynamics because it allows creating a library of readymade grids for standard shapes such as rudders, struts, fins, possibly parameterized so that they can be customized [49].

Another important application of overlapping grids is the refinements on the singleblock of structured grids. Often stern region of the ship is expected to have denser grids than other regions. In order to refine the grid only at the desired region such as stern, overlapping grids works with high accuracy and cost effective.

2.10 Propeller Simulation

An operating propeller will affect the flow by creating a sudden pressure jump across the propeller plane. Due to the pressure difference, the flow ahead of the propeller will be accelerated in both the axial and tangential directions. In Shipflow CFD code, Viscous Flow module simulates the effect of the propeller with the body force approach induced in a cylindrical component in overlapping grid [49]. The body forces are calculated with propeller design and analysis software OpenProp. OpenProp is the design and analysis tool for propellers and turbines developed by MIT. In 2012, the OpenProp project has moved from MIT to Thayer School of Engineering at Dartmouth [50].

The code is written in MATLAB M-code and the numerical model is based on moderately-loaded lifting line theory, in which a propeller blade is represented by a lifting line, with trailing vorticity aligned to the local flow velocity (i.e. the vector sum of free-stream plus induced velocity). Using a vortex lattice with helical trailing vortex filaments shed at discrete stations along the blade, induced velocities can be computed. The blade is sectioned discretely, having 2D section properties at each radius. Loads are computed by integrating the 2D sections load over the span of the blade. The velocities and forces (per unit span) on a 2D blade section can be seen in both the axial and tangential directions in Figure 2.11.

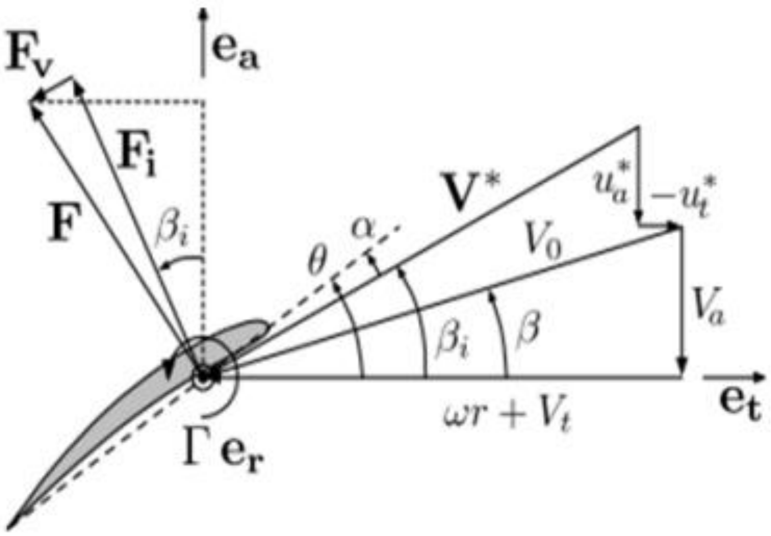

Figure 2.11: Propeller velocity/force diagram, as viewed from the tip towards the root of the blade. All velocities are relative to a stationary blade section at radius r.

Apparent tangential inflow at radius r is $-\omega r e_t$, while the propeller shaft rotates with angular velocity $-\omega e_a$. Total resultant inflow velocity, V^* and its orientation pitch angle can be computed by equation (2.64) and equation (2.65), respectively.

Total resultant inflow velocity:

$$V^* = \sqrt{\left(V_a + u_a^*\right)^2 + \left(\omega r + V_a + u_t^*\right)^2} \tag{2.64}$$

$$\beta_i = \arctan\left(\frac{V_a + u_a^*}{\omega r + V_a + u_t^*}\right) \tag{2.65}$$

where $V_a = -V_a e_a$ and $V_t = -V_t e_t$ are the axial and tangential inflow velocities, $u_a^* = -u_a^* e_a$ and $u_t^* = -u_t^* e_t$ are induced axial and tangential velocities, α is the angle of attack, $\theta = \alpha + \beta_i$ is blade pitch angle, Γe_r is circulation, $F_i = \rho V^* (\Gamma e_r)$ is Kutta-Joukowski lift force, and F_v viscous drag force aligned with V^*. Assuming the $u_t^* = -u_t^* e_t$ blades are identical, the total thrust and torque on the propeller are:

$$T = z\int_{r_h}^{R}\left(F_i \cos\beta_i - F_v \sin\beta_i\right)dr\left(\hat{e}_a\right) \tag{2.66}$$

$$Q = z\int_{r_h}^{R}\left(F_i \sin\beta_i - F_v \cos\beta_i\right)rdr\left(-\hat{e}_a\right) \tag{2.67}$$

where $F_i = \rho V^{*}\Gamma$ and $F_v = \frac{1}{2}\rho V^{*2}\left(C_D\right)c$ are the magnitude of inviscid and viscous force per unit radius, ρ is the fluid density, C_D is the section drag coefficient, c is the section chord, and r_h and R re the radius of the hub and blade tip, respectively.

The body forces calculated by Lifting Line program of OpenProp are then added to the momentum equations at the grid elements where the propeller is located. The flow passes through the cylindrical propeller grid, linear and angular momentum of the flow increase as if it passed a propeller of infinite number of blades [51]. The forces induced by body forces vary in space but are independent of time.

Rotating speed of the propeller is determined by balancing the propeller thrust and ship's resistance. Viscous flow around ship is then calculated by treating propeller forces as body force terms. The flow computation is performed iteratively until convergent results are obtained. The interaction between hull and propeller with changing position of rudder is then predicted to improve propulsive efficiency

2.11 Verification and Validation Study

Computational Fluid Dynamics has progressed rapidly in the past sixty years. It has been used in many industrial fields and plays an irreplaceable role in engineering design and scientific research. Unfortunately, inherent in the solutions from the CFD code is error or uncertainty in the results. In order for computational simulation to achieve its full potential as a predictive tool, engineers must have confidence that the simulation results are an accurate representation of reality. Verification and validation provide a framework for building confidence in computational simulation predictions.

In this thesis, the flow around ship hull considering rudder-propeller interaction has been determined using Shipflow CFD code. Verification and Validation of the results is provided according to the ITTC recommended procedures and guidelines [26].

The convergence ratio R_G is defined as:

$$R_G = \frac{\varepsilon_{21}}{\varepsilon_{32}} \tag{2.68}$$

Where $\varepsilon_{k21} = S_2 - S_1$ $\varepsilon_{k32} = S_3 - S_2$ give the change of solutions between the medium-fine and coarse-medium grids. Three convergence conditions are possible:

i. Convergence condition: $0 < R_G < 1$

ii. Oscillatory condition: $R_G < 0$

iii. Diverging condition: $R_G > 0$

According to the ITTC procedure, the Richardson extrapolation can be used to compute the error for the fine grid.

$$\delta^*_{R_G} = \frac{\varepsilon_{21}}{r_G^{P_G} - 1} \tag{2.69}$$

Where P_G is the estimated order of accuracy which can be computed as:

$$P_G = \frac{\ln(\frac{\varepsilon_{32}}{\varepsilon_{21}})}{\ln r_G} \tag{2.70}$$

According to the ITTC recommended procedures a correction factor C_G should be used for estimating the error and the uncertainty of the finest grid solution.

$$C_G = \frac{r_G^{P_G} - 1}{r_G^{P_{Gest}} - 1} \tag{2.71}$$

Where $P_{Gest} = P_{th} = 2$

For C_G considered as sufficiently less than or great than 1 and lacking of confidence, the uncertainty is estimated as:

$$U_G = \left|C_G \delta^*_{R_G}\right| + \left|(1 - C_G)\delta^*_{R_G}\right| \tag{2.72}$$

For C_G considered as close to 1 and having confidence both $\delta^*_{R_G}$ and U_{GC} are estimated as:

$$\delta^*_G = C_G \delta^*_{R_G} \tag{2.73}$$

$$U_{GC} = \left|(1 - C_G)\delta^*_{RE_G}\right| \tag{2.74}$$

The corrected solution is defined as:

$$S_C = S_G - \delta^*_G \tag{2.75}$$

Simulation certainty defined as: $U_{SN} = \sqrt{U_G^2 - U_I^2}$ (2.76)

Validation certainty defined as: $U_V = \sqrt{U_{SN}^2 - U_D^2}$ (2.77)

Chapter 3

Geometry and Condition

The geometry of the MOERI Container Ship- KCS and propeller KP 505 are obtained from Simman 2008 Workshop, Copenhagen [52]. The geometry of Japan Bulk Carrier, JBC is designed jointly by National Maritime Research Institute (NMRI), Yokohama National University and Ship Building Research Centre of Japan (SRC) [32].

3.1 Description of Hull

Two modern benchmark ship hull namely KCS (Kriso Container Ship) and JBC (Japan Bulk Carrier) shown in Figure3.1, are used for CFD validation. The principal particulars in full and model scale are described in Table 3.1.

a) KCS

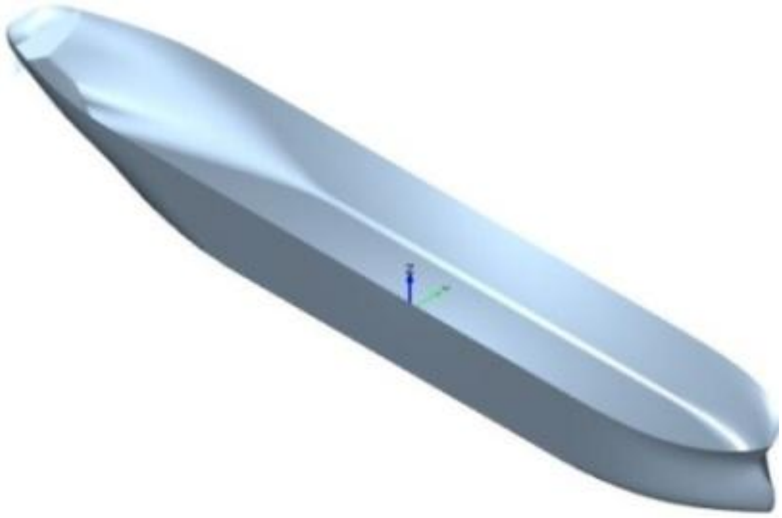

b) JBC

Figure 3.1: Description of hull: a) KCS; b) JBC

Table 3.1: Principal particulars for KCS and JBC hull.

Hull type	KCS		JBC	
Main particulars	Full scale	Model scale	Full scale	Model scale
Length between perpendiculars (m)	230.0	7.279	280.0	7.0
Maximum beam of waterline (m)	32.2	1.0190	45.0	0.561
Depth (m)	19.0	0.6019	25.0	0.630
Draft (m)	10.8	0.342	16.5	0.423
Block coefficient (C_B)	0.651	0.651	0.859	0.858

3.1.1 Hull Offset Generation in Shipflow

Hull offset file is generated as an input file for Shipflow CFD analysis. In Shipflow, hull offset is divided into four different groups for main hull, stern, bulb and boss designated by H1GR, OGRP, FBGR and ABGR respectively as shown in Figure 3.2.

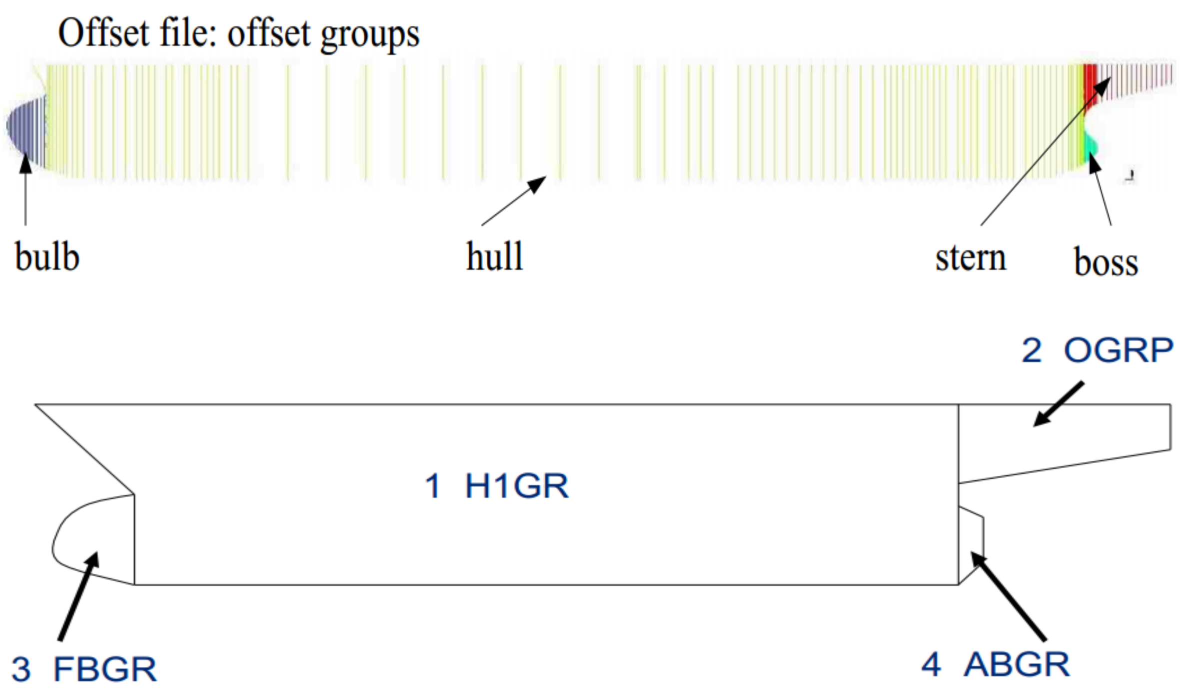

Figure 3.2: Offset file of shiphull in Shipflow

3.2 Description of Propeller

3.2.1 KP 505 Propeller

For KCS hull propeller openwater and self-propulsion characteristics are determined for KP 505 marine propeller as shown in Figure 3.3.

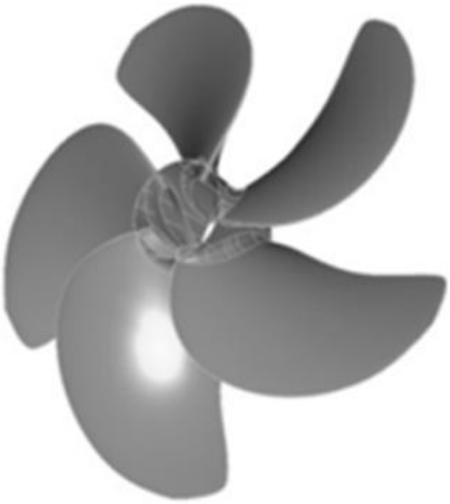

Figure 3.3: KP 505 propeller

Detail description of propeller blades main particulars and section geometry are shown in Table 3.2 and Table 3.3 respectively.

Table 3.2: KP 505 propeller blade main particulars

Number of Blade	5
Section Profile	NACA66 Thickness form + a=0.8 mean line Camber
Propeller Diameter	7.9m (Model: 250mm)
Hub Ratio	0.180
Blade Area Ratio	0.80

Table 3.3: KP 505 propeller blade section geometry

r/R	P/D	Rake	Skew	C/D	fo/C	to/D
0.18	0.834700	0.0	-4.720	0.231300	0.028448	0.045850
0.25	0.891200	0.0	-6.980	0.261800	0.029641	0.040710
0.30	0.926900	0.0	-7.820	0.280900	0.029477	0.037120
0.40	0.978300	0.0	-7.740	0.313800	0.026769	0.030470
0.50	1.007900	0.0	-5.560	0.340300	0.022010	0.024590
0.60	1.013000	0.0	-1.500	0.357300	0.017324	0.019470
0.70	0.996700	0.0	4.110	0.359000	0.014039	0.014920
0.80	0.956600	0.0	10.480	0.337600	0.011996	0.010730
0.90	0.900600	0.0	17.170	0.279700	0.010440	0.006930
0.95	0.868300	0.0	20.630	0.222500	0.010067	0.005280
1.00	0.833100	0.0	24.180	0.000100	0.000000	0.003690

3.2.2 DTMB 4119 Propeller

For JBC hull propeller open water test and self-propulsion tests are performed using DTMB 4119marine propeller as shown in Figure 3.4. Detail description of propeller blades main particulars and section geometry is shown in Table 3.4 and Table 3.5.

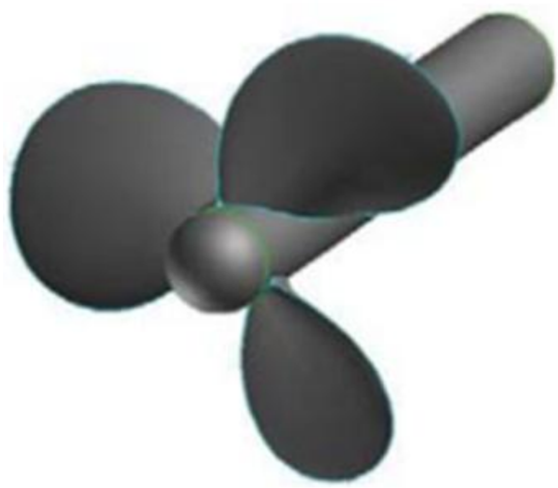

Figure 3.4: DTMB 4119propeller

Table 3.4: DTMB 4119 propeller blade main particulars

Number of Blade	3
Section Profile	NACA66 Thickness form + a=0.8 mean line Camber
Propeller Diameter	0.3048 m
Hub Ratio	0.26
Blade Area Ratio	0.66

Table 3.5: DTMB 4119 propeller blade section geometry

r/R	P/D	Rake	C/D	fo/C	to/D
0.20	1.1050	0.0	0.3200	0.01429	0.20550
0.30	1.1020	0.0	0.0	0.02318	0.15530
0.40	1.0980	0.0	0.4048	0.02303	0.11800
0.50	1.0930	0.0	0.4392	0.02182	0.09160
0.60	1.0880	0.0	0.4610	0.02072	0.06960
0.70	1.0840	0.0	0.4622	0.02003	0.05418
0.80	1.0810	0.0	0.4347	0.01967	0.04206
0.90	1.0790	0.0	0.3613	0.01817	0.03321
0.95	1.0770	0.0	0.2775	0.01631	0.03228
1.00	1.0750	0.0	0.0000	0.01175	0.03160

3.3 Description of Rudder

To determine the effect of varying rudder position on self-propulsion characteristics of propeller semi balanced horn rudder is used for both ships. Shipflow has the ability to model the rudder geometry by writing a specific command by which the rudder geometry data is imported into the computations. The geometry definition of the rudder which are given as an input file of Shipflow is shown in Figure 3.5.

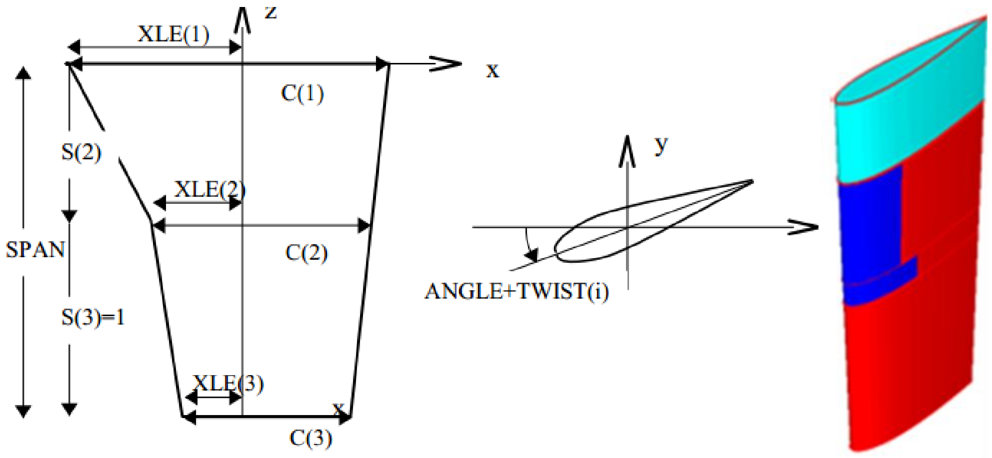

Figure 3.5: Geometry definition of semi balanced horn rudder

Detail description of semi balanced horn rudder's dimension is shown in Table 3.6.

Table 3.6: Semi balanced horn type rudder dimension

Particulars	Value
Span	0.36 m
Angle	0 degree
Origin (x, y, z)	(0,0,0.36)
XLE(1)	0.080
XLE(2)	0.060
XLE(3)	0.040
C(1)	0.260
C(2)	0.188
C(3)	0.135
S(1)	0.000
S(2)	0.500
S(3)	1.000

3.4 Various Longitudinal Positions of Rudder from Propeller

To determine self propulsive characteristics at varying longitudinal rudder positions different longitudinal distances of rudder (b) to propeller diameter (D) are taken. Definition sketch of different b/D ratio for KCS and JBC hulls are shown in Figures. 3.6 and 3.7 respectively.

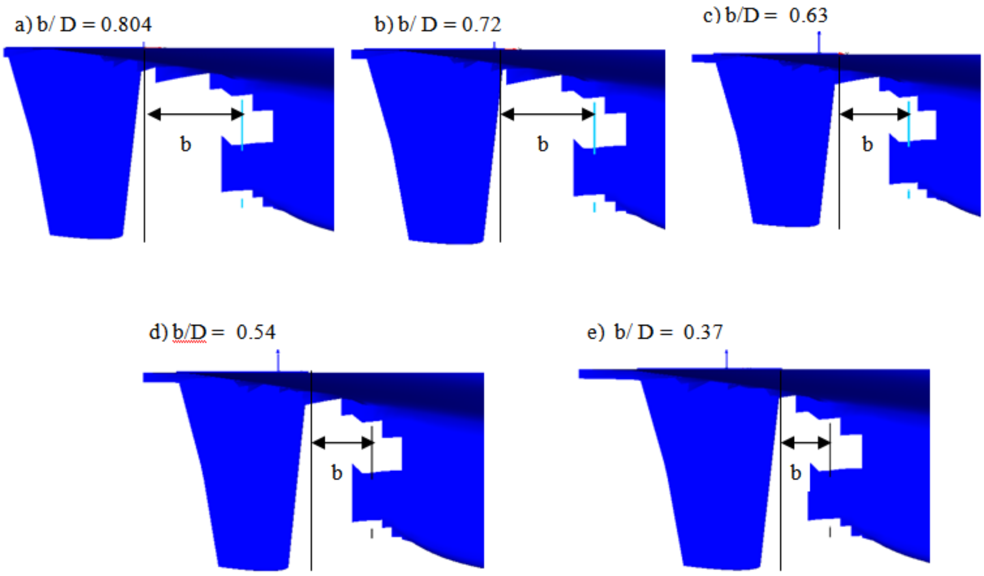

Figure 3.6: Definition sketch of different b/D ratio for KCS hull

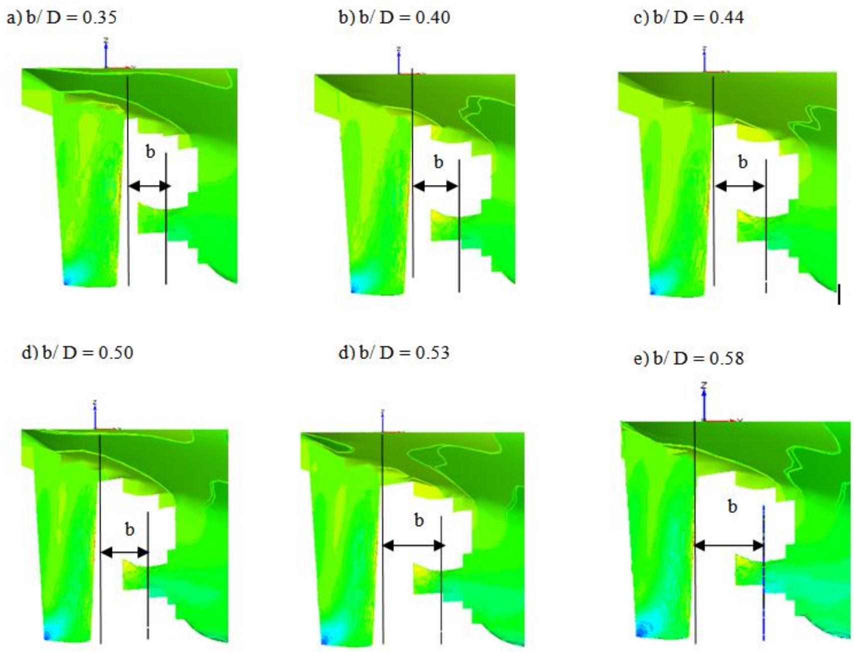

Figure 3.7: Definition sketch of different b/D ratio for JBC hull

Self-propulsion test has been performed with Shipflow for calculating the propeller characteristics with hull-propeller interaction. The reason for applying self-propulsion test is to adjust the J value to achieve the balance between thrust and drag. The wave drag which is computed by ‘Potential Flow solver’ is included in total drag. As zonal approach is used for computing flow around the ship hull with propeller and rudder, frictional drag is computed by ‘Thin Boundary Layer solver’ for the fore body is also added to the total drag. The external tow force then is subtracted from the drag. The towing force is computed according to the ITTC 78 procedure. CWTO which is the towing force coefficient is calculated by Equation (3.1) and imported as an input data into computation.

$$CWTO = CF_m - (CF_s + dCF_s) \tag{3.1}$$

$$CF_s = \frac{0.075}{\left(\log R_{nL} - 2\right)^2} \tag{3.2}$$

$$CF_m = \frac{0.075}{\left(\log R_{nL} - 2\right)^2} \tag{3.3}$$

where CF_m and CF_s are the ITTC57 friction drag coefficients for model and ship respectively and dCF_s is a correction depending on the surface condition of the ship, which normally is dCF_s = 0.0004 [53].

Chapter 4

Results and Discussions

In this chapter, the results of the thesis work are discussed. First, the results of the potential flow solution have been presented. After discritizing the inviscid region with flat quadrilateral panels, pressure coefficient on hulls, free-surface wave pattern and wave elevation have been obtained as the outcome of potential flow solution. Wave cuts are obtained at different transverse locations using viscous flow solver by capturing the free-surface with VOF method.

RANS is used at the stern region where the viscosity effect is significant. Different types of grids are generated around bare hull, rudder and propeller. Grid convergency with verification and validation study has been performed and is presented here. Propeller open water performance curves are obtained through Lifting Line program and coupled with RANSE solver to determine self-propulsion characteristics at varying rudder positions. A comparison between zonal and global approach has been shown to outline the efficiency of the present approach.

4.1 Panel Mesh Generation for Potential Flow Solver

The non-linear free-surface potential flow problem is solved by discretizing the hull and the free-surface by flat quadrilateral panels with constant source strength as shown in Figure 4.1. This means that the only unknown parameter for each panel is the source strength. An equation corresponding to the boundary condition is applied to one point on each panel, which gives N points with N equations and N unknown source strengths. Solving this system of equations velocity at every point in the flow is calculated to get the potential flow around the hull.

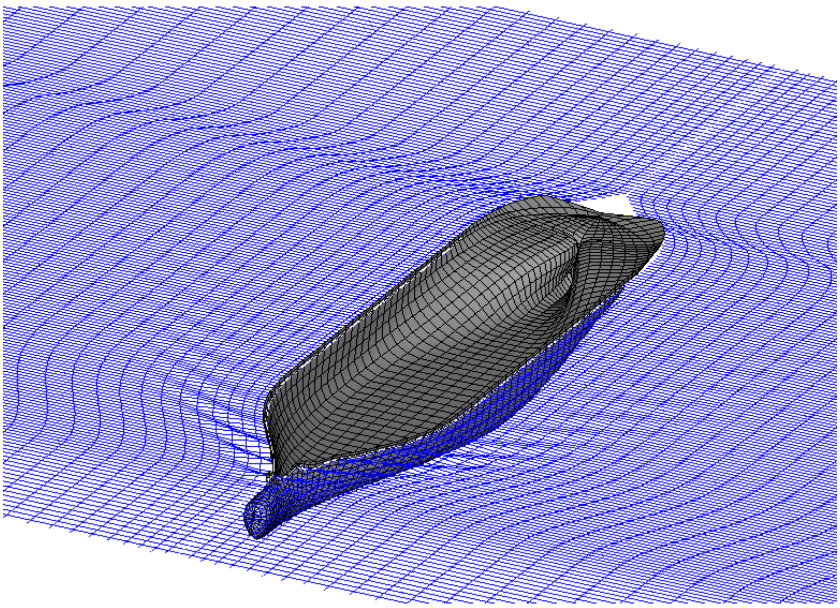

a) KCS

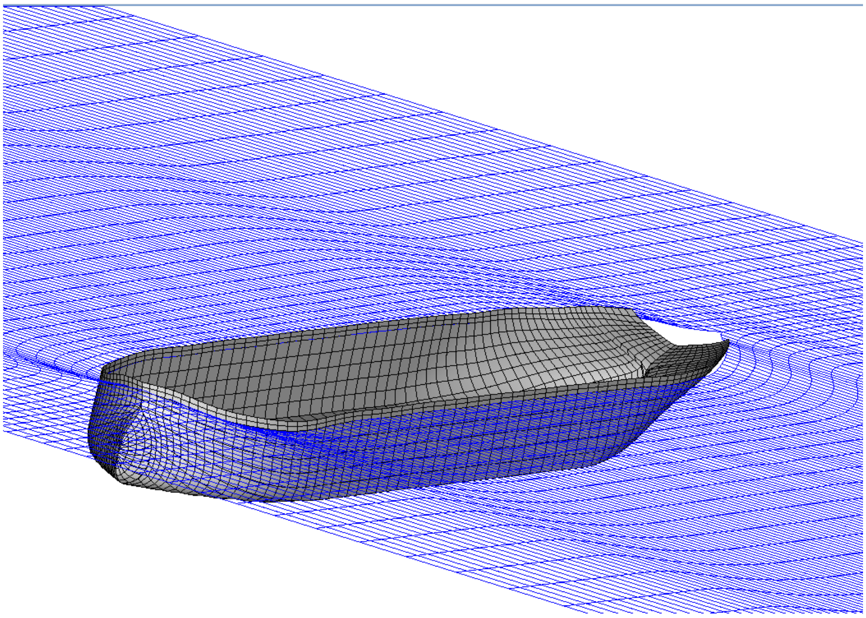

b) JBC

Figure 4.1: Discretization of hulls and free-surface for potential flow solution: a) KCS; b) JBC

4.2 Grid Generation at Transom Stern for KCS Hull

When free-surface has been captured with viscous flow solver with VOF method, additional grid along the transom stern of KCS hull needs to be created as shown in Figure 4.2. This additional structured grid at the stern helps to capture wet transom stern effect for free-surface.

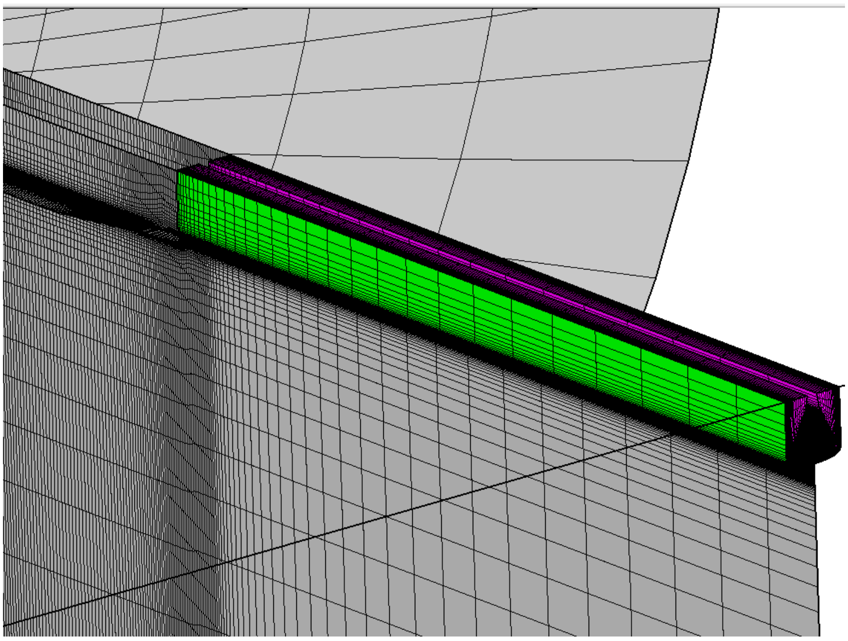

Figure 4.2: Additional grid at transom stern of KCS hull

4.3 Pressure Coefficient on Ship Hull

Pressure coefficient on KCS and JBC hull is obtained from potential flow solution by integrating pressure on hull surface. Figure 4.3 shows pressure coefficient on KCS and JBC hull at Fn. 0.316 and 0.142 respectively. Both hulls show that maximum pressure occurs at the bow of the ship where the velocity is minimum.

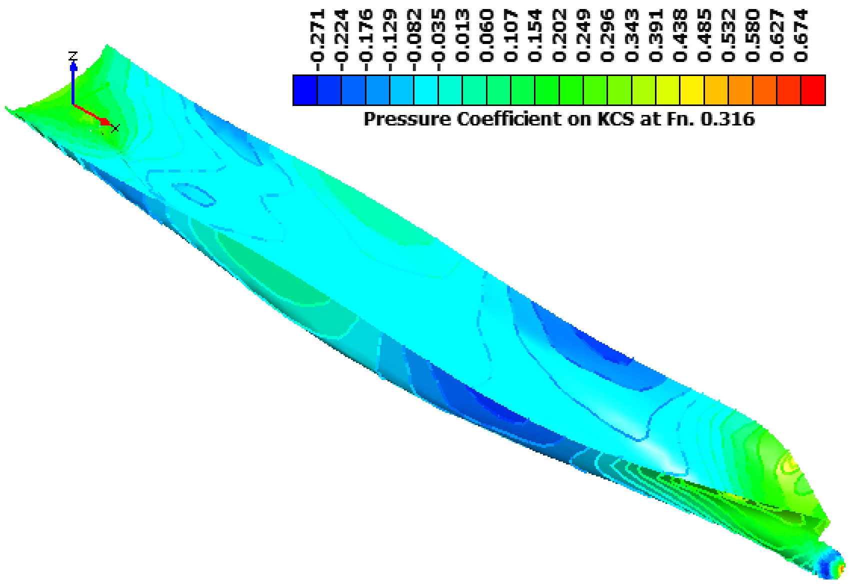

a) KCS

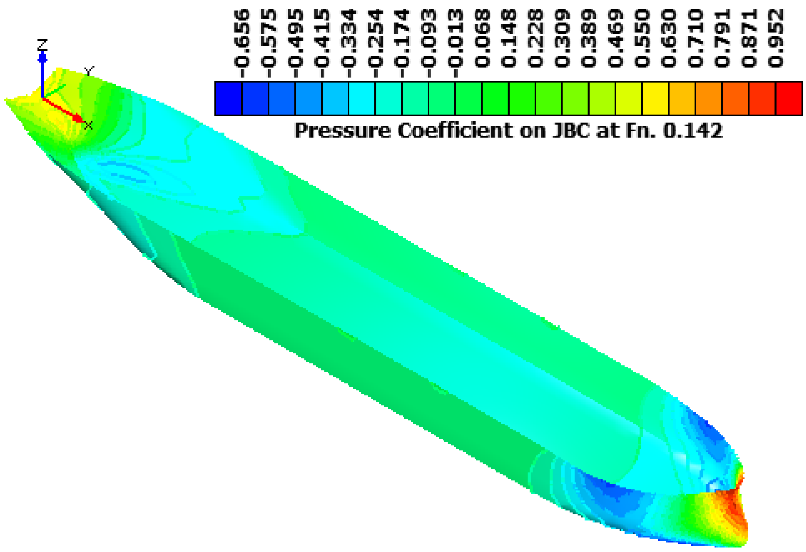

b) JBC

Figure 4.3: Pressure coefficient on ship hull: a) KCS; b) JBC

4.4 Free-Surface Wave Pattern

4.4.1 Potential Flow Solver for KCS Bare Hull

Free-surface wave pattern around KCS at Fn. 0.26 is computed from potential flow solver using 3D Rankine source panel method and compared with the measured results from experiment [55].

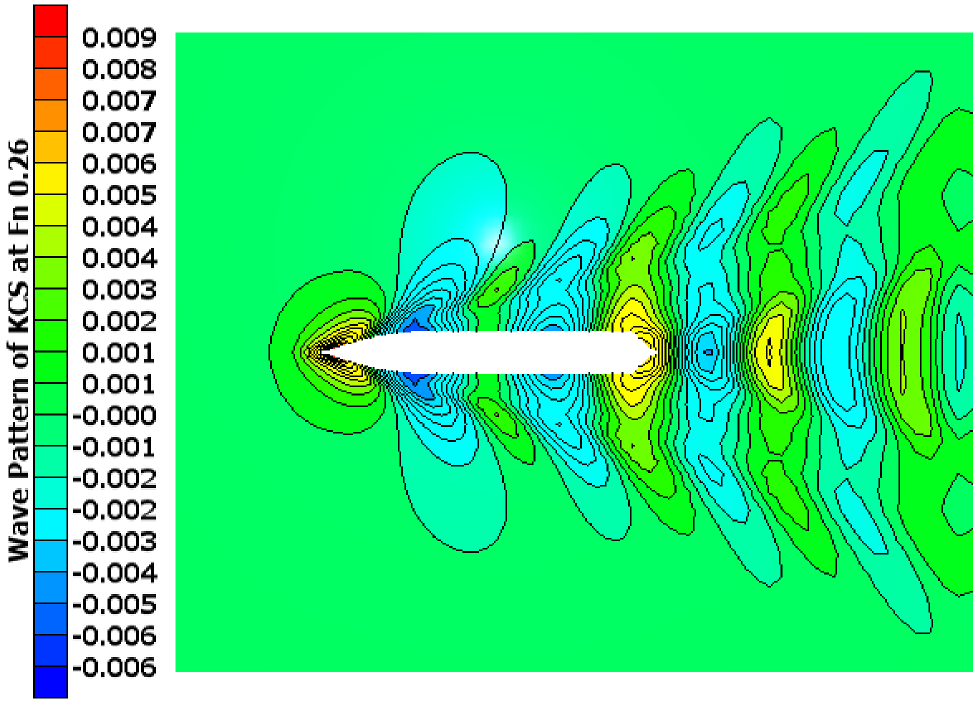

a) Computed

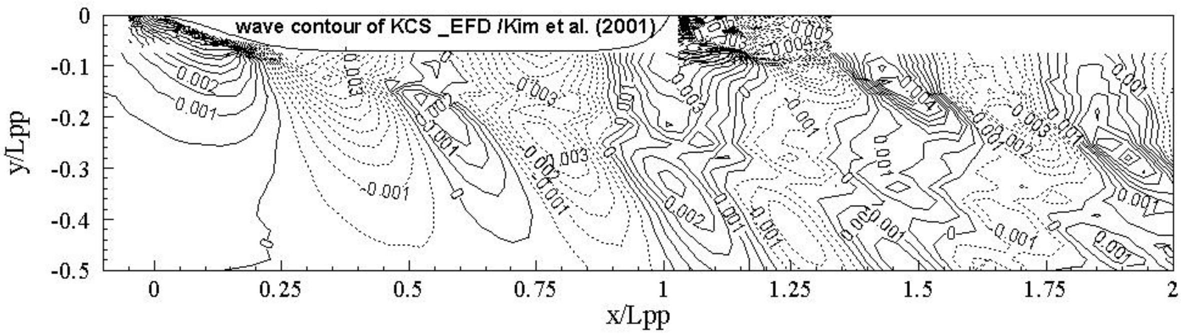

b) Measured [55]

Figure 4.4: Wave pattern around KCS hull at Fn.0.26 a) Computed result;
b) Measured result [55]

From Figure 4.4 it is apparent that both computed and measured wave pattern consist of a series of divergent and transverse waves maintaining a constant Kelvin angle of $19^{\circ}28'$ with the line of motion. However, at the stern region, some discrepancies are observed between the computational and experimental results. At the stern region, the viscosity effect is significant and also the presence of wet transom stern can make the wave pattern from potential flow solver to deviate from the experimental wave pattern. Therefore, in the next section the results of the computed free-surface wave pattern obtained from viscous flow solver is described.

4.4.2 Viscous Flow Solver for KCS Bare Hull and Hull with Rudder and Propeller

When Global approach is applied, Viscous/ RANS solver is used throughout the whole domain considering rudder-propeller interaction. With Global approach only the results can be obtained with very coarse or coarse grids. Here viscous free-surface with VOF method has been applied with coarse grid for bare hull and very coarse grid for hull considering rudder-propeller interaction as shown in Figures 4.5 and 4.6 respectively.

From Figures 4.5 and 4.6 it is found that viscous free-surface for both bare hull and hull with rudder and propeller show some change in wave pattern. But, the wave pattern does not show any contour at the far way of the ship stern which may be due to very coarse grids of the domain. As the Global approach of Shipflow only provides result for coarse grids due to limitation of computational resources, this approach cannot be used to predict the wave pattern accurately.

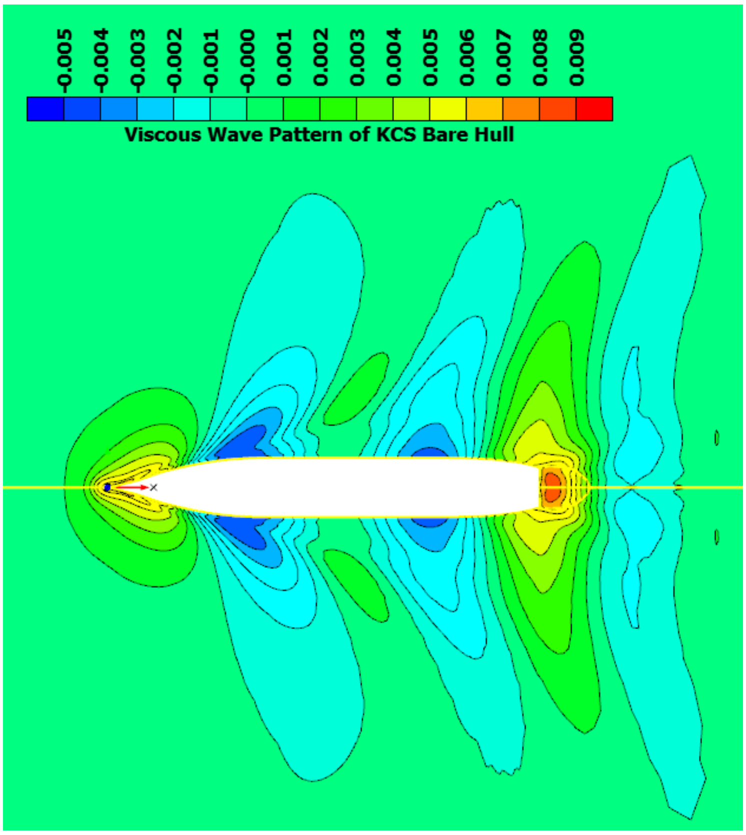

Figure 4.5: Viscous wave pattern around KCS hull at Fn.0.26

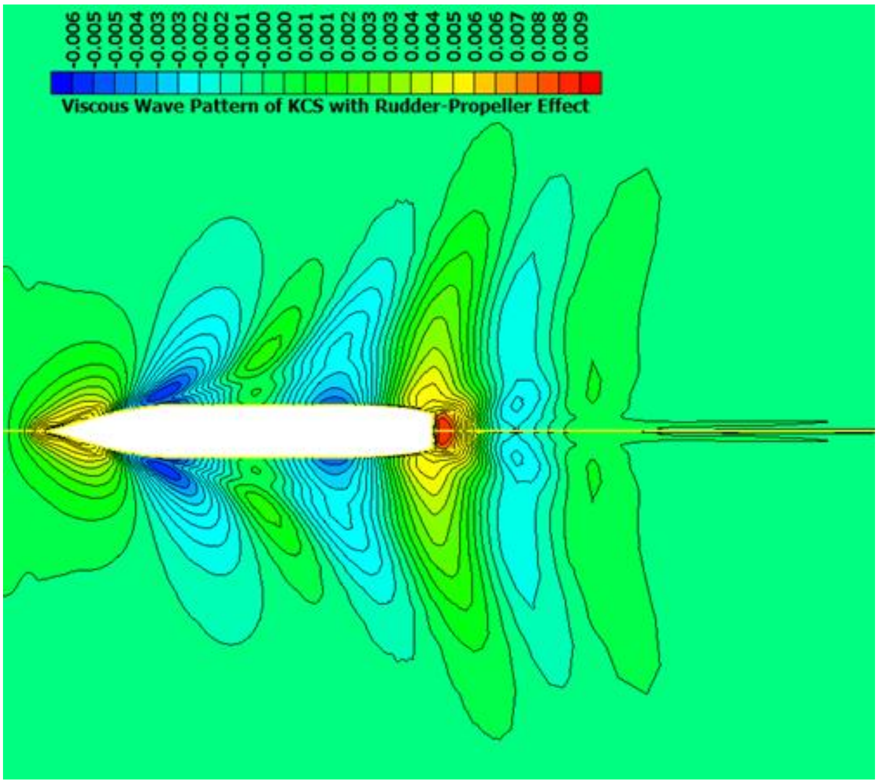

Figure 4.6:Viscous wave pattern around KCS hull with propeller-rudder effect at Fn.0.26

4.4.3 Potential Flow Solver for JBC Bare Hull

Computed wave pattern at Fn. 0.142 around JBC hull starboard side shows good agreement with the experimental wave pattern [23] as shown in Figure 4.7.

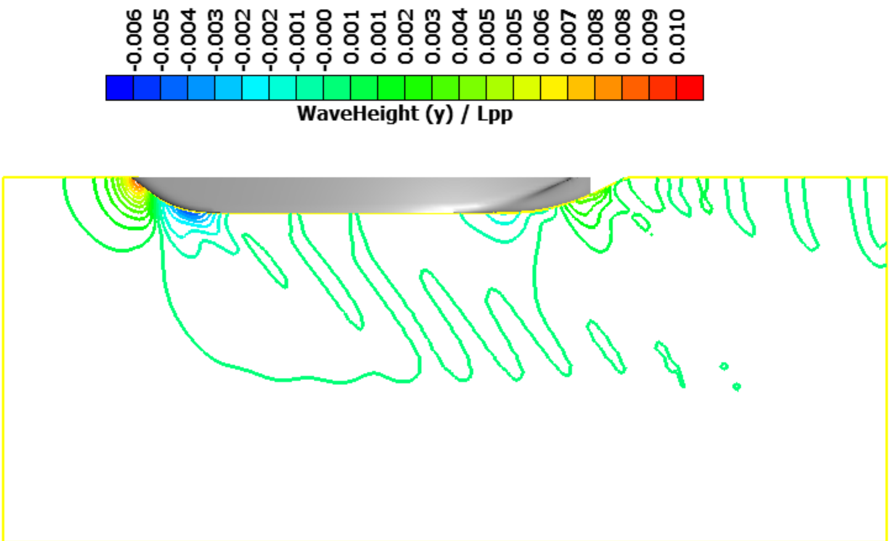

a) Computed

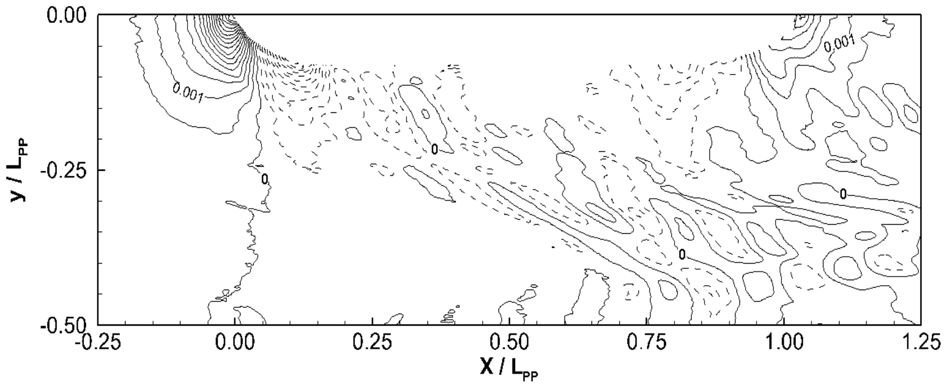

b) Measured [23]

Figure 4.7: Wave pattern around JBC hull at Fn.0.142: a) Computed; b) Measured result [23]

4.4.4 Viscous Flow Solver for JBC Bare Hull and Hull with Rudder and Propeller

When Global approach is applied, Viscous/ RANS solver is used throughout the whole domain considering rudder propeller interaction. As with Global approach only the results can be obtained with very coarse or coarse grids due to limitation of computational resources, here viscous free-surface with VOF method has been applied with coarse grid for bare hull and very coarse grid for hull considering rudder-propeller interaction as shown in Figures 4.8 and 4.9 respectively.

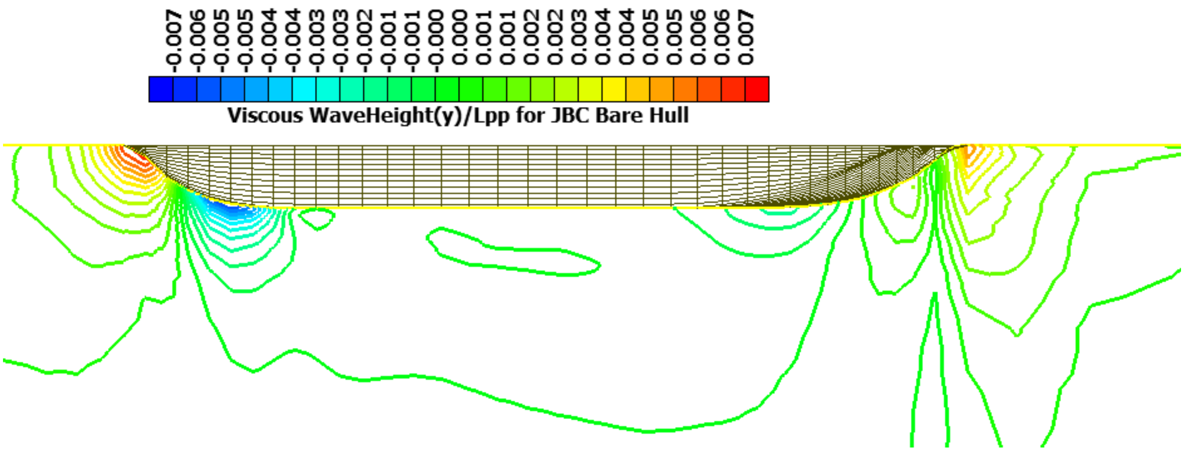

Figure 4.8: Viscous wave pattern around JBC hull at Fn. 0.142

From Figures 4.8 and 4.9, it is found that viscous free-surface for both bare hull and hull with rudder and propeller show some change in wave pattern. The maximum value of wave height/length ratio has been obtained at the bow and stern of the ship. Similarly for the JBC hull, as Global approach of Shipflow only provides result for coarse grids due to limitation of computational resources, this approach cannot be used to predict the wave pattern accurately.

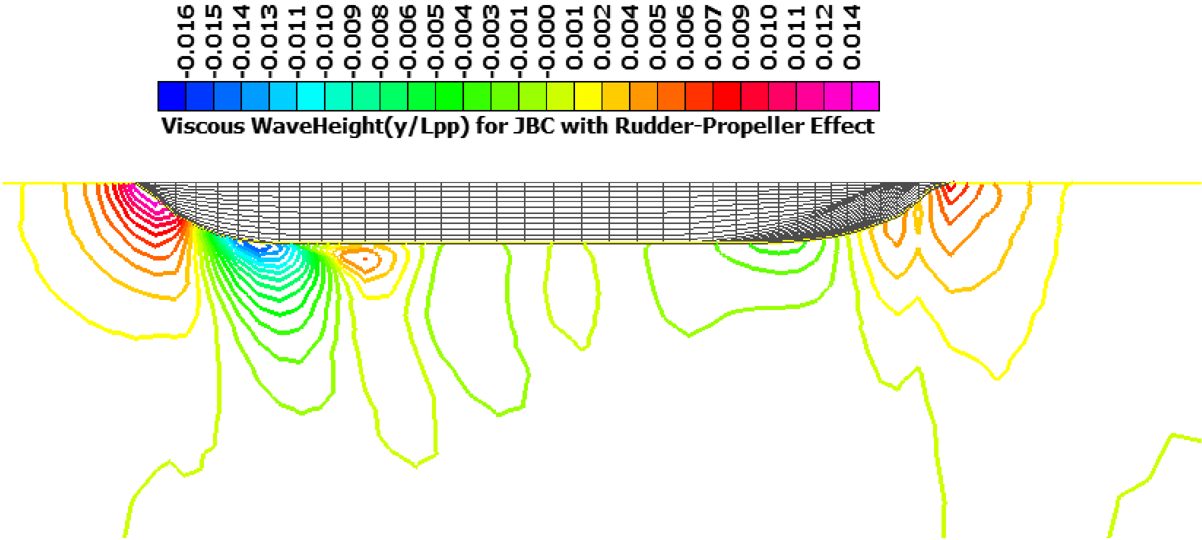

Figure 4.9: Viscous wave pattern around JBC hull with propeller-rudder effect at Fn.0.142

4.5 Free-Surface Wave Elevations

4.5.1 Wave Elevation along KCS Hull at Fn. 0.26

The computed free-surface wave elevations from potential flow solver around KCS hull at Fn. 0.26 are shown in Figures 4.10. Here the computed result is also compared with experimental results [55].

From Figure 4.10, it is found that computed wave elevation along ship hull show good agreement with experimental results. Some discrepancies between computed and experimental wave height are found at the wake region of the KCS hull as the computed results obtained from potential flow solution without considering viscosity effect.

Wave cuts are obtained as the intersection of the wave pattern with different planes. In Figure 4.11 transverse wave cuts with planes separated from the center plane to the portside distances of y = - 0.1, - 0.2 and - 0.3 are shown respectively at Fn. 0.26.

Figure 4.11 shows transverse wave cuts for bare hull condition for KCS hull. It is obvious that as the wave cuts move further away from the ship hull the magnitude of wave height decreases. The maximum wave height/length (z/Lpp) occurs at transverse plane y = - 0.1 which is the closest transverse cutting plane at the portside whereas the minimum wave height/length (z/Lpp) occurs at transverse plane y = - 0.3 which is the furthest transverse cutting plane also at the portside.

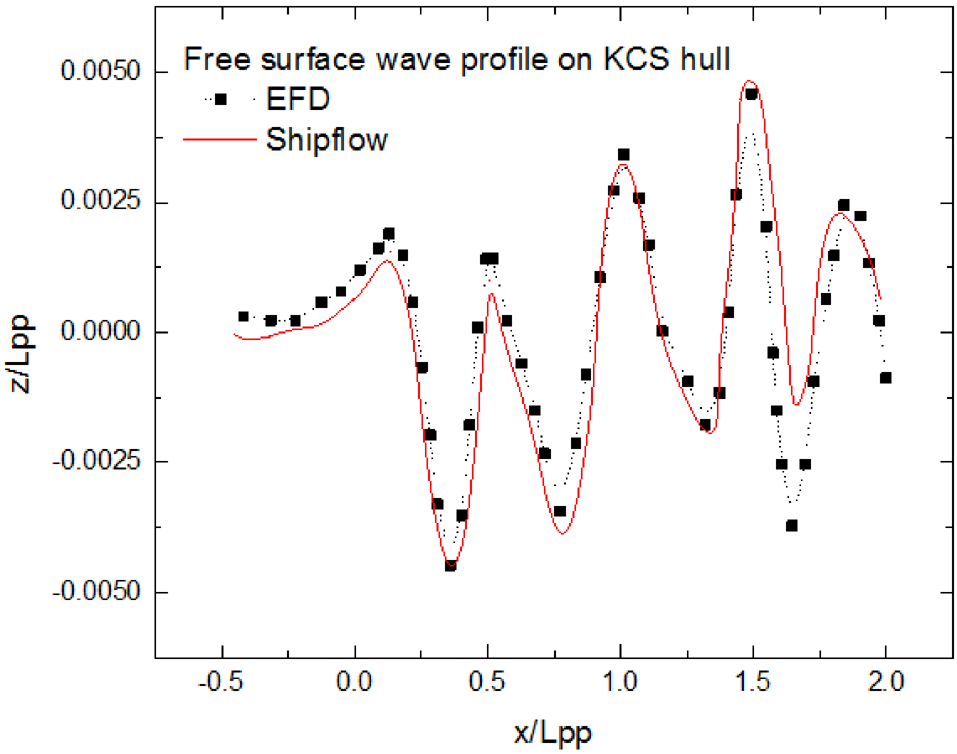

Figure 4.10: Free-surface wave elevations around KCS hull from potential flow solution

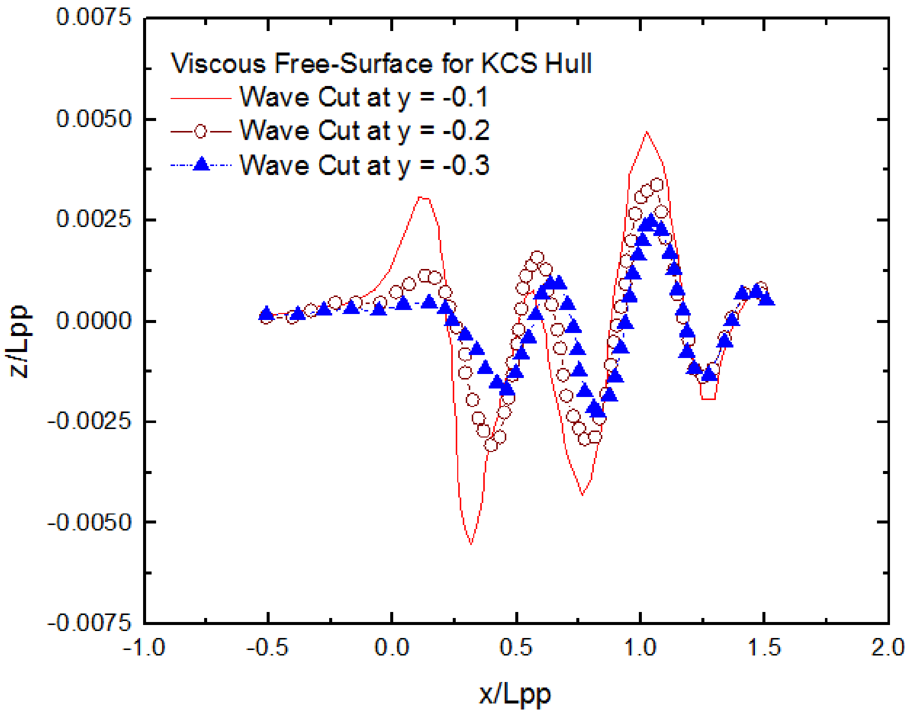

Figure 4.11: Transverse wave cuts for KCS hull at Fn.0.26

At Fn. 0.26, the comparison of different wave cuts between bare hull and hull with rudder-propeller effect is shown fromFigures 4.12-4.14.

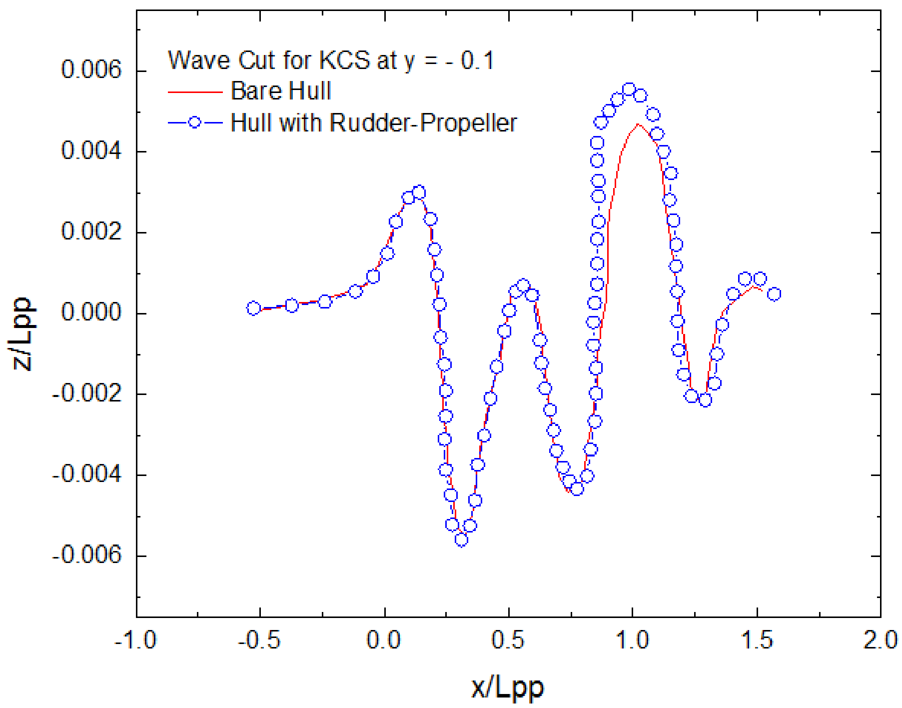

Figure 4.12: Comparison between transverse wave cuts for KCS Hull at y = - 0.1

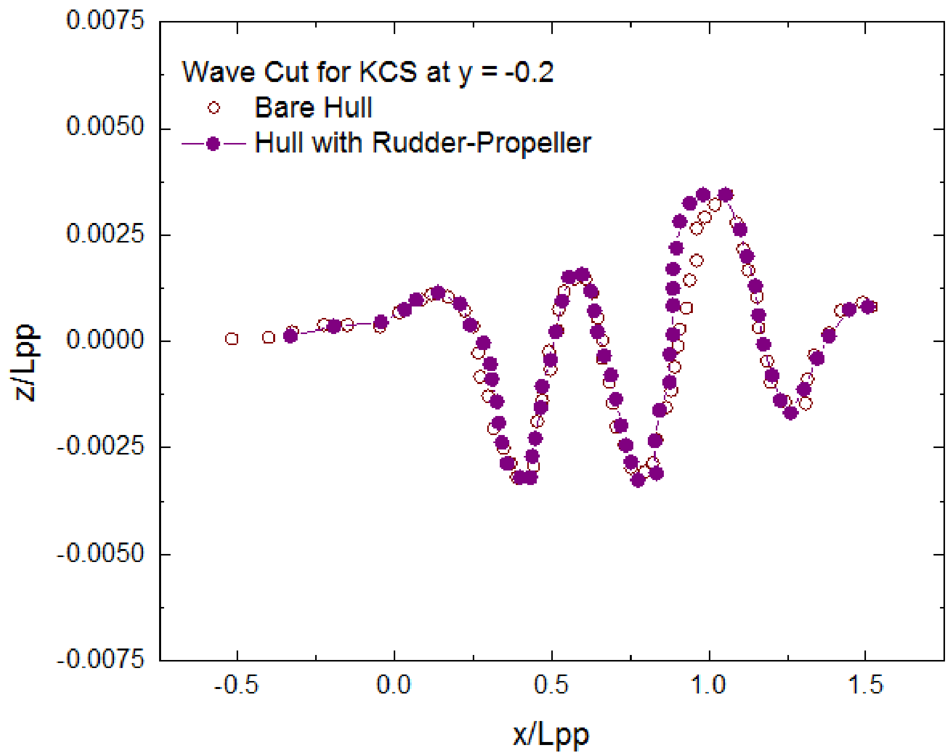

Figure 4.13: Comparison between transverse wave cuts for KCS hull at y = - 0.2

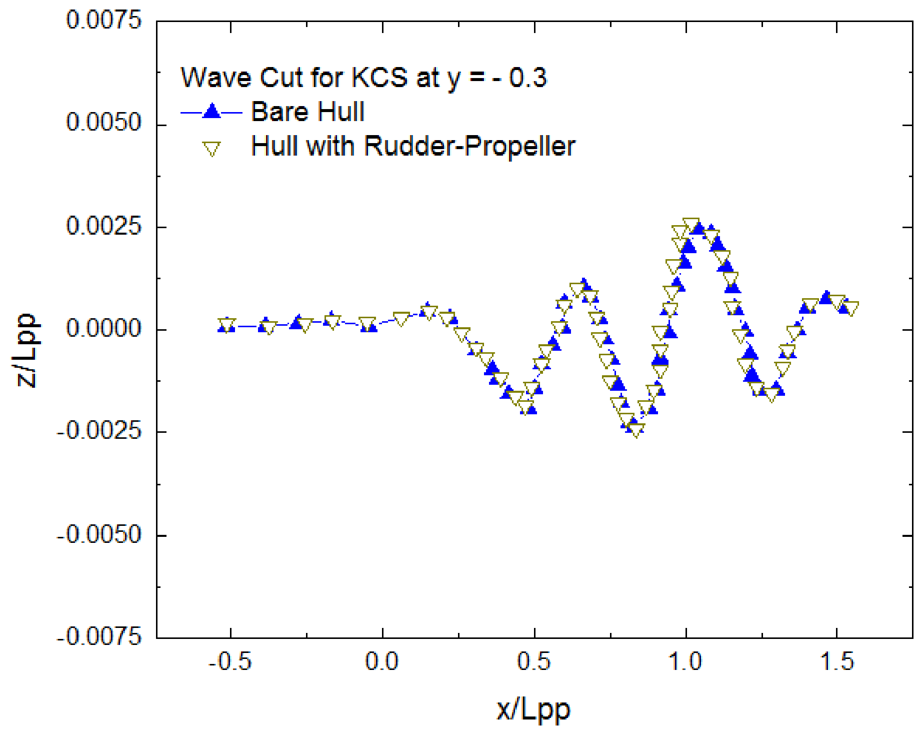

Figure 4.14: Comparison between transverse wave cuts for KCS hull at y = - 0.3

From Figures 4.12-4.14, it is observed that the value of the wave height remains same for bare hull and hull with rudder-propeller condition until the location of propeller plane. At the propeller plane which is at x = 0.9747, a sudden increase of wave height occurs. The maximum increase in wave height occurs when the wave cut is very close to hull, i.e., y = - 0.1 as shown in Figure 4.12. At the propeller plane a sudden acceleration of flow occurs which may lead to the increase of wave height at this location due to hull-propeller-rudder interaction.

4.5.2 Free-Surface along JBC Hull at Fn.0.142

The computed free-surface wave elevations from both potential flow and viscous flow solvers around JBC hull at Fn. 0.142 are shown in Figures 4.15 and 4.16 respectively. A comparison between computed potential flow and experimental results [23] is also shown in Figures 4.15. It is observed that the computed wave elevation show good agreement with experimental results along the JBC hull.

Wave cuts are obtained as the intersection of the wave pattern with different planes. In Figure 4.16, transverse wave cuts with planes separated from the center plane to the portside distances of y = - 0.1, - 0.2 and - 0.3 for JBC hull are shown respectively at Fn. 0.142. It is apparent that as the wave cuts move further away from the ship hull the magnitude of wave height decreases. The maximum wave height/length (z/Lpp) occurs at transverse plane y = - 0.1 which is the closest transverse cutting plane at the portside whereas the minimum wave height/length (z/Lpp) occurs at transverse plane y = - 0.3 which is the furthest transverse cutting plane also at the portside.

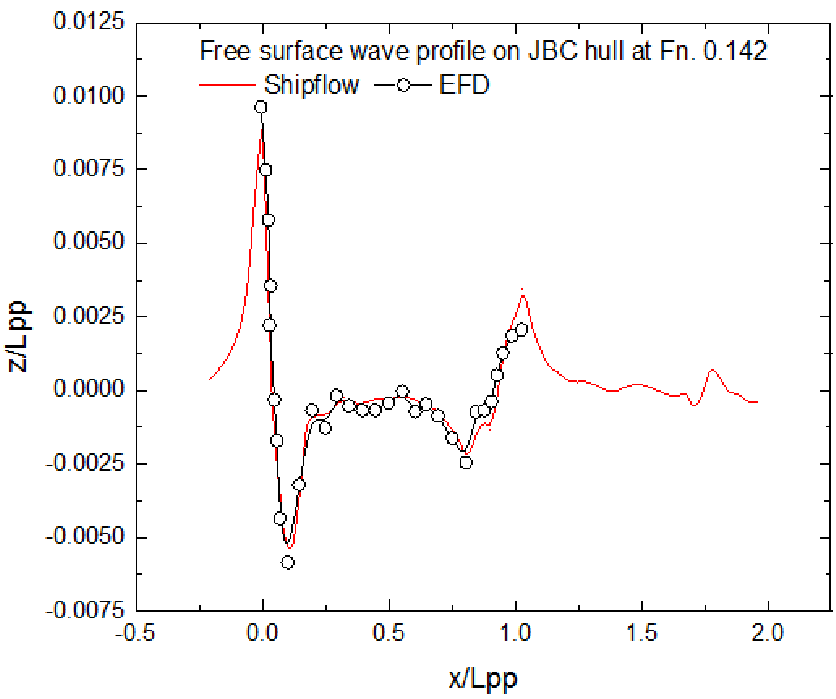

Figure 4.15: Free-surface wave elevations around JBC hull from potential flow solution

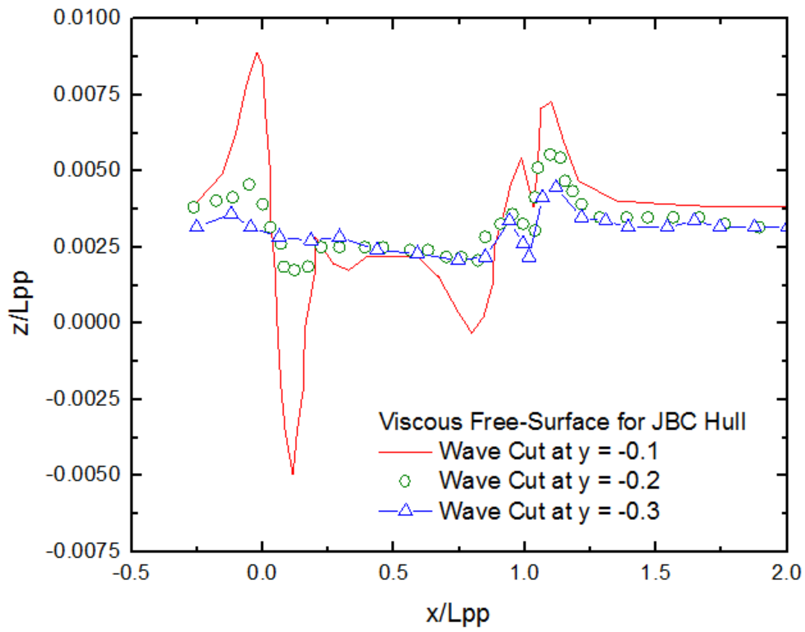

Figure 4.16: Transverse wave cuts for JBC hull at Fn.0.142

At Fn. = 0.142, the comparison of different wave cuts between bare hull and hull with rudder-propeller effect is shown from Figures 4.17-4.19 which show that the value of the wave height remains same for bare hull and hull with rudder-propeller condition until the location of propeller plane. At the propeller plane which is at x = 0.9747, a sudden increase in wave height occurs due to acceleration of flow by propeller. The maximum increase in wave height occurs when the wave cut is very close to hull i.e. y = - 0.1 as shown in Figure 4.17.

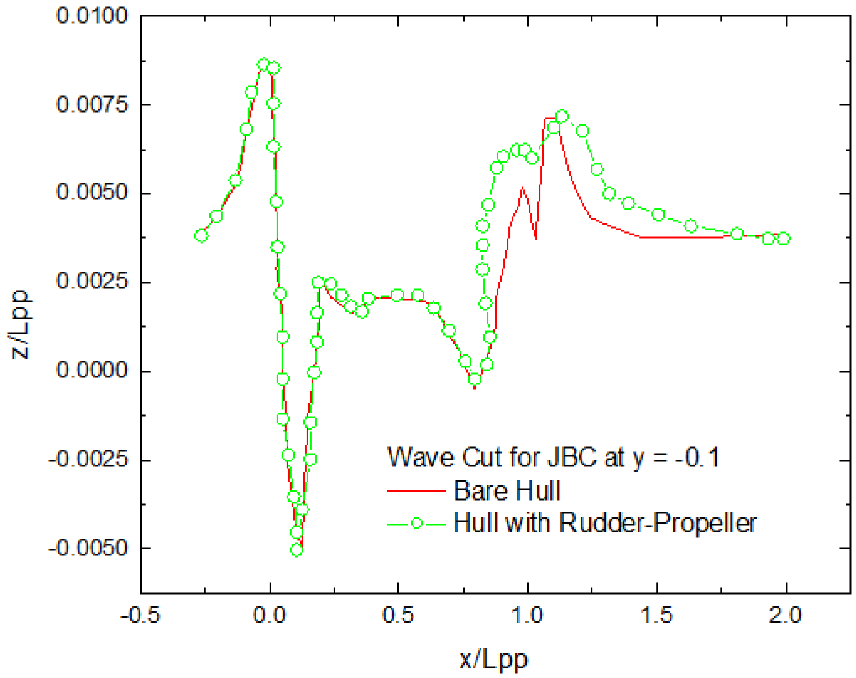

Figure 4.17: Comparison between transverse wave cuts for JBC hull at y = - 0.1

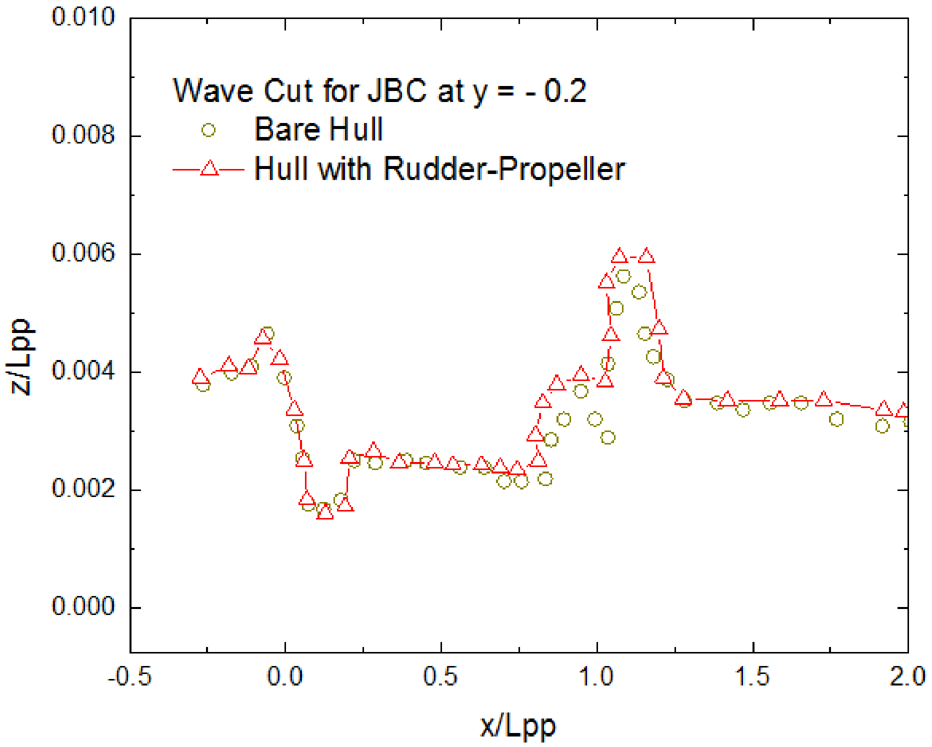

Figure 4.18: Comparison between transverse wave cuts for JBC hull at y = - 0.2

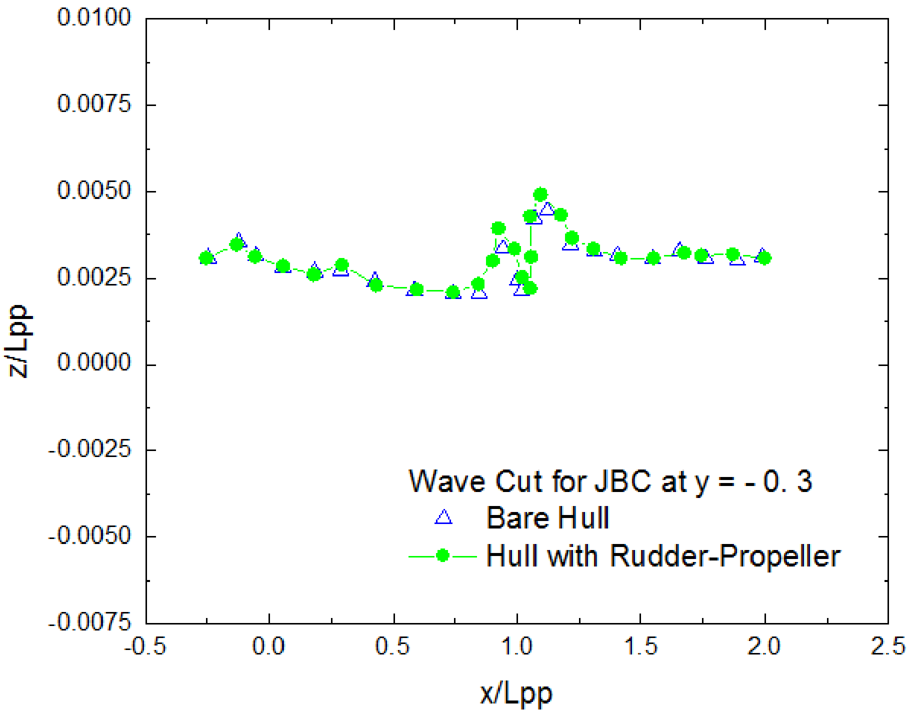

Figure 4.19: Comparison between transverse wave cuts for JBC hull at y = - 0.3

4.6 Computational Domain for Viscous Flow Solver

Due to symmetry on the x-z plane, quarter of a cylinder is used as computational domain with radius 0.5 L, downstream length 1.8L and for zonal approach viscous computation starts from 0.5L behind the F.P of the ship as shown for in Figure 4.20.

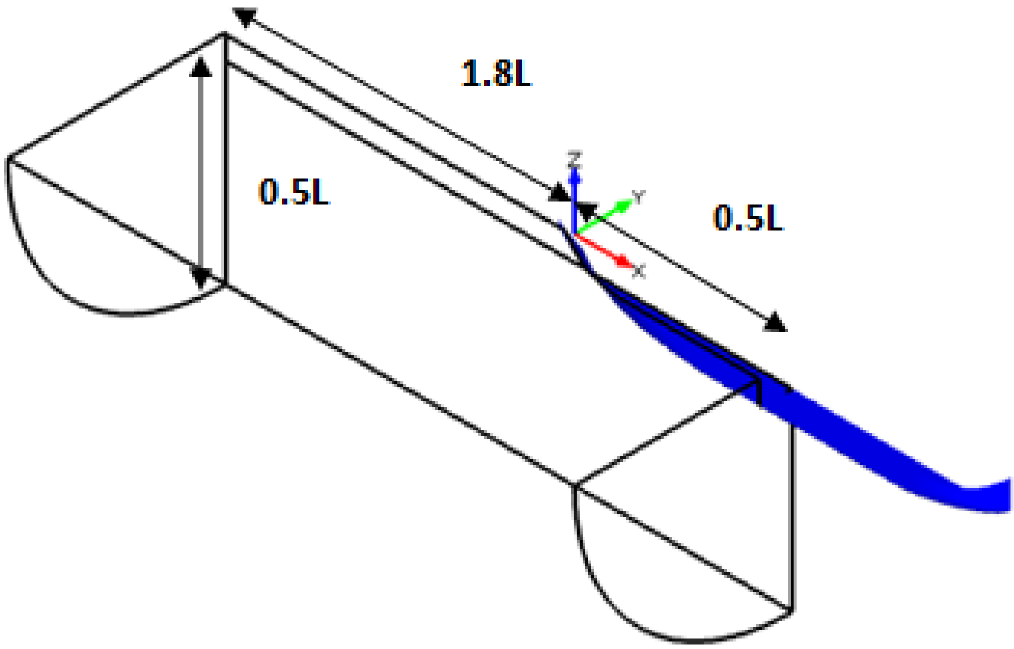

Figure 4.20: Computational domain for viscous flow solver

4.7 Grid Generation

Finite volume method requires grid cells in order to discretize the partial differential equations and approximate algebraic equations. In viscous flow module only structured grids are used. Computational domain along with hull geometry is represented by a single block structured grid of H-O type with 0.45 M cells as shown in Figure 4.21.

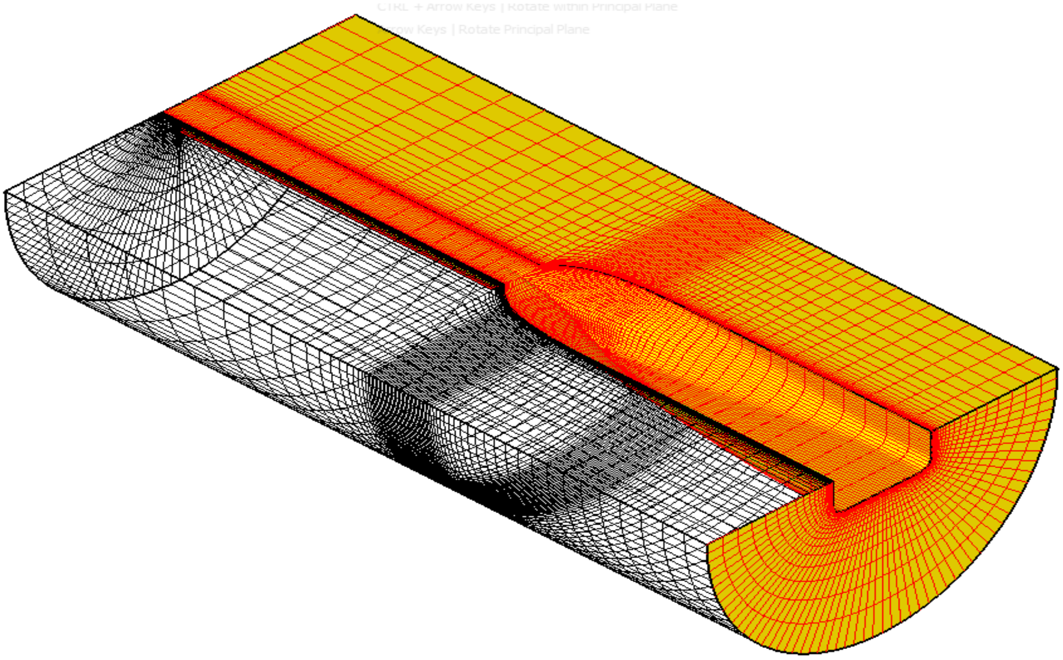

a) KCS hull

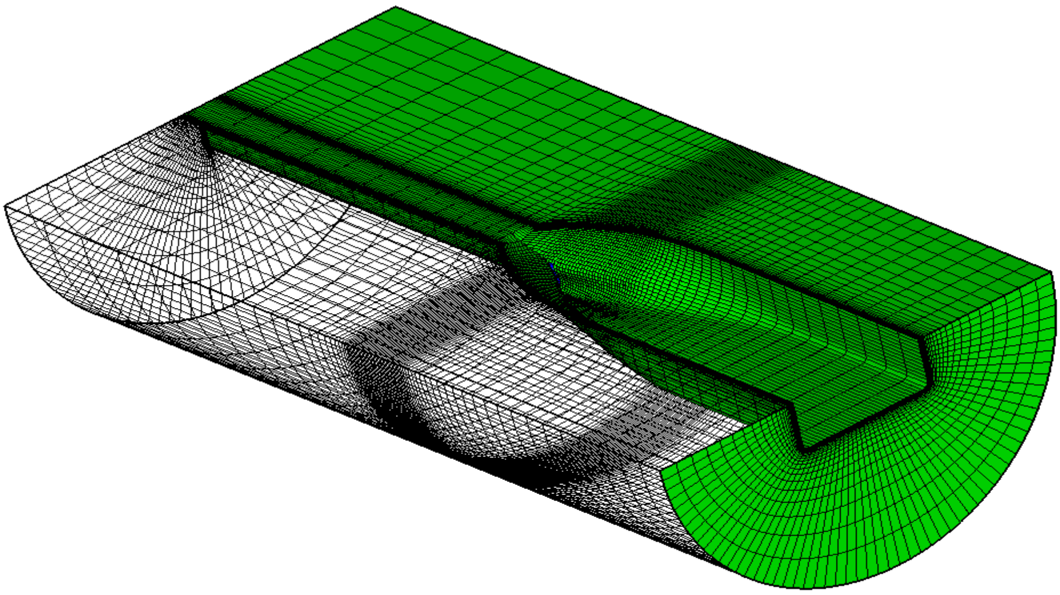

b) JBC hull

Figure 4.21: Single block structured grid of H-O type around bare ship hull

Grid generation around rudder is done with O-O type structured grid. Propeller is modeled as an actuator disc and gridded with cylindrical grids which are shown in Figure 4.22.

Additional grids for the propeller and the rudder is fitted with hull by *Chimera or overlapping* grid generation technique where complex geometries are added to hull with geometrically simple grid generation technique. Overlapping grid of propeller disc with ship hull is shown in Figure 4.23. The whole grid around rudder-propeller overlapped with ship hull is shown in Figure 4.24.

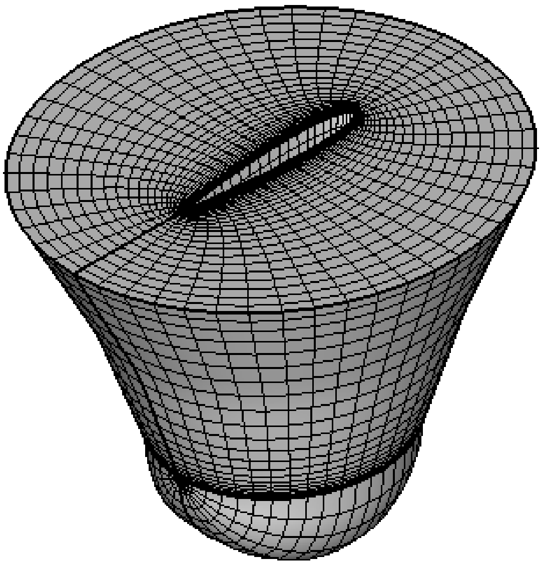

a) O-O type grid

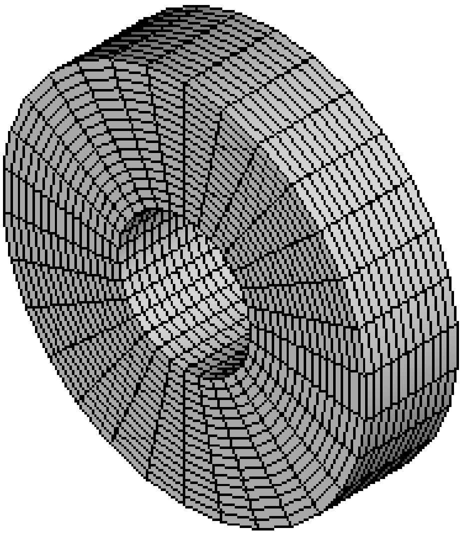

b) Cylindrical grid

Figure 4.22: Grid around rudder and propeller: a) O-O type grid around rudder;
a) Cylindrical grid around propeller disc

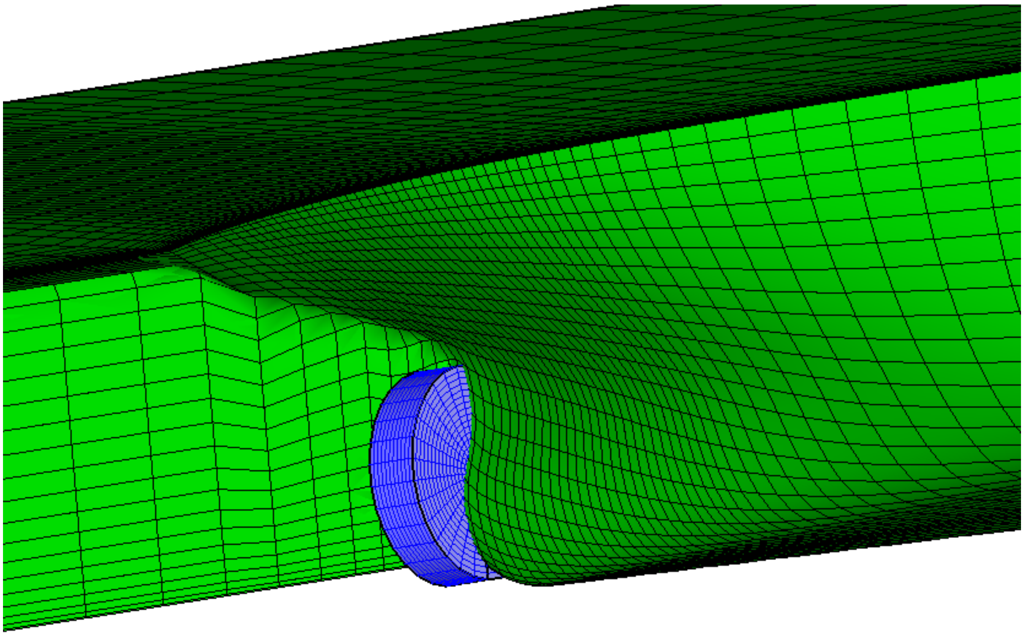

Figure 4.23: Overlapping grid of propeller disc with ship hull

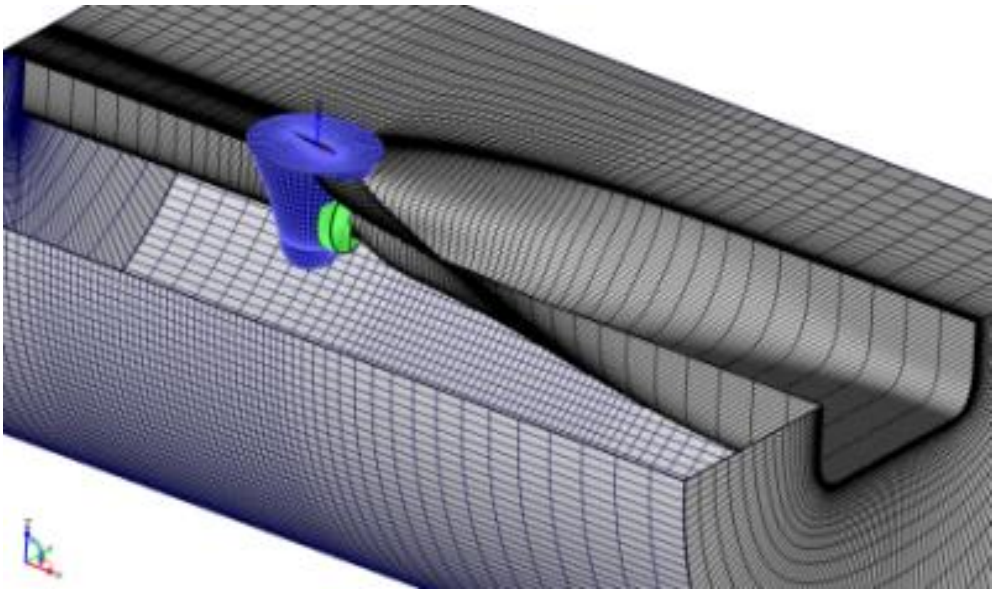

Figure 4.24: The whole grid around rudder-propeller overlapped with ship hull

4.7.1 Grid Convergence Study

The first step of CFD verification is grid convergence study which is a procedure where the grid is systematically refined. It is assumed that as the number of grid point increases and the grid spacing tend to zero, the discretization error should tend to zero as well. As the grid is refined the solution should approaches the solution of the continuous equations. This assumption is qualified by the condition of consistency and convergence. Grid convergence study is useful for deciding the level of discretization error existing in the CFD solution.

In this thesis, three sets of systematically refined grids are generated as shown in Figure 4.25. The multiblock structured grid is used. The number of numerical grid in Millions (M) is listed in Table 4.1 for all three sets of grids.

Table 4.1: Number of grids for grid convergence study

	Coarse	Medium	Fine
Number of grids	0.148 M	0.423 M	1.247 M

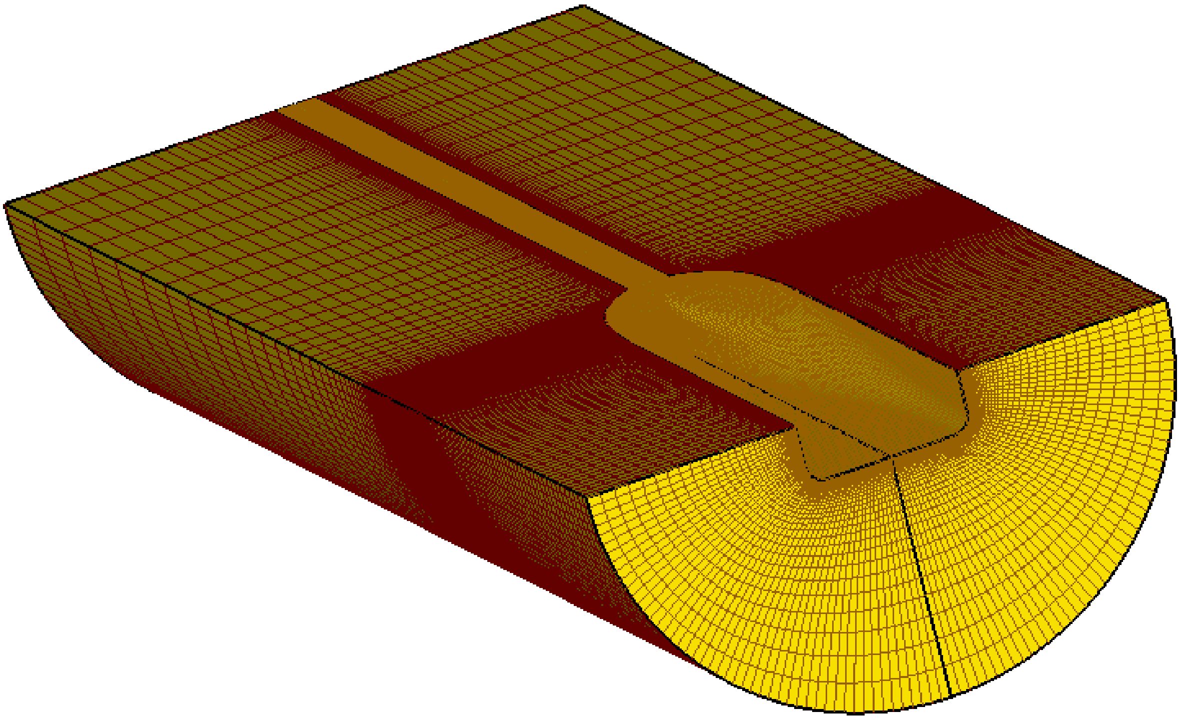

a) Coarse

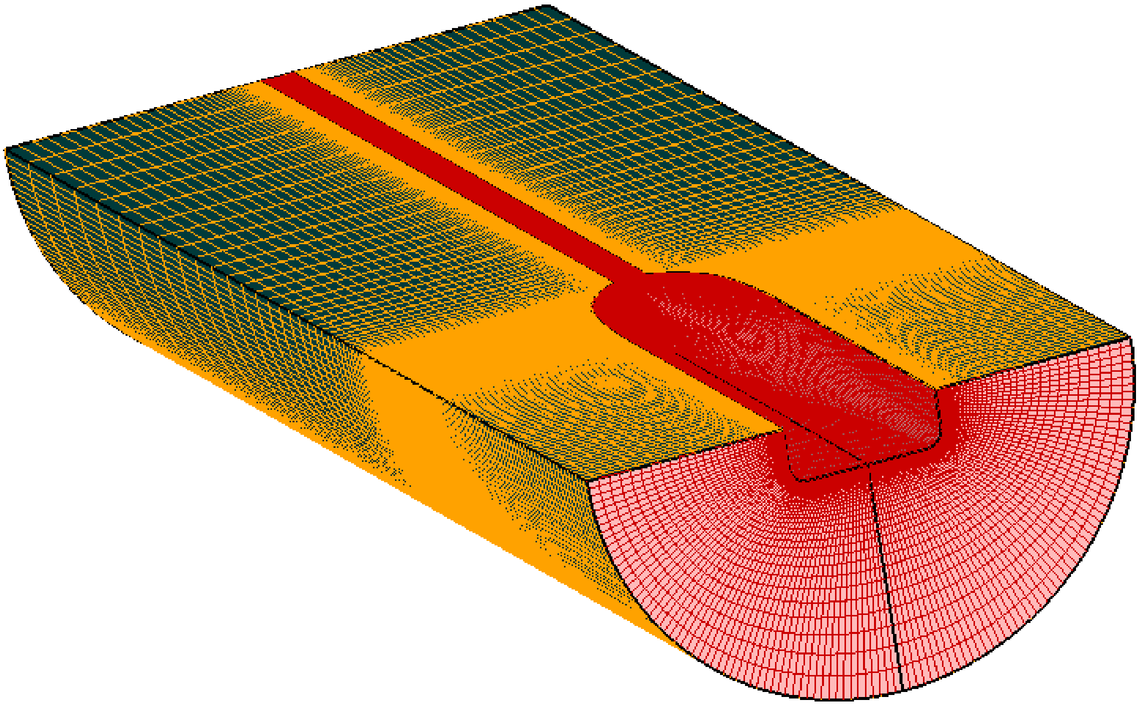

b) Medium

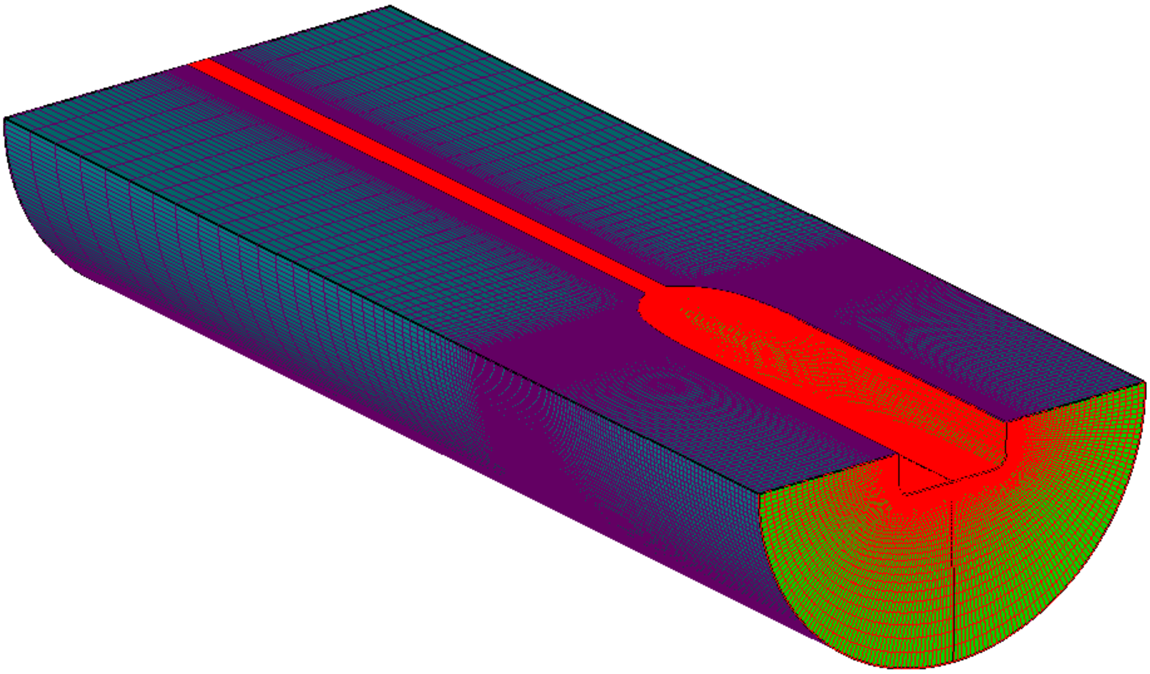

c) Fine

Figure 4.25: Three sets of systematically refined grids: a) Coarse; b) Medium; c) Fine

4.7.2 Verification and Validation

Verification of the total resistance was performed according to ITTC recommended procedures as described in section 2.11 for three different grid densities from fine (S_1) to coarse (S_3) as shown in Table 4.2 for KCS and Table 4.3 for JBC. For determining validation errors numerical solutions are evaluated against experimental data. EFD result and data uncertainty are provided for C_T and U_D%D is reported as 1% (NMRI, 2015) [32].

Table 4.2.V&V study for KCS bare hull resistance prediction, Re =1.26×10^7, Fr = 0.260

			V & V Study				
Parameters		**EFD (D)**	**Grid#3 (S_3)**	**Grid#2 (S_2)**	**Grid#1 (S_1)**	**U_D %S_1**	**U_{SN} %**
$C_t\times10^3$	Value	3.711	3.968	3.763	3.738	1.0	0.715
	E%D		-6.925	-1.401	-0.728		
$C_w\times10^3$	Value		1.6172	1.4962	1.4952		
$C_v\times10^3$	Value		2.3508	2.2668	2.2428		

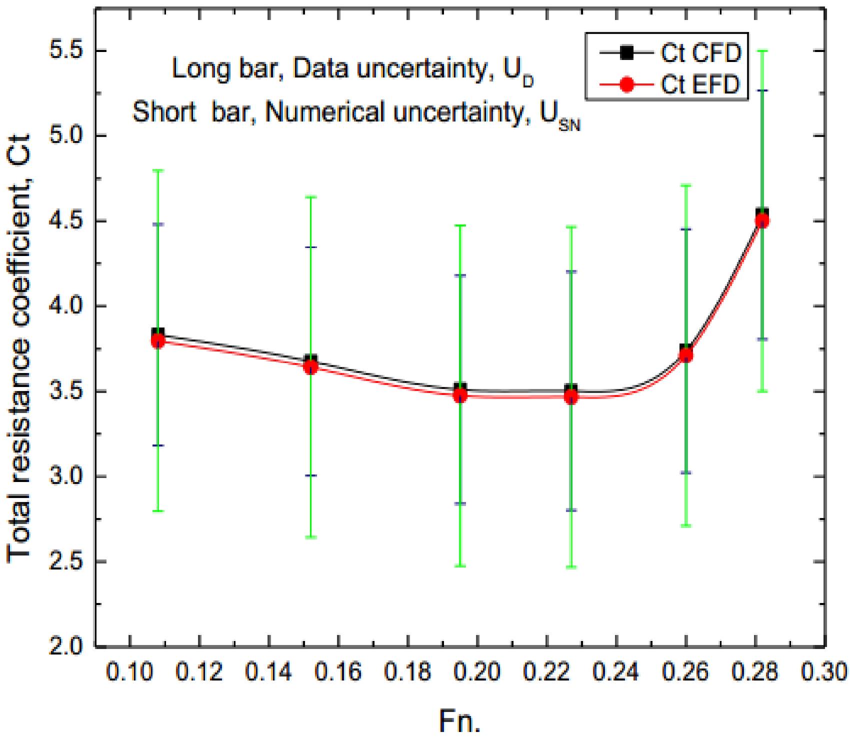

Figure 4.26: Verification and Validation of resistance coefficients for KCS

For KCS at Re =1.26×10^7, Fn = 0.260 computed C_T values and experimental data are presented in Table 4.2 and Figure 4.26 together with numerical and data uncertainties. Green long vertical bars represent the data uncertainties (U_D), while black short vertical bars denote the numerical uncertainties (U_{SN}). From Table 4.2 it is observed that from coarse grid to finer grids, CFD predictions get closer to EFD measurement.

Table 4.3.V&V study for JBC bare hull resistance prediction, Re =7.46×10[6], Fr = 0.142

			V & V Study				
Parameters		**EFD (D)**	**Grid#3 (S_3)**	**Grid#2 (S_2)**	**Grid#1 (S_1)**	**U_D %S_1**	**U_{SN} %**
$C_t \times 10^3$	Value	4.289	4.175	4.196	4.22	1.0	0.825
	E%D		2.658	2.168	1.61		
$C_w \times 10^3$	Value		0.313	0.3318	0.3318		
$C_v \times 10^3$	Value		3.862	3.864	3.868		

For JBC at Re =7.46×10[6], Fn. = 0.142 computed C_T values and experimental data are presented in Table 4.3 and Figure 4.27 together with numerical and data uncertainties. Red long vertical bars represent the data uncertainties (U_D), while black short vertical bars denote the numerical uncertainties (U_{SN}). From Table 4.3 it is observed that from coarse grid to finer grids, CFD predictions get closer to EFD measurement.

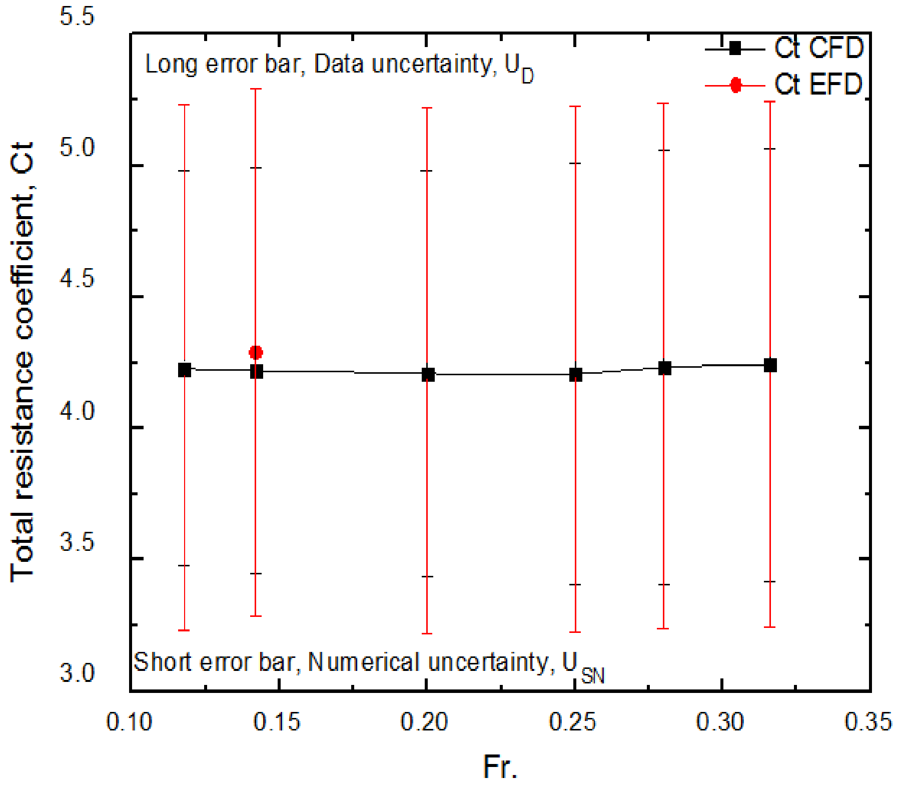

Figure 4.27: Verification and Validation of resistance coefficients for JBC

4.8 Propeller Open Water Characteristics (POW)

Propeller Open Water (POW) simulations are performed using OpenProp software [50] as described in Section 2.10. Propeller open water characteristics are investigated for various advance ratios. Forces and moments are calculated in the propeller grid with Lifting Line (LL) program of OpenProp are applied to the RANS method as body forces.

4.8.1 KP 505 Propeller Open Water Results

The geometric particulars from Table 3.2 and 3.3 are provided as input into OpenProp in the Single Propeller Design GUI as shown in Figure 4.28. The thickness form of the KP 505 propeller is the NACA 66.

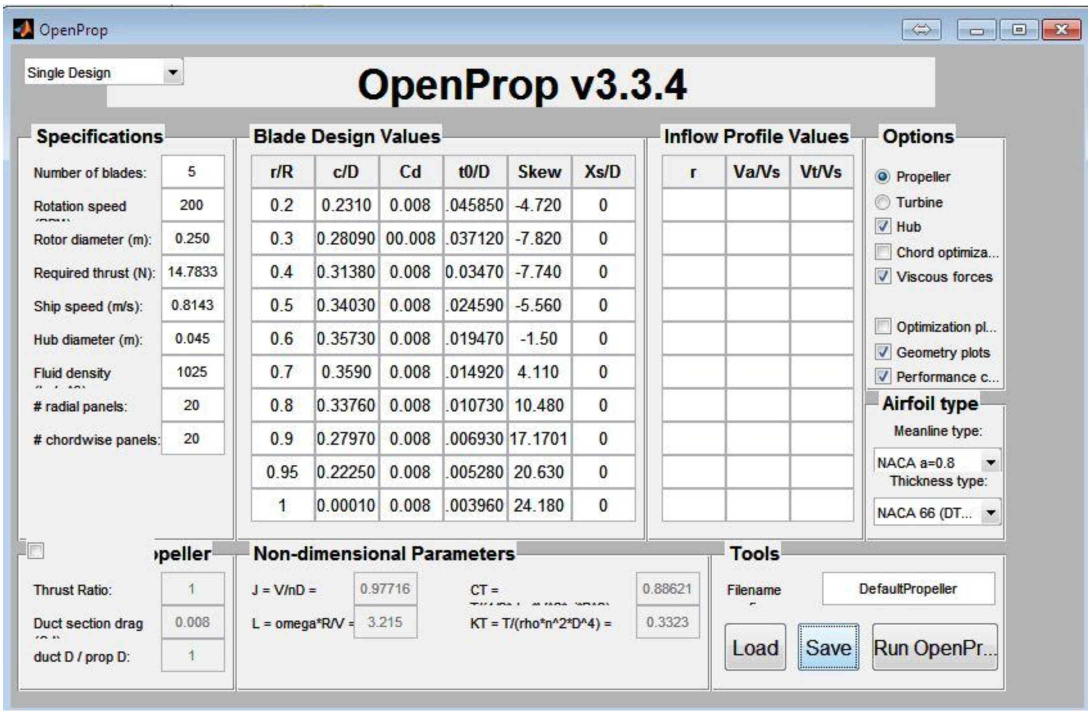

Figure 4.28: OpenProp input parameters for the KP 505 propeller

With these inputs the three dimensional KP 505 propeller geometry produced by OpenProp with 20 radial and chordwise panels for Lifting Line analysis as shown in Figure 4.29.

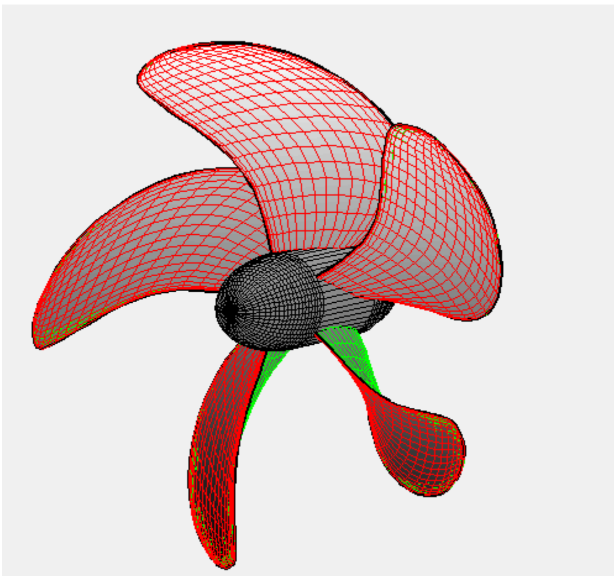

Figure 4.29: OpenProp representation of the KP 505 propeller

The propeller performance results for the KP 505 propeller generated by the MATLAB® code is shown with the solid lines in Figure 4.30. The dashed lines represent the experimentally derived performance values as reported by National Maritime Research Institute [32].

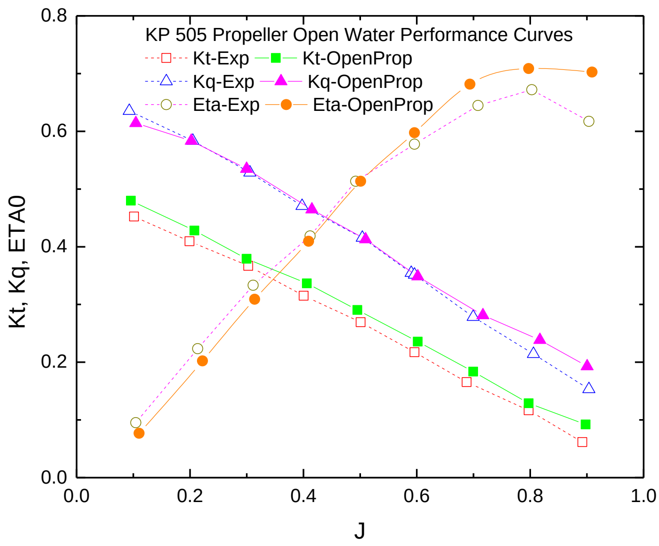

Figure 4.30: Comparison between CFD and EFD results of open water hydrodynamic characteristics of KP 505 propeller

4.8.2 DTMB 4119 Propeller Open Water Results

The geometric particulars from Table 3.4 and 3.5 are entered into OpenProp in the Single Propeller Design GUI as shown in Figure 4.31.

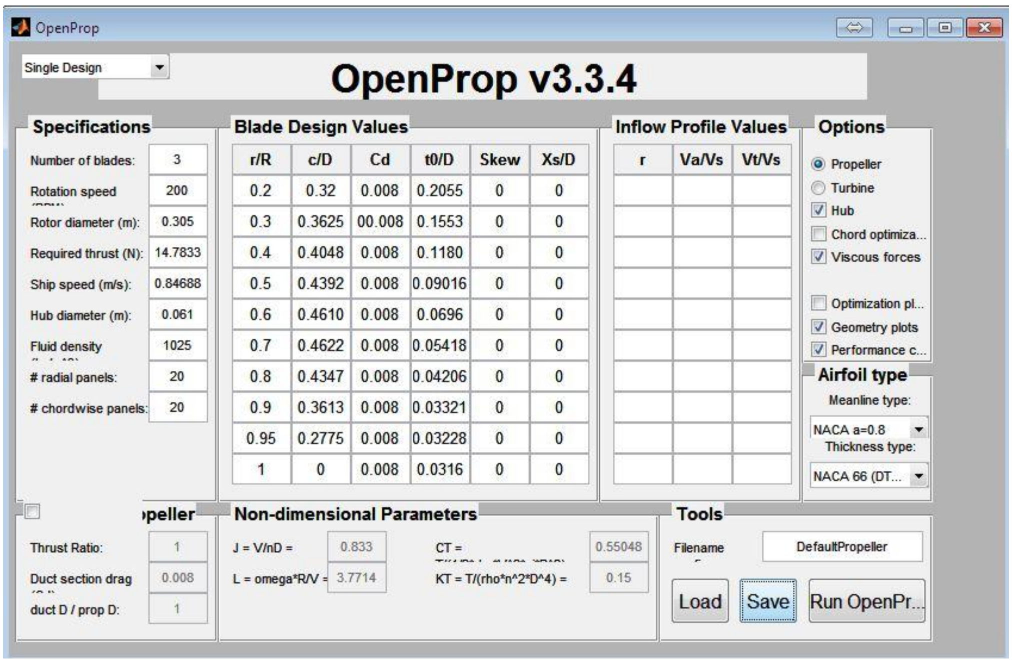

Figure 4.31: OpenProp input parameters for the DTMB 4119 propeller

The thickness form of the DTMB 4119 propeller is the NACA 66. With these inputs the three dimensional DTMB 4119 propeller geometry produced by OpenProp with 20 radial and chordwise panels for Lifting Line analysis as shown in Figure 4.32.

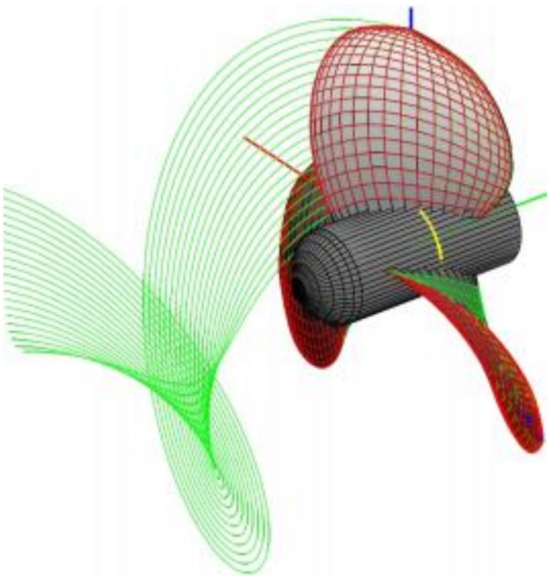

Figure 4.32: OpenProp representation of the DTMB 4119 propeller

The propeller performance results for the DTMB 4119 propeller generated by the MATLAB® code is shown with the solid lines in Figure 4.33. The dashed lines represent the experimentally derived performance values as reported by Hsin and Kerwin [56].

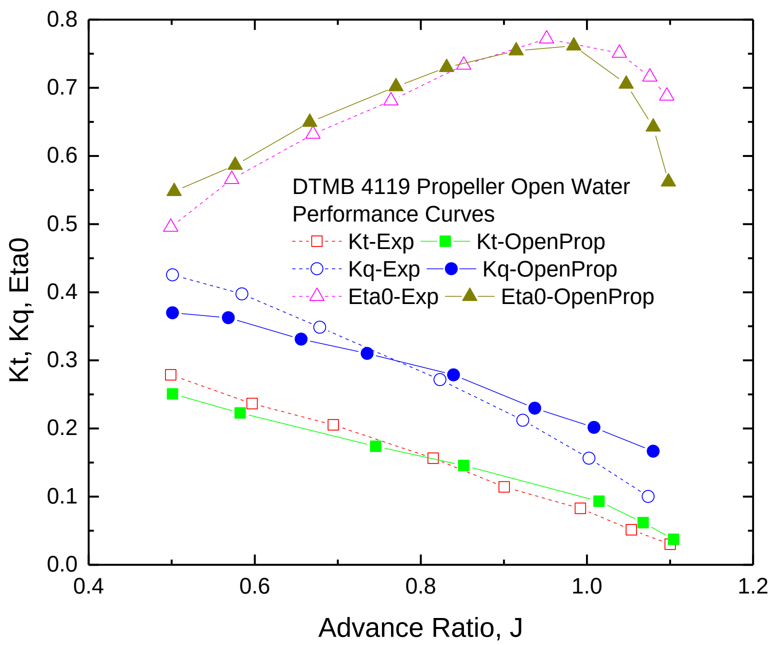

Figure 4.33: Comparison between CFD and EFD results of open water hydrodynamic characteristics of DTMB 4119propeller

From Figures 4.29 and 4.32 it is clear that the most significant differences occur in the torque coefficient and efficiency values at low and high values of advance ratio. One possible reason for the deviations at low J values is that the Lerbs Lifting Line method is only valid for moderately loaded propellers. The load increases with decreases in the advance ratio therefore some error in this region is expected.

4.9 Self Propulsion Results at Varying Rudder Positions

The summary of the computed self-propulsion characteristics for KCS hull for four different longitudinal rudder positions are shown in Table 4.4.

From Table 4.4 it is found that at the position b/D = 0.72 maximum thrust with minimum torque and minimum total resistance are obtained. Therefore maximum efficiency of propeller has also been obtained here.

Table 4.4.Summary of the self propulsion characteristics for KCS hull

b/D	**J**	**Ct**	**T (kN)**	**Q (kN-m)**
0.37	0.87044	0.00597	4147.98	1167.76
0.54	0.87250	0.00597	4154.3	1168.09
0.63	0.87271	0.00596	4159.7	1163.58
0.72	0.87282	0.00468	4395.65	640.175

The computed variation of total resistance coefficient Ct, thrust T and torque Q at varying rudder positions for KCS are shown in Figures 4.34-4.36 respectively.

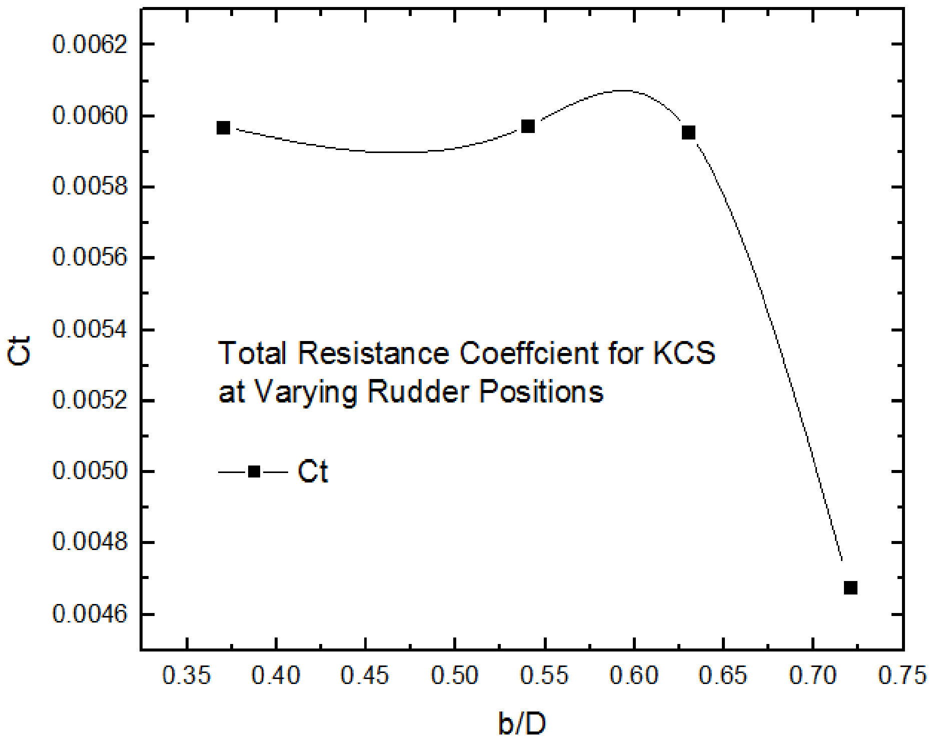

Figure 4.34: Total resistance coefficient for KCS at varying rudder positions

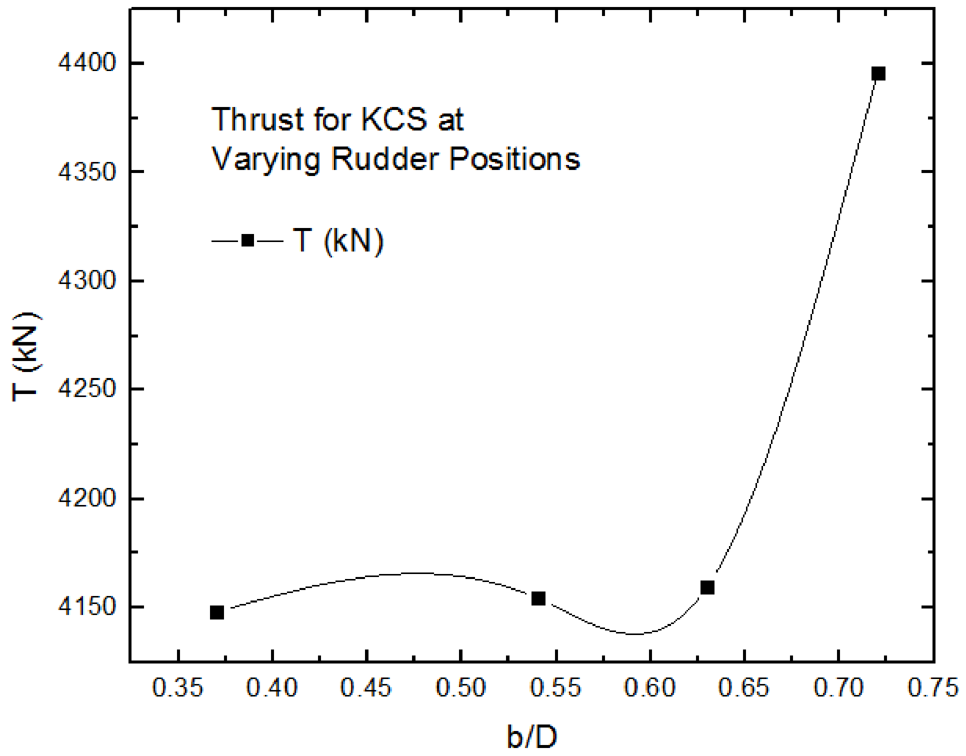

Figure 4.35: Thrust for KCS at varying rudder positions

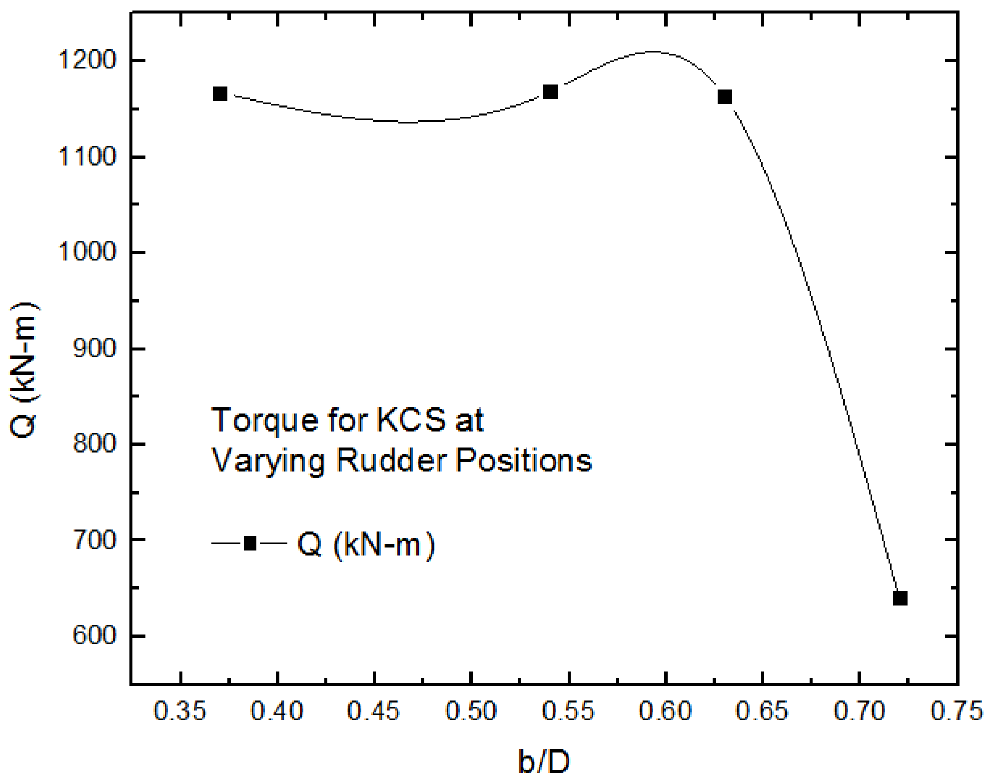

Figure 4.36: Torque for KCS at varying rudder positions

Figures 4.34-4.36, it is found that as the rudder moves further away from the propeller the maximum thrust is obtained with minimum torque. Therefore, the rudder position of b/D = 0.72 is considered as the optimum position with respect to thrust and torque.

Table 4.5.Summary of the self propulsion characteristics for JBC hull

b/D	J	Ct	T (kN)	Q(kN-m)
0.35	0.86567	0.00503	1449.33	587.309
0.4	0.86613	0.00499	1500.13	585.309
0.44	0.86696	0.00497	1506.78	576.234
0.5	0.86873	0.00491	1512.22	564.832
0.53	0.86909	0.00482	1516.28	559.448
0.58	0.86943	0.00478	1533.29	558.288

From Table 4.5, it is observed that at the position of b/D = 0.58 maximum thrust with minimum torque and minimum total resistance are obtained here.

The computed variation of total resistance coefficient Ct, thrust T and torque Q at varying rudder positions for JBC are shown in Figures 4.37, 4.38 and 4.39 respectively.

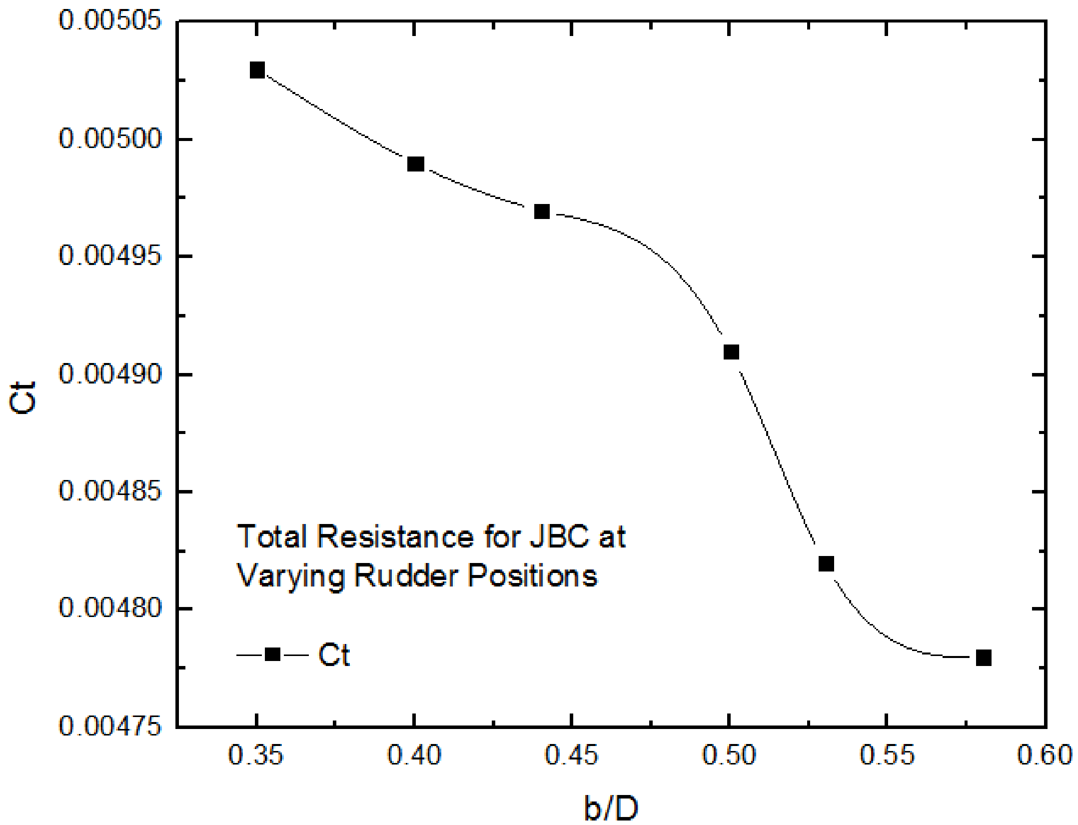

Figure 4.37: Total resistance coefficient for JBC at varying rudder positions

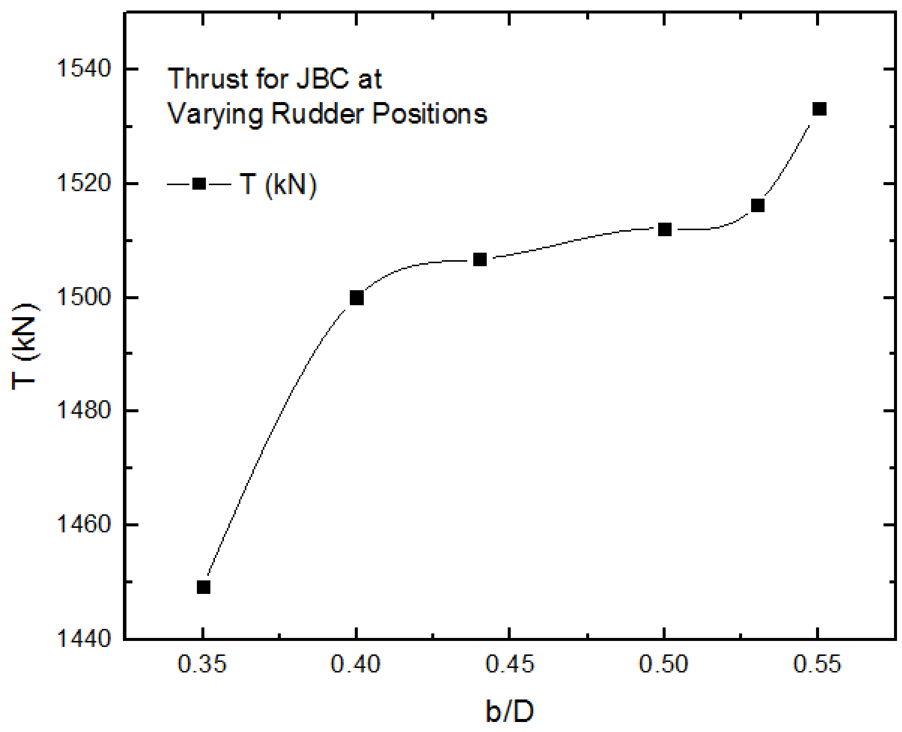

Figure 4.38: Thrust for JBC at varying rudder positions

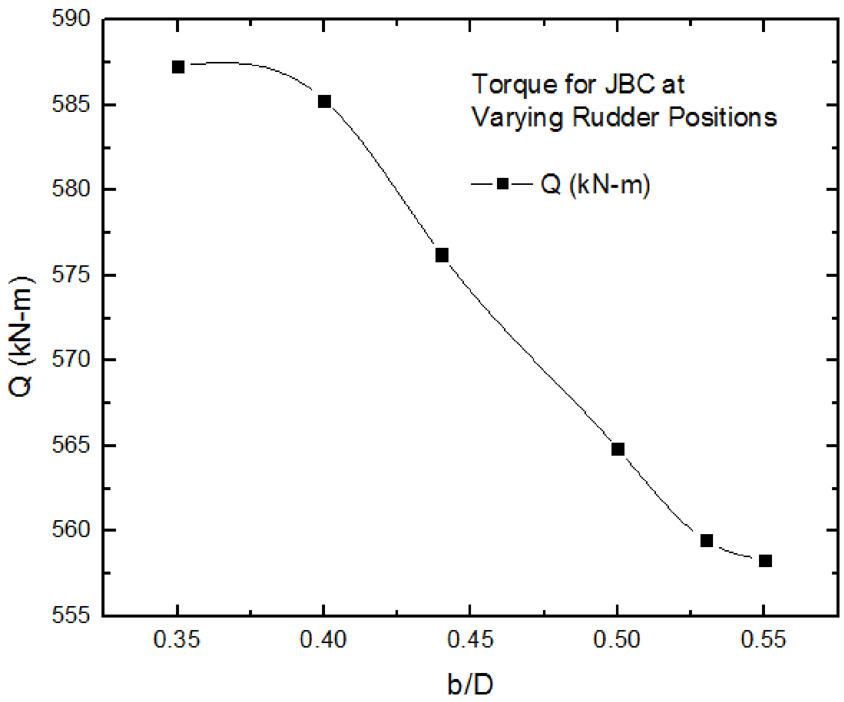

Figure 4.39: Torque for JBC at varying rudder positions

From Figures 4.37-4.39, it is found that as the rudder moves further away from the propeller the maximum thrust is obtained with minimum torque. Therefore, the rudder position of b/D = 0.58 is considered as the optimum position with respect to thrust and torque.

4.10 Wake Field at Stern

The wake field is strongly dependent on ship type and each vessel can be considered to have a unique wake field. The wake velocities with the propeller operating behind the ship and developing thrust is called effective wake which is smaller than nominal wake due to the effect of propeller and rudder on hull flow.

4.10.1 Wake Field behind KCS Hull

The nominal wake is the wake behind the hull without propeller as shown in Figure 4.40.

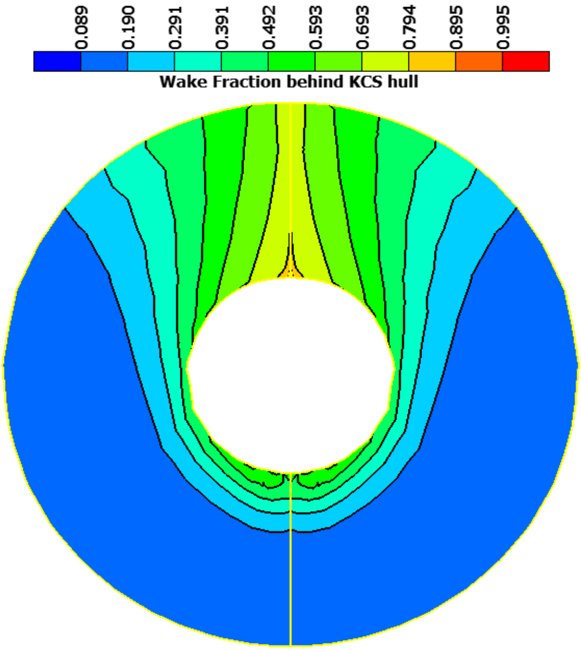

Figure 4.40: Nominal wake (without propeller) behind KCS hull

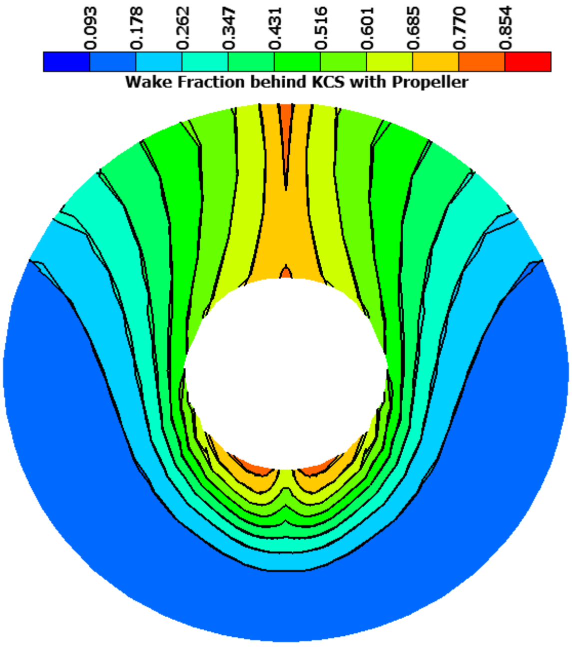

Figure 4.41: Effective wake (with propeller) behind KCS hull

The effective wake field with propeller and with both rudder-propeller at optimum rudder position (b/D = 0.72) are shown in Figures 4.41 and 4.42 respectively.

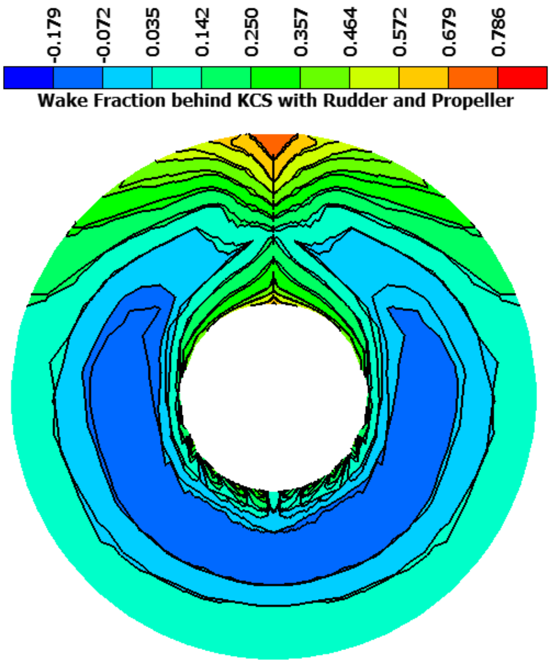

Figure 4.42: Effective wake (with propeller and rudder) behind KCS hull

From Figures 4.41 and 4.42 it is found that the value of maximum wake fraction decreases with increasing interaction behind hull due to presence of rudder and propeller. Therefore velocity of advance increases through the acceleration of the flow field at stern.

4.10.2 Wake Field behind JBC Hull

Nominal wake (without propeller) behind JBC hull is shown in Figure 4.43.

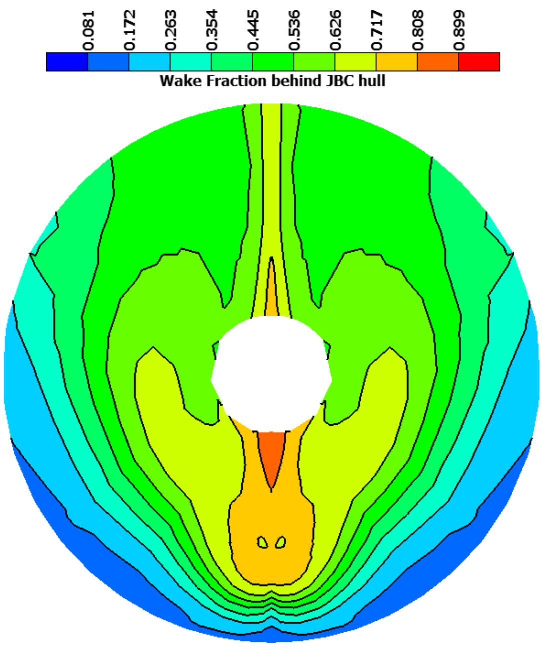

Figure 4.43: Nominal wake (without propeller) behind JBC hull

The effective wake field with propeller and with both rudder-propeller are shown in Figure 4.44 and Figure 4.45 respectively.

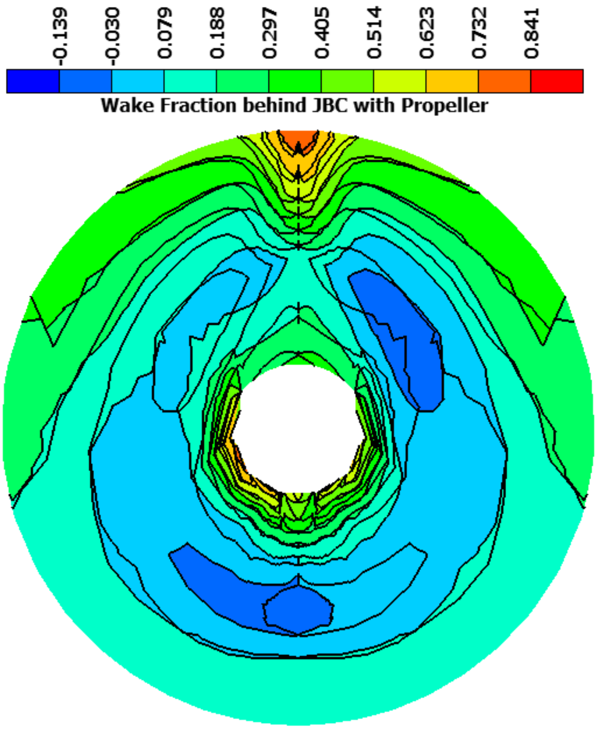

Figure 4.44: Effective wake (with propeller) behind JBC hull

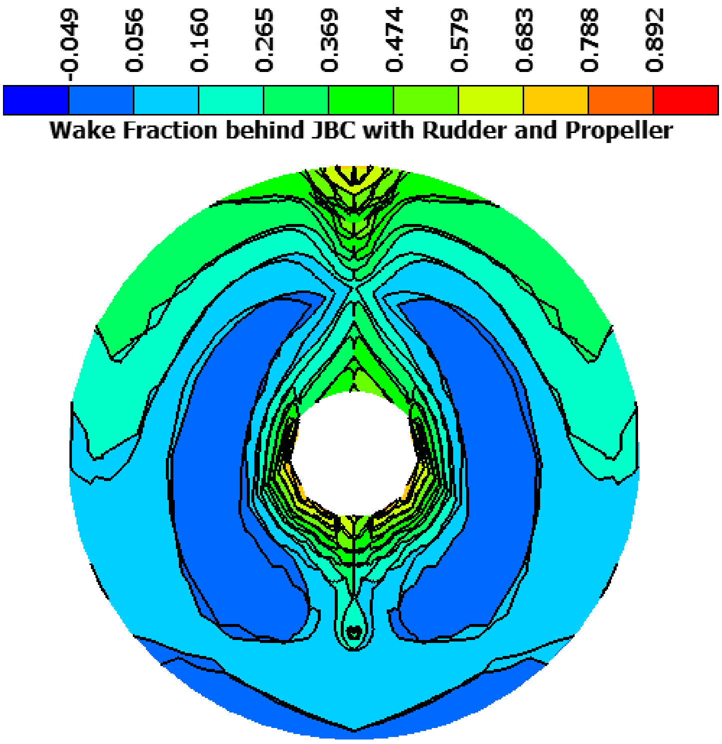

Figure 4.45: Effective wake (with propeller and rudder) behind JBC hull

4.11 Axial Velocity Contour at Stern

Axial velocity at stern is also affected by the presence of rudder and propeller. Axial velocity contour at the stern region of the KCS hull with rudder and propeller for different longitudinal distance from propeller plane (x) are shown in Figure 4.46.

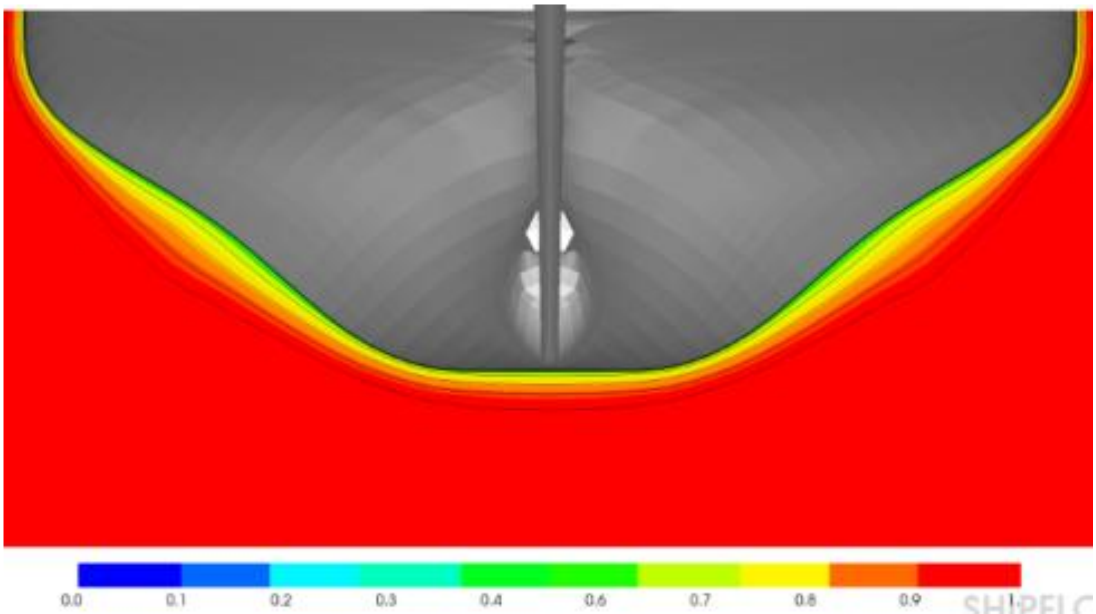

a) x = 0.80

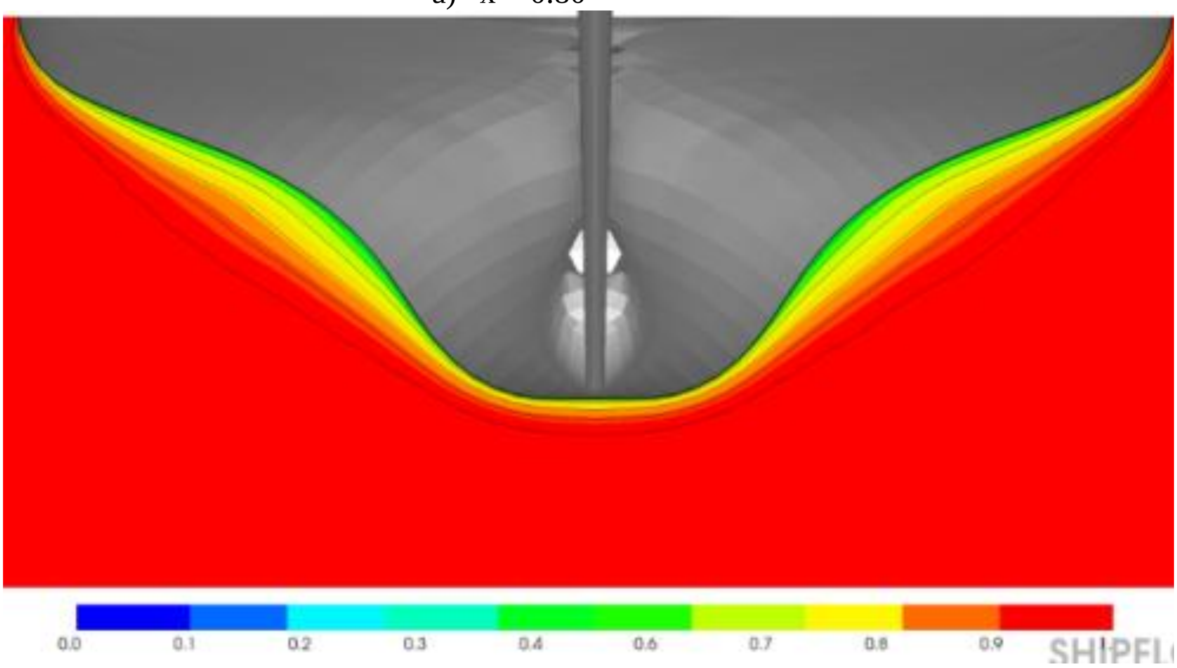

b) x = 0.85

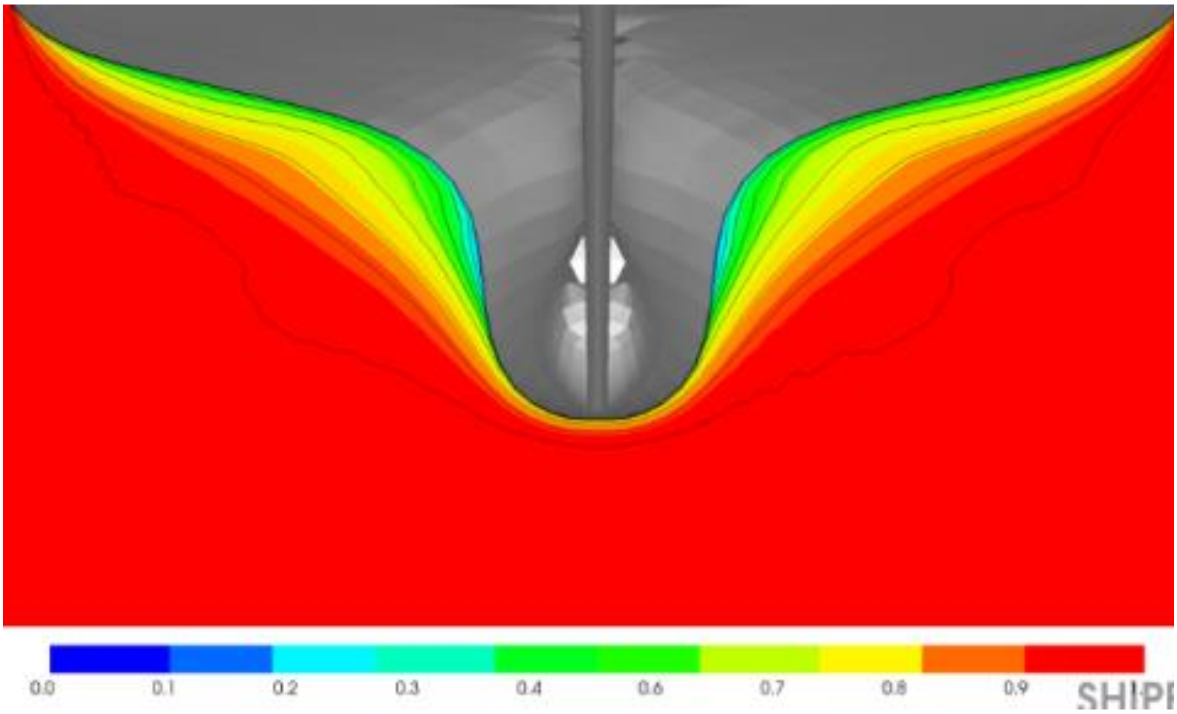

c) x = 0.90

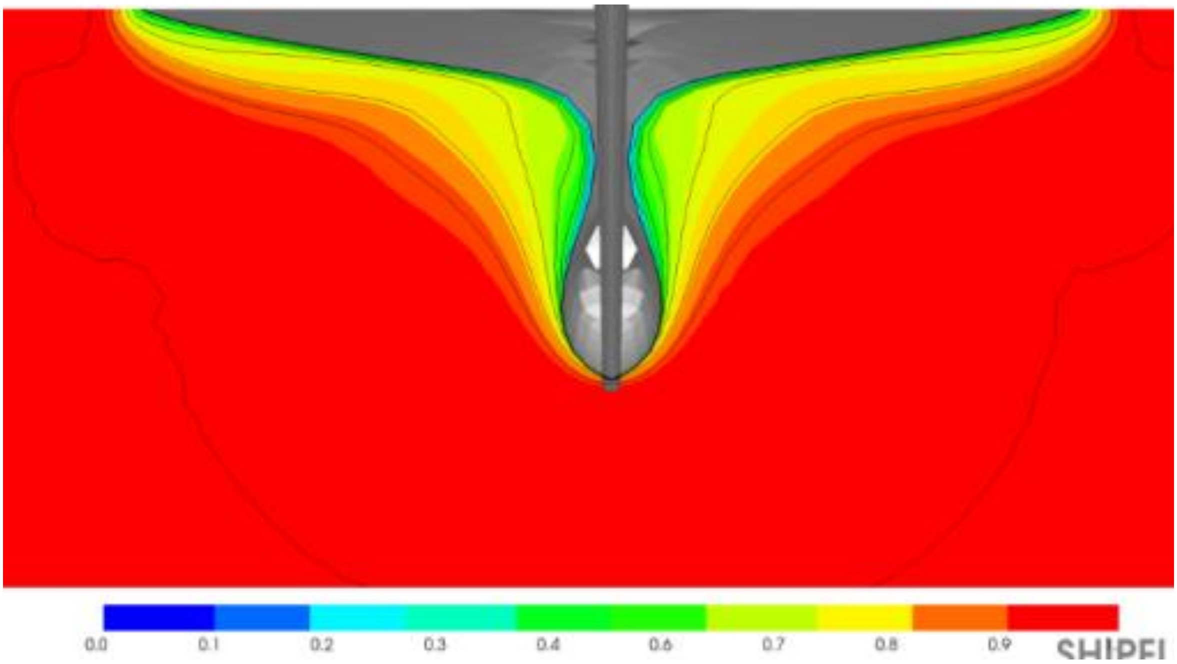

d) x = 0.95

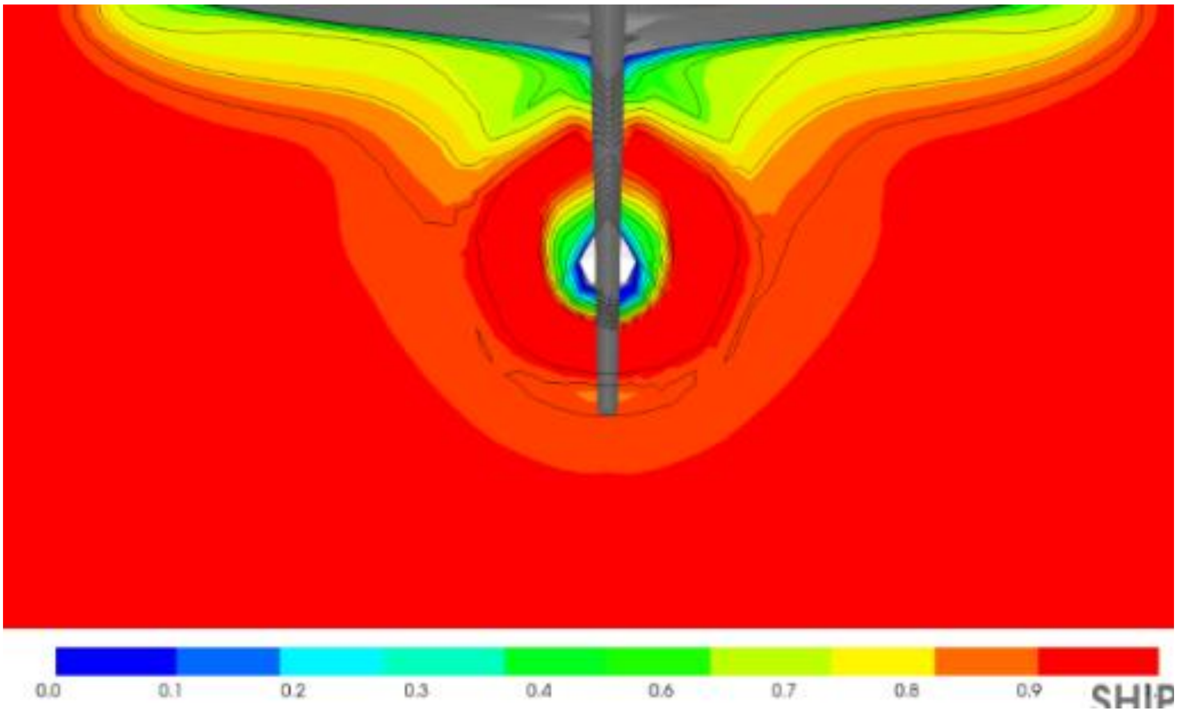

e) x = 0.9747

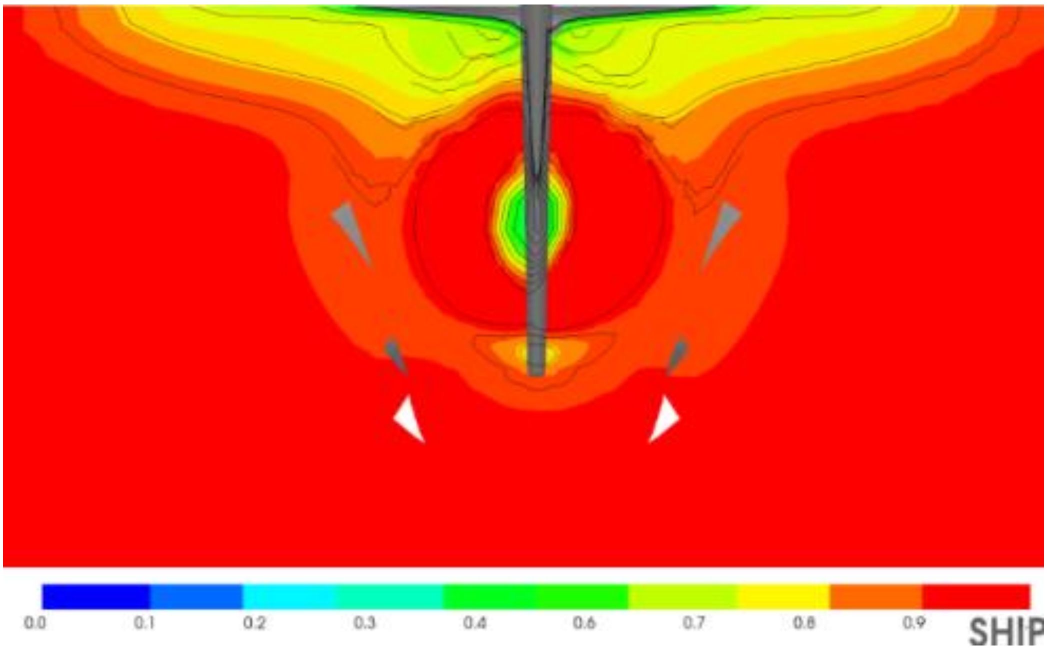

f) x = 1.00

Figure 4.46: Axial velocity contour at the stern region of the KCS hull with rudder and propeller effect

From Figure 4.46 (a-f) it is found that axial velocity at stern changes both its pattern and magnitude as the distance from propeller plane changes.

Axial velocity contour at the stern region of the JBC hull with rudder and propeller for different longitudinal distance from propeller plane are shown in Figure 4.47.

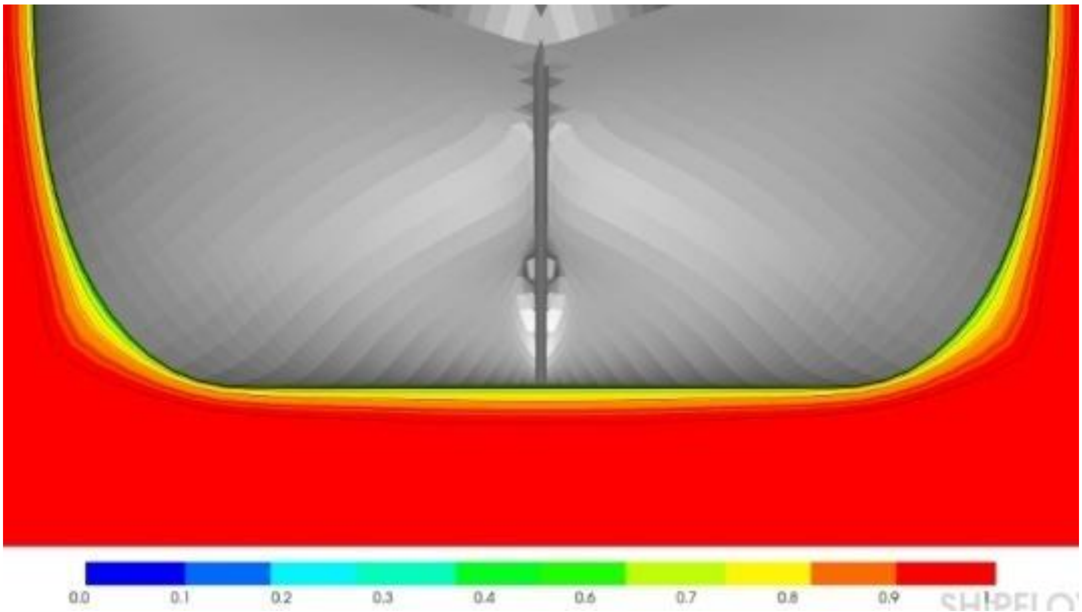

a) x = 0.80

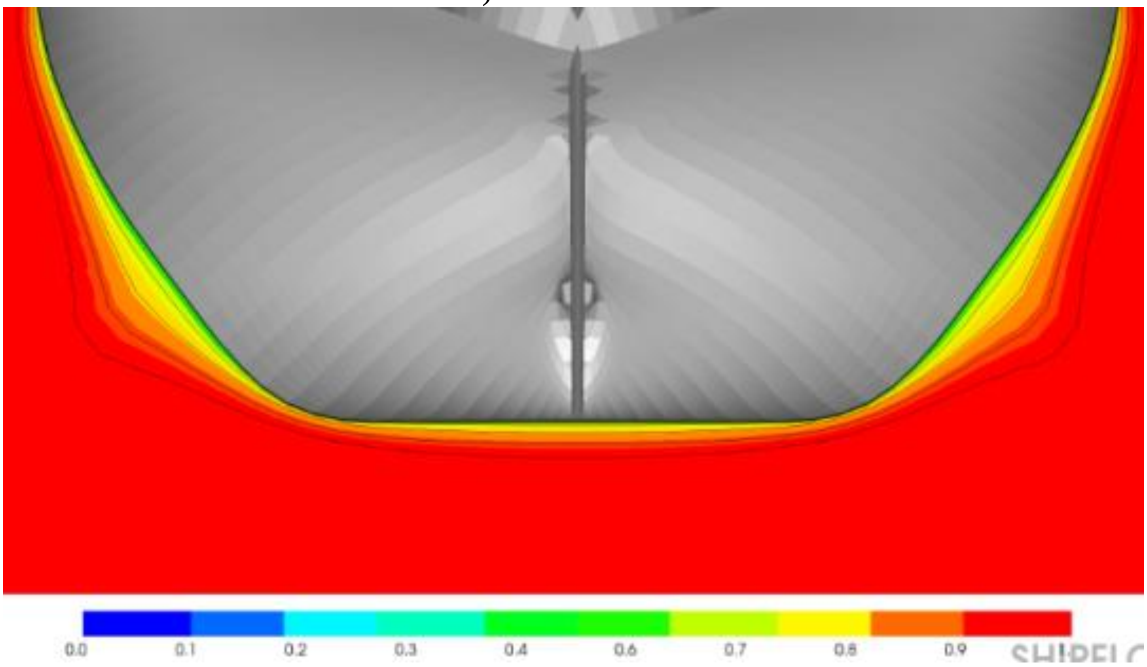

b) x = 0.85

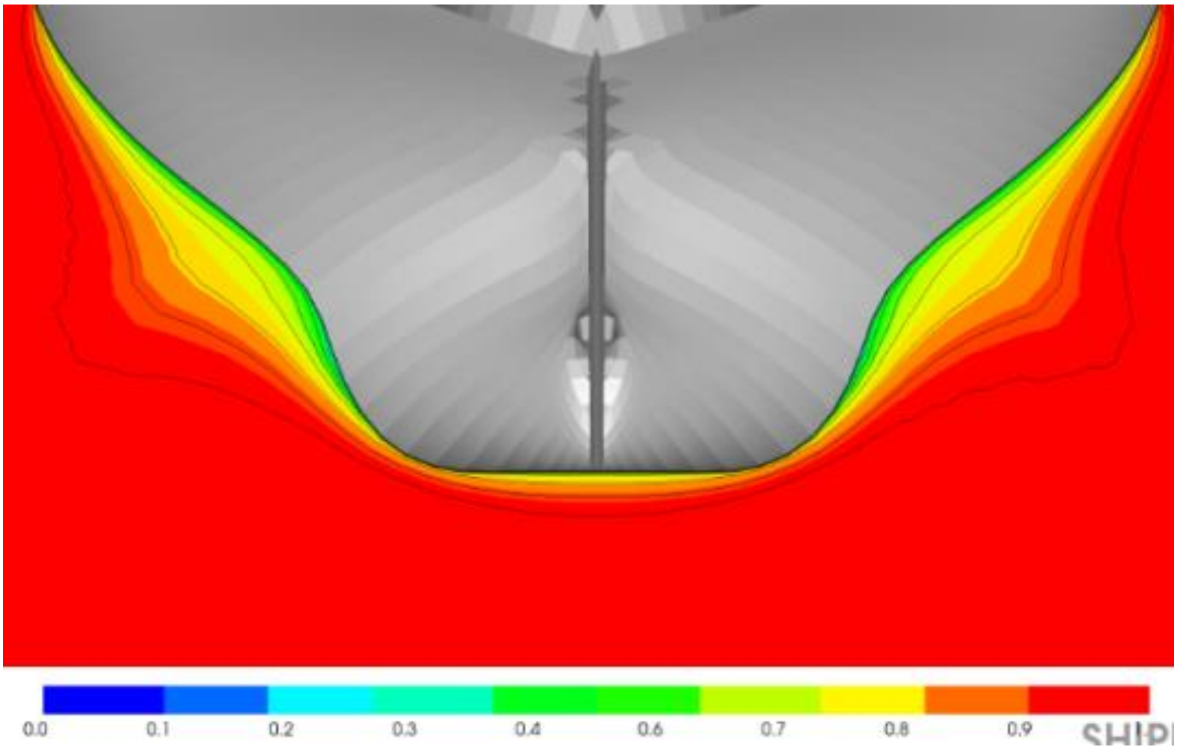

c) x = 0.90

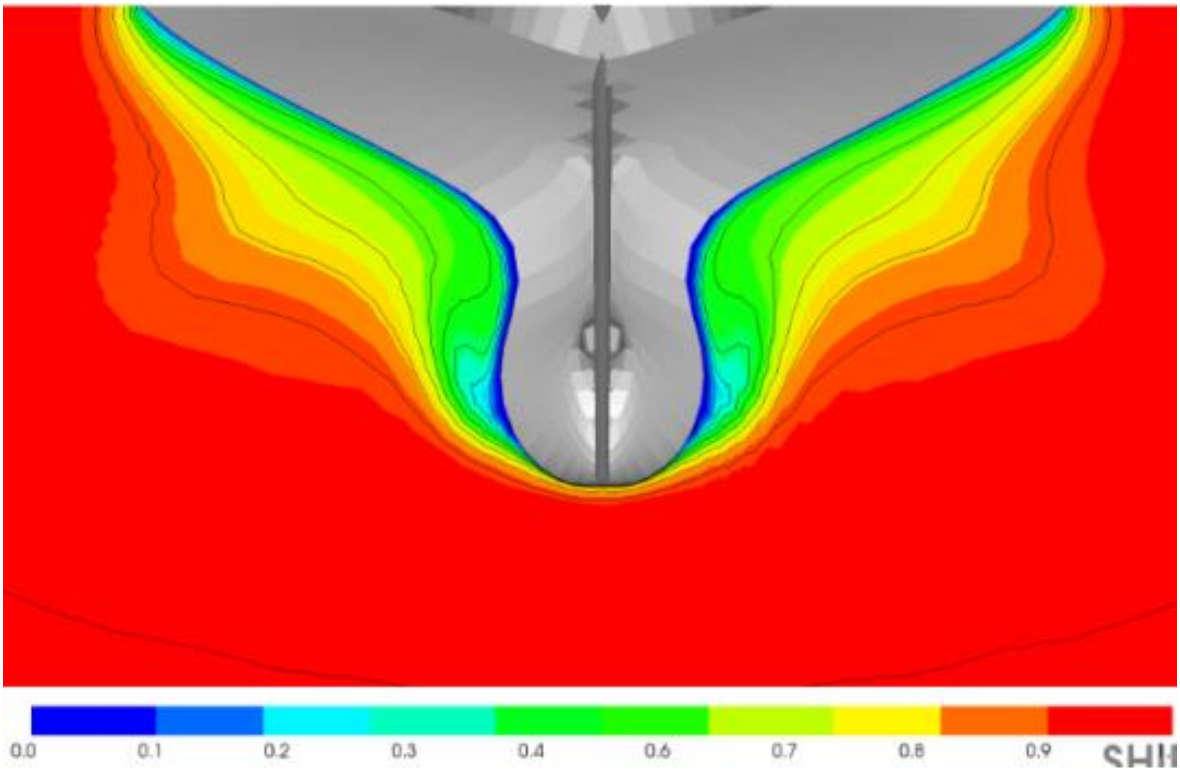

d) x = 0.95

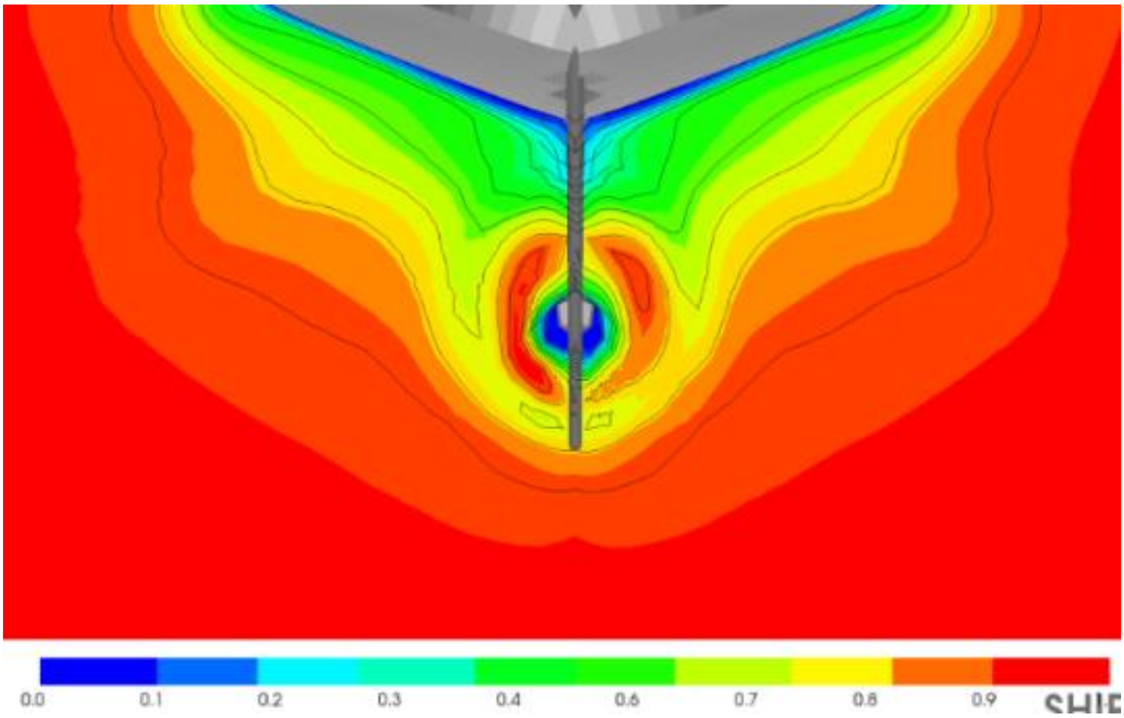

e) x = 0.9747

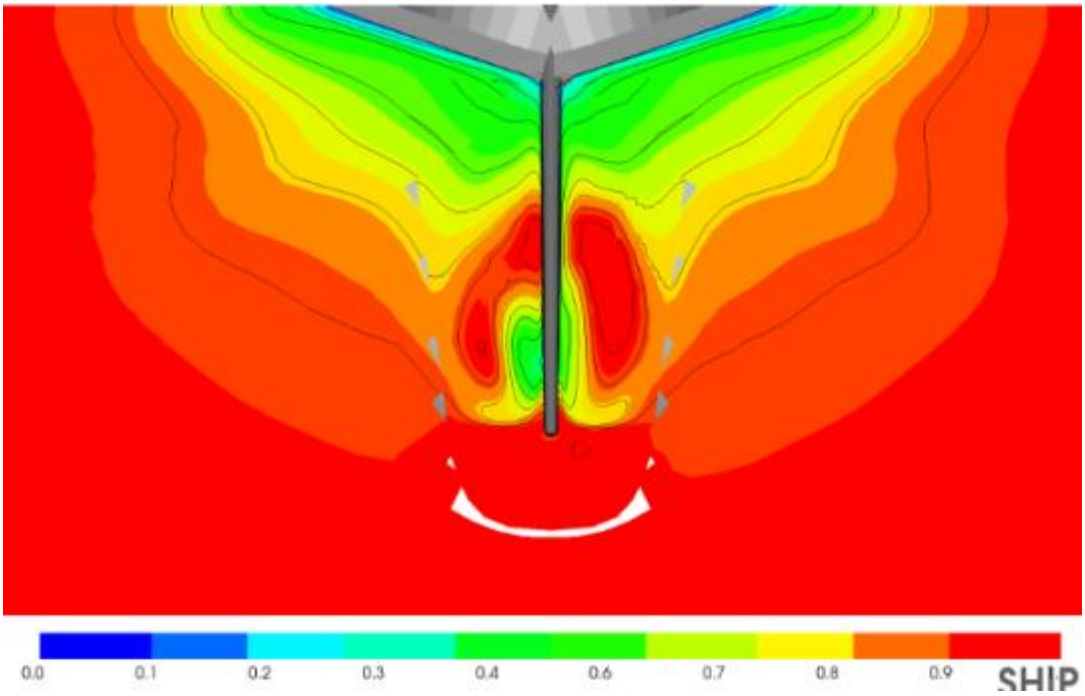

f) x = 1.00

Figure 4.47: Axial velocity contour at the stern region of the JBC hull with rudder and propeller effect

From Figure 4.47 (a-f) it is found that axial velocity at stern changes both its pattern and magnitude as the distance from propeller plane changes.

From both Figures 4.46 and 4.47 it is observed that the propeller thrust creates strongly axial flow acceleration behind the propeller comparing with the bare hull conditions.

Contours of axial velocity at x = 0.90 show that the maximum thickness of boundary layer are found at the concave surface as shown in Figures 4.46 c) and 4.47 c) respectively for both hulls. It is likely that the streamlines from bilge area converge onto the concave surface after the midship, resulting in a thickening of the boundary layer thereafter. It is also observed that the boundary layer is very thin along the convex keel region, since low momentum fluids are moved towards the concave side. The axial velocity contour at the propeller plane at x = 0.9747 are of round shape as shown in Figures 4.46 e) and 4.47 e) respectively for both hulls which is favorable to the propeller efficiency.

4.12 Comparison of Computed Axial Velocity Contour with EFD

The numerical solution reveals a rather complex flow field in the stern region where the velocity distribution and propeller loading reflects changes in the flow field. To determine the complex flow field at stern with rudder and propeller axial velocity contours are determined for both hulls.

Axial velocity contour around the KCS and JBC hull at stern positions of x = 0.95 with rudder is shown in Figure 4.48. From 4.48 it is found that the computed results from Shipflow CFD show good agreement with the experimental results [57] for both hulls.

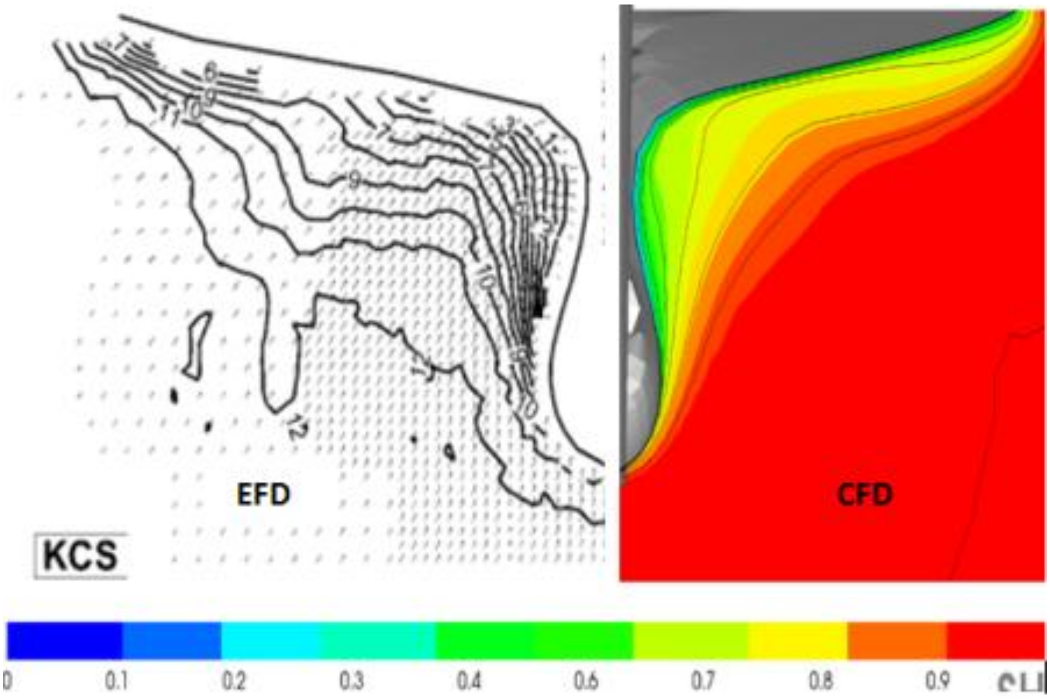

a) KCS at x = 0.95

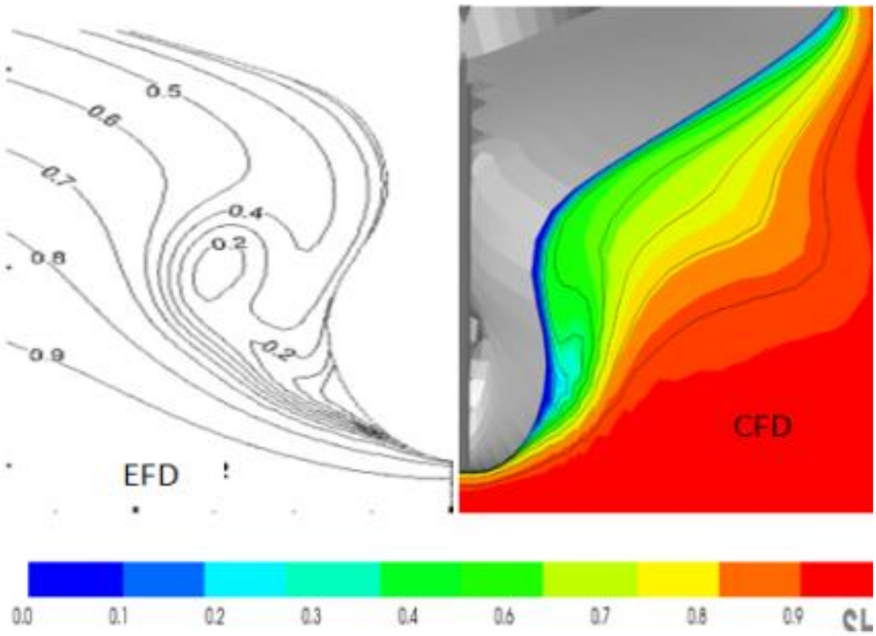

b) JBC at x = 0.95

Figure 4.48: Comparison of Computed Axial Velocity Contour with EFD at x = 0.95: a) KCS b) JBC hull

4.13 Efficiency of Zonal Approach over Global Approach

Bare ship hull resistance is computed first with zonal approach and compared with global approach. It has been found that the former approach complete the whole analysis in far more less time than the latter approach for very coarse and coarse mesh size. Furthermore, with zonal approach results have been obtained for both hull with medium and fine mesh sizes whereas, global approach is incapable of dealing with the similar mesh size as shown in Table 4.6 Consequently, it is also failed to compute self propulsion characteristics.

Table 4.6: Comparison between zonal and global approach.

	KCS		JBC	
	Zonal	Global	Zonal	Global
Mesh Size (Million, M)	Time (min)	Time (min)	Time (min)	Time (min)
Very Coarse (0.213 M)	18	145	18	157
Coarse (0.446 M)	30	230	33	243
Medium (0.744 M)	53	-----	57	-----
Fine (1.218 M)	77	-----	83	-----

Global Approach represents the state of the art among all numerical approaches. This approach is very onerous in terms of calculation time and computational resources since both the space and time scales of the propeller, rudder and of the hull flows are of quite different order of magnitude with requirement of complex grid generation around the whole system.

To compute the flow field around ship hull considering rudder-propeller interaction using "Zonal Approach" of Shipflow iteration number with grid size are carefully chosen to obtain the result with less computational effort.

Comparison of different iteration numbers and grid densities for KCS and JBC hulls are shown in Table 4.7.

Table 4.7: Comparison of different iteration numbers and grid densities for KCS and JBC.

	KCS	JBC
Mesh Size (Million, M)	No. of Iterations for convergence	
Very Coarse (0.213 M)	10,000	10,000
Coarse (0.446 M)	5000	5200
Medium (0.744 M)	3000	3500
Fine (1.218 M)	2500	3000

Table 4.7 it is found that with increasing grid sizes the number of iterations to reach convergence decreases and less difference in iterations numbers are obtained between medium and fine grid for both hulls. Therefore medium grids can be used for both hulls to get convergent results with less computational effort.

Conclusions and Recommendation

5.1 Conclusions

In this thesis work, commercial Computational Fluid Dynamics (CFD) software 'Shipflow' has been used to predict the flow around two modern benchmark ship hulls with and without rudder-propeller interaction. Based on the predicted results and discussions following conclusions can be drawn:

- The numerical simulation of flow around bare hull shows significant variation from the hull with rudder and propeller especially at the stern region. Therefore, the effect of propeller and rudder cannot be ignored in order to obtain accurate prediction of flow around ship.
- The computed viscous free-surface wave cuts for hull with rudder and propeller show increase in wave height compared to bare hull condition at the location of propeller especially when the cutting plane is closer to hull.
- There exists a significant change in wake due to hull-propeller-rudder interaction. The presence of propeller causes the reduction of wake by accelerating the flow.
- Axial velocity contours at different upstream and downstream transverse plane of propeller show that the contour of velocity changes with the change in distance of cutting plane from propeller.
- From the Verification and Validation (V&V) study of total resistance coefficients for both hulls, it is observed that when grid density is changed from coarse grid to finer grids, CFD predictions gets closer to EFD measurement.
- Lifting Line method determines propeller open water characteristics more or less precisely.
- The effect of rudder positions plays a significant role on propulsive characteristics. It is observed that as the rudder moves far away from the propeller, the interaction effect becomes less; consequently efficiency of the propeller increases.
- The RANS solver coupled with Lifting line method predictseffective wake and axial velocity contour well to numerically simulate flow around ship considering hull-propeller-rudder interaction.
- The CFD software 'Shipflow' can be successfully implemented in maritime industry for prediction of the preliminary resistance and propulsive power of ship.

5.2 Recommendation for Further Study

In this thesis work, main focus was placed on prediction of resistance and propulsive factors with numerical computations. Some sources of numerical errors and modeling errors have been addressed. Therefore, this thesis recommends the following topics as possibilities for further work:

- Though overlapping grid technique with Zonal approach has been implemented in this research to simplify the grid generation technique; moving mesh technique around the propeller with fully Global approach can be used for better analysis of self-propulsion characteristics.
- Effect of changing position of rudder on propulsive efficiency has been analyzed. However, maneuverability of rudder will also be changed with their variation of distance from propeller which is not considered in this analysis. In order to determine optimum position various rudder forces need to be computed for evaluating how much maneuverability will be lost or gained for different rudder positions.

References

[1] Maritime Propulsion, URL: http://articles.maritimepropulsion.com/ accessed on 20th Dec, 2016.

[2]Wartsila Marine Propulsion Technology, URL: http://www.wartsila.com/encyclopedia/cavitation-tunnel/ accessed on 20th Dec, 2016.

[3] J. H., Michell, "The Wave Resistance of a Ship", Philosophical Magazine Series 5, vol.45, no. 272(1898), pp. 106-123.

[4] W. Froude., "Observations and suggestions on the subject of determining by experiment the resistance of ships", The Papers of William Froude, Royal Institution of Naval Architects, (1810-1879).

[5] Poland Sea, URL: http://www.polandatsea.com/ accessed on 22nd Dec, 2016.

[6] Wikipedia, URL:https://en.wikipedia.org/wiki/Water_tunnel (hydrodynamic)/ accessed on 22nd Dec, 2016.

[7] International Maritime Consultancy, URL: http://www.imcs.qinetiq.com/facilities/ cavitation-tunnel.aspx/ accessed on 23rd Dec, 2016.

[8] J. H. Ferziger and M. Peric., "Computational Methods For Fluid Dynamics", Berlin: Springer-Verlag, (2002).

[9] L. Larsson and H. C. Raven., "Ship Resistance and Flow", Jersey City, New Jersey: The Society of Naval Architects and Marine Engineers, (2010).

[10] K. Kim, M. L. Andersen, and M. Orych, "Hydrodynamic Optimization of Energy Saving Devices in Full Scale", 30th Symposium on Naval Hydrodynamics, Australia, (2014).

[11] H. Takeshi, T. Hino, M. Hinatsu, Y. Tsukada, and J. Fujisawa, "ITTC cooperative experiments on a Series 60 Model at Ship Research Institute-flow measurement and test", 17thInternational Towing Tank Conference, Washington DC, (1987), pp. 10-13.

[12] U. Gietz, J. Kux, "Flow Investigations on the Hamburg Test case Model in the Wind Tunnel", Technical

[13] E. Oyan, "Speed and Powering Prediction for Ships based on Model Testing", Master's Thesis, Department of Marine Technology, Norwegian University of Science and Technology, (2012).

[14] J. Kayano, H. Yabuki, N. Sasaki, and R. Hiwatashi, "A Study on the Propulsion Performance in the Actual Sea by means of Full-scale Experiments", The International Journal on Marine Navigation and Safety of Sea Transportation, vol. 7, no. 4 (2013), pp. 521–526.

[15] H. B., Moraes, J.M., Vasconcellos, and R.G., Latorre, "Wave Resistance of High-Speed Catamarans", Ocean Engineering, vol. 31 (2004), pp. 2253-2282.

[16] A. F. Molland, and S. R. Turncock, “Wind tunnel investigation of the influence of propeller loading on ship rudder performance”, Technical report, Ship Science, Report No. 46. (1991).

[17] C. Simonsen, “Propeller – Rudder interaction by RANS”, PhD thesis, University of Denmark, (2000).

[18] V. Bertram, “Fuel Saving Options for Ships”, Annual Marine Propulsion Conference, London, (2009).

[19] A.B. Phillips, S.R. Turnock, and M.E. Furlong, “Accurate capture of rudder-propeller interaction using a coupled blade element momentum-RANS approach”, Ship Technology Research, (Schiffstechnik), vol. 57, no.2 (2010), pp. 128-139.

[20] J. Kim, K.S. Kim, G.D. Kim, I.R. Park, and S.H. Van, “Hybrid RANS and Potential Based Numerical Simulation for Self-Propulsion Performances of the Practical Container Ship”, Journal of Ship and Ocean Technology, vol. 10 (2006), pp. 1-11.

[21] V. I. Krasinikov, “Self-Propulsion RANS Computations with a Single-Screw Container Ship”, Third International Symposium on Marine Propulsors, Tasmania, Australia, (2013),pp. 430- 438.

[22] D. Rijpkema, B. Starke, and J. Bosschers, “Numerical Simulation of Propeller-Hull Interaction and Determination of The Effective Wake Field using a Hybrid RANS-BEM Approach”, Third International Symposium on Marine Propulsors, Tasmania, Australia, 2013), pp. 421- 429.

[23] N. Sakamoto and K. Kume, “Numerical Towing Tank Procedure for JBC in Self-Propulsion with Rotating Propeller and Energy Saving Duct”, JASNAOE Spring Annual Meeting, Fukuoka, Japan, May (2016).

[24] M. Kawabuchi, M. Kubota, and S. Ishikawa, “Development of Technology to Estimate the Flow Field around Ship Hull Considering Wave Making and Propeller Rotating Effects”, Mitsubishi Heavy Industries Technical Review, vol. 53, no. 2 (2016), pp. 53–57.

[25] P.J. Roache, “Verification and Validation in Computational Science and Engineering”, Hermosa Publishers, New Mexico, (1998).

[26] ITTC – Recommended procedures and guidelines 7.5-03-02-01, “Uncertainty analysisin CFD examples for resistance and flow”, (1999).

[27] V. R. Wilson, F. Stern, H. W. Coleman, and E. G. Paterson, “Comprehensive Approach to Verification and Validation of CFD Simulations—Part 2: Application for RANS Simulation of a Cargo/Container Ship”, Journal of Fluids Engineering, vol. 123 (2001),pp. 803-810.

[28] L. Eca, and M. Hoekstra, “An Evaluation of Verification Procedures for CFD Applications”, 24th Symposium on Naval Hydrodynamics, Fukuoka, Japan, (2002).

[29] L. Eca, and M. Hoekstra, “Discretization Uncertainty Estimation based on a Least Squares Version of the Grid Convergence Index”, Proceedings of the Second Workshopon CFD Uncertainty Analysis, Instituto Superior Tecnico, (2006).

[30] L. Eca, G. Vaz, and M. Hoekstra, “Assessing Convergence Properties of RANS SolversWithManufactured Solutions”, European Congress on Computational Methods inApplied Sciences and Engineering, Vienna, Austria, (2012).

[31] L. Larsson, F. Stern, and M. Visonneau, “Numerical Ship Hydrodynamics”, An Assessment of the Gothenburg 2010 Workshop, Dordrecht: Springer, (2014).

[32] National Maritime Research Institute (NMRI), Tokyo 2015: A Workshop on CFD in Ship Hydrodynamics, URL: http://www.t2015.nmri.go.jp/, accessed on 25th Dec, (2016).

[33] K. Boumediene, S. E. Belhenniche, “Numerical Analysis of the Turbulent Flow around DTMB 4119 Marine Propeller”, International Journal of Mechanical, Aerospace, Industrial, Mechatronic and Manufacturing Engineering, vol. 10, no. 2 (2016), pp.347- 351.

[34] L. Broberg, B. Regnstrom, and M. Ostberg, “SHIPFLOW Theoretical Manual”, FLOWTECH International AB, Gothenburg, Sweden, (2007).

[35] K. M. Flood, “Propeller performance analysis using lifting line theory”, M.Sc. Engg. Thesis, Department of Mechanical Engineering, Massachusetts Institute of Technology, Massachusetts Avenue, USA, (2009).

[36] H. K. Versteeg, and W. Malalasekera, “An Introduction to Computational Fluid Dynamics (2nd ed.)”, Harlow, Essex CM20 2JE, England: Pearson Education Limited,(2007).

[37] L. Zou, “CFD Predictions Including Verification and Validation Hydrodynamic Forces and Moments on Ship in Restricted Water Doctoral dissertation)”, Department of Shipping and Marine Technology, Chalmers University of Technology, Gothenburg, (2012).

[38] F. R. Menter, “Two-Equation Eddy-Viscosity Turbulence Models for Engineering Applications”, AIAA Journal, vol. 32, no.8 (1994), pp. 1598-1605.

[39]Lecture Notes on Modeling of Turbulence Flow Features, URL: http://www.southampton.ac.uklectures/Turbulence/,accessed on 18th Jan, 2017.

[40] Presence of Ship Wake, URL: http://www.research.ncl.ac.uk/cavitation/, accessed on5th Jan, 2017.

[41] L. Broberg, B. Regnstrom, and M. Ostberg, “ XCHAP Theoretical Manual”, FLOWTECH International AB, Gothenburg, Sweden, (2007).

[42] L. Da-Qing, “Investigation on Propeller-Rudder Interaction by Numerical Methods”, Department of Shipping and Marine Technology, Chalmers University of Technology, Gothenberg, Sweden, (1994).

[43] MAN Diesel and Turbo, URL: www.manbw.com/files/news/Hydrodopropellers.pdf/, accessed on 26th Dec, 2016.

[44] K. J. Han, "Numerical optimization of hull/propeller/rudder configurations", Department of Shipping and Marine Technology, Chalmers University of Technology, Gothenburg, Sweden, (2008).

[45] H.C. Raven, "A solution method for the nonlinear ship wave resistance problem" PhD Thesis, MARIN/Delft University of Technology, Netherlands, (1996).

[46] J. Katz, and A. Plotkin, "Low speed aerodynamics", Cambridge University Press, (2001).

[47] C.E. Janson, "Potential flow panel methods for the calculation of free surface flows with lift", Department of Shipping and Marine Technology, Chalmers University of Technology, Gothenburg, Sweden, (1997).

[48] C.E. Janson, and D. Spinney , "A comparison of four wave cut analysis methodsfor wave resistance prediction ", Ship Technology Research, vol. 51 (2004).

[49] B. Regnström, "Introduction to Overlapping Grids in SHIPFLOW", FLOWTECH International AB, Gothenburg, Sweden. (2008).

[50] OpenProp Home Page, URL: engineering.dartmouth.edu/epps/openprop/, accessed on20th Dec, 2016.

[51] L. Broberg, and M. Orych, "An Efficient Numerical Technique to Simulate the Propeller Hull Interaction", International Journal of Innovative Research & Development, vol. 14, (2012).

[52]MOERI Container, URL: http://www.simman2008.dk/KCS/container.html/accessed on 26th Dec, 2016.

[53] D. Zhang, "Numerical Computation of Ship Stern/Propeller Flow", Doctoral Dissertation, Department of Shipping and Marine Technology, Chalmers University of Technology, Gothenburg, Sweden (1990).

[54] L. Larsson, and H. C. Raven, "MMA 155 Ship Resistance and Flow", Göteborg and Wageningen, Chalmers University of Technology, (2004).

[55] W. J. Kim, S. H. Van. And D. H. Kim, "Measurement of flows around modern commercial models", Experiments in fluids, Springer Verlag, vol. 31(2001), pp. 567-578.

[56] C. Y. Hsin, Kerwin, and E. Justin, "Steady Performance for Two Propellers usingMIT-PSF-10", 20th ITTC Propulsor Committee Comparative Calculation of Propellers by Surface Panel Methods, (1992).

[57] Tokyo 2015: A Workshop on CFD in Ship Hydrodynamics, Tokyo, Japan, (2015).

Appendix-A

A.1 Sample ShipflowInput File for KCS Hull

xflow *// Selection of geometry of ship hull and program*

title(title = "Self Propulsion KCS")

program(all)

vship(fn = [0.316], rn = [10000000])

control(spauto, all)

hull(mono, h1gr = "main", ogrp = "aft", fbgr = "bulb", abgr = "boss", fsflow, coarse)

offset(file = "as_as_off_kcs_model", lpp = 7.2786, xaxdir = -1, ysign = 1,

xori = 7.2786, zori = 0.3418)

symmetr(nosym) *// Selection of non symmetric flow due to presence of propeller*

selfpr(on) *// Selection of self propulsion simulation*

ittc78(on, lm = 7.2786, ls = 230, ds = 7.9,

a_t = 264.04, npow = 18)*// Model scale to full scale conversion*

propel(id = "KP505", dpro = 0.23, dhub = 0.1, *// Set up propeller dimension and geometry*

xsh = 0.185, zsh = 0.14, jv = 0.8, ear = 0.8, nbla = 5, number = 11,

r_rt = [0.18,0.25,0.3,0.4,0.5,0.6,0.7,0.8,0.9,0.95,1],

p_d = [0.8347,0.8912,0.9269,0.9783,1.0079,1.013,0.9967,0.9566,0.9006,0.8683,0.8331],

c_d = [0.2313,0.2618,0.2809,0.3138,0.3403,0.3573,0.359,0.3376,0.2797,0.2225,0.0001],

t_d = [0.04585, 0.04071, 0.03712, 0.03047, 0.02459, 0.01947, 0.01492, 0.01073, 0.00693

, 0.00528, 0.00369],

f_c = [0.028448, 0.029641, 0.029477, 0.026769, 0.02201, 0.017324, 0.014039, 0.011996,

0.01044, 0.010067, 8.7])

rudder(span = 0.36, angle = 0, origin = [0,0,0.36], *// Set up rudder geometry*

s = [0,0.5,1], c = [0.26,0.188,0.135], xle = [0.1,0.08,0.06])

```
end

xpan                                           // Potential Flow Solver
parall(nthread = 6 )
end

xgrid                                          // Grid generation for viscous flow solver
size(etamax = 30, zetamax = 40 )
xdistr(xstart = 0.5, nm = 25, xapu = 0.9, na = 30, xapd = 0.98, nw = 20,
xend = 1.5 )
radius( radius = 0.25 )
end

xchap                                          // Viscous flow solver
parall(nthread = 6 )
control( start, maxit = 100 )
pow( start, maxit = 50, output = "POW.dat", j = [0.2,0.9], coupled )
lline( id = "KP505", on, cf = 0.004 )
end
```

A.2 Sample ShipflowOutput File for KCS Hull

SHIPFLOW-XFLOW VERSION 5.1.00 2016-07-25 AT 10:51:24

==

*** XFLOW WARNING: XZ-SYMMETRY IS ENFORCED FOR STANDARD CASES

Revision: Rev. 9136

- COMMANDS AND KEYWORDS FOR XFLOW

Both input and default values are printed

- TITLE

titl = Self Propulsion KCS

- POST PROCESSOR

Default post-processor SHIPFLOW is used.

- PROGRAM

xmes
xpan
xbou
xgri
xcha

- HULLTYPE

mono
xmau
h1gr = main
ogrp= aft
fbgr= bulb
abgr = boss
fsfl

bden= 5.00000E-01
fden= 5.00000E-01
trxd
xwlp= 6.00000E-01

- OFFSETFILE
file= ../as_as_off_kcs_model
lpp= 7.27860E+00
xori= 7.27860E+00
yori= 0.00000E+00
zori= 3.41800E-01
ztem= 0.00000E+00
ztop= 0.00000E+00
xaxd= -1.00000E+00
ysig = 1.00000E+00
itte= 4

- IPOSITION
roll= 0.00000E+00
trim= 0.00000E+00
xcof= 5.00000E-01
zvcg= 0.00000E+00

- OSFLOW
numb= 1
flow= 0.00000E+00

- VSHIP
numb= 1
fn= 3.16000E-01
rn= 1.00000E+07

- SYMMETRY
xzpl

- FLUID
dens= 1.00000E+03
grav = 9.80665E+00
visc= 1.00400E-06

- PROPELLER
dpro = 2.30000E-01
dhub = 1.00000E-01

xsh=   1.85000E-01
ysh=   0.00000E+00
zsh=   1.40000E-01
xdir= -1.00000E+00
ydir=   0.00000E+00
zdir=   0.00000E+00
cts=   0.00000E+00
nbla=   5
jv=   8.00000E-01
ear=   8.00000E-01
numb =   11

R/RT	**P/D**	**THIC**	**LENG**	**CAMB**
0.1800	0.8347	0.0105	0.0532	0.0015
0.2500	0.8912	0.0094	0.0602	0.0018
0.3000	0.9269	0.0085	0.0646	0.0019
0.4000	0.9783	0.0070	0.0722	0.0019
0.5000	1.0079	0.0057	0.0783	0.0017
0.6000	1.0130	0.0045	0.0822	0.0014
0.7000	0.9967	0.0034	0.0826	0.0012
0.8000	0.9566	0.0025	0.0776	0.0009
0.9000	0.9006	0.0016	0.0643	0.0007
0.9500	0.8683	0.0012	0.0512	0.0005
1.0000	0.8331	0.0008	0.0000	0.0002

- RUDD
id= UnnamedObject
span = 0.36
angl= 0
cant= 0
orig= [0,0,0.36]
s   = [0, 0.5, 1]
c   = [0.26, 0.188, 0.135]
xle= [0.1, 0.08, 0.06]
rmax = 1

===

SHIPFLOW-XMESH VERSION 5.1.00 2016-07-25 AT 10:51:41

===

Licensed under the SHIPFLOW EDUCATIONAL LICENSE AGREEMENT
--- To be used only in academic education ---
- Estimated memory requirement for XPAN
memory requirement in integer words :   14918611
available memory (SHIPFLOWMEM)   :   200000000

- Estimated disk space requirement for XPAN
disk space in Mbyte : 1
- COMMANDS AND KEYWORDS FOR XMESH
Both input and default values are printed

- BODY

grno = 1
high
gene
fsin
onei
offs = main
poin = 11
stat = 72
expa = 2
str1 = 0
  df1 = 0.00000E+00
  dl1 = 0.00000E+00
str2 = 5
  df2 = 5.00000E-03
  dl2 = 5.00000E-03
str3 = 0
  df3 = 0.00000E+00
  dl3 = 0.00000E+00
str4 = 5
  df4 = 5.00000E-03
  dl4 = 5.00000E-03
xtra = 0.00000E+00
ytra = 0.00000E+00
ztra = 0.00000E+00
xrot = 0.00000E+00
yrot = 0.00000E+00
zrot = 0.00000E+00
xsca = 1.00000E+00
ysca = 1.00000E+00
zsca = 1.00000E+00
velb = 0.00000E+00

- BODY

grno = 2
high
gene
fsin
onei
offs = aft
poin = 7

```
stat  =   10
expa  =    2
str1  =    0
   df1   =   0.00000E+00
   dl1   =   0.00000E+00
str2  =    0
   df2   =   0.00000E+00
   dl2   =   0.00000E+00
str3  =    0
   df3   =   0.00000E+00
   dl3   =   0.00000E+00
str4  =    0
   df4   =   0.00000E+00
   dl4   =   0.00000E+00
xtra  =   0.00000E+00
ytra  =   0.00000E+00
ztra  =   0.00000E+00
xrot  =   0.00000E+00
yrot  =   0.00000E+00
zrot  =   0.00000E+00
xsca  =   1.00000E+00
ysca  =   1.00000E+00
zsca  =   1.00000E+00
velb  =   0.00000E+00
```

- BODY

```
grno  =    3
high
gene
fsin
onei
offs  =  bulb
poin  =   11
stat  =    7
expa  =    0
str1  =    0
   df1   =   0.00000E+00
   dl1   =   0.00000E+00
str2  =    0
   df2   =   0.00000E+00
   dl2   =   0.00000E+00
str3  =    0
   df3   =   0.00000E+00
   dl3   =   0.00000E+00
```

str4 = 0
  df4 = 0.00000E+00
  dl4 = 0.00000E+00
xtra = 0.00000E+00
ytra = 0.00000E+00
ztra = 0.00000E+00
xrot = 0.00000E+00
yrot = 0.00000E+00
zrot = 0.00000E+00
xsca = 1.00000E+00
ysca = 1.00000E+00
zsca = 1.00000E+00
velb = 0.00000E+00

- BODY
grno = 4
high
gene
fsin
onei
offs = boss
poin = 5
stat = 5
expa = 0
str1 = 0
  df1 = 0.00000E+00
  dl1 = 0.00000E+00
str2 = 0
  df2 = 0.00000E+00
  dl2 = 0.00000E+00
str3 = 0
  df3 = 0.00000E+00
  dl3 = 0.00000E+00
str4 = 0
  df4 = 0.00000E+00
  dl4 = 0.00000E+00
xtra = 0.00000E+00
ytra = 0.00000E+00
ztra = 0.00000E+00
xrot = 0.00000E+00
yrot = 0.00000E+00
zrot = 0.00000E+00
xsca = 1.00000E+00
ysca = 1.00000E+00

zsca = 1.00000E+00
velb = 0.00000E+00

- FREE
grno = 5
firs
gene
poin = 22
str1 = 1
df1 = 1.76400E-02
dl1 = 0.00000E+00
stau = 10
stru = 1
dfu = 0.00000E+00
dlu = 4.00000E-02
stam = 26
strm = 0
dfm = 0.00000E+00
dlm = 0.00000E+00
stad = 26
strd = 1
dfd = 4.00000E-02
dld = 0.00000E+00
xups = -5.63707E-01
xbow = 0.00000E+00
xste = 1.00000E+00
xdow = 2.44112E+00
y2si = 0.00000E+00
y4si = -1.19547E+00
smoo = 10
nbd2 = 4
ibd2 = 1
nbd4 = 0
nbde = 0
xu2 = -1.00000E-02
yu2 = 0.00000E+00
xd1 = 1.10000E+00
yd1 = 0.00000E+00
Total no. of panels : 2293
Total no. of nodes : 2508

SHIPFLOW-XPAN VERSION 5.1.00 2016-07-25 AT 10:51:50

==

Licensed under the SHIPFLOW EDUCATIONAL LICENSE AGREEMENT

--- To be used only in academic education ---

Non-lifting potential flow

with free surface

and without the dry transom stern option

- COMMANDS AND KEYWORDS FOR XPAN

Both input and default values are printed

- CONTROL

nonl
itso
eqsi = 1.00000E-05
eqav = 5.00000E-03
eqco = 1.00000E-03
nodi
sing
four
free
save
nola
zrai = 6.05000E-01
xshi = 3.00000E-01
zfac = 7.50000E-01
afss

- CONVERGENCE

eptr = 1.00000E-02
epsi = 1.00000E-05
epwa = 5.00000E-05
wchm = 1.00000E+00

- EXFORCE

cvfo = 0.00000E+00
cvli = 0.00000E+00
cvbo = 0.00000E+00

- EXMOMENT

towx = LCB
towz =VPoR
towa = 0.00000E+00
zmli = 0.00000E+00
zmbo = 0.00000E+00

- ITERATION
maxi = 20

- RELAXATION
rftr = 1.00000E+00
rfsi = 1.00000E+00
rfso = 7.00000E-01
rfwa = 1.00000E+00

- TWCUT
xstt = 1.65685E+00
xent = 2.28427E+00
ytwc = -1.19547E+00
stat = 8
strt = 1
dftw = 3.92134E-02
dltw = 0.00000E+00
nval = 100
nwav = 100

==
Case no 1: Flow Angle = 0.0Fn= 0.316 Iteration no 1
==

- Iterations
IT (iterations): 1

- Hull data, non-dimensionalized by Lpp

LPP (length): 0.100000000000000E+01
B (breadth): 0.140179568748244E+00
T (draught): 0.469612227159516E-01
WPA (water plane area): 0.116293812478914E+00
CWPA (water plane area coefficient) : 0.829606008331876E+00
CB (blockcoefficient): 0.649573998445778E+00
CPRISM (prismaticcoefficient):0.663464676475108E+00
LCB (x - center of buoyancy): 0.514882373361259E+00
VCB (z - center of buoyancy): -0.213880626963686E-01
S (wetted surface area): 0.180393621334547E+00
V (displacement): 0.427614819642463E-02

- Resistance coefficients (force/(0.5*density*Sref*U2))**

CW (Wave resist. coeff. press. int.): 0.155234332500422E-02
CWTWC (Wave resist. coeff. wave cut) : 0.837421095815139E-03
Sref(Wetted surface at zero speed) : 0.180393621334547E+00
- Sinkage and Trim calculation

-CZSINK(coefficient of sinking force) : -0.366049463260299E-01
CMTRIM (coefficient of trim moment) : 0.147273363291664E-03
XCOF (center of flotation) : 0.556826297600560E+00
BML (metacentric radius, long.) : 0.165612091096940E+01
TRIMAN (trim angle in degree) : 0.617313209693709E-01
ZSINK (draft change at Lpp/2) : -0.277374480027616E-02
ZSINKF (draft change at XCOF): -0.283497029448347E-02
ZSINKB (draft change at bow) : -0.223503739901569E-02
ZSINKS (draft change at stern) : -0.331245220153663E-02
==
Case no 1 : Flow Angle = 0.0 Fn = 0.316 Iteration no 2
==
- Iterations
IT (iterations) : 2

- Hull data, non-dimensionalized by Lpp

LPP (length): 0.100000000000000E+01
B (breadth): 0.140146230013787E+00
T (draught): 0.501934820398469E-01
WPA (water plane area): 0.122331749431455E+00
CWPA (water plane area coefficient) : 0.872886480210137E+00
CB (blockcoefficient): 0.654283933682649E+00
CPRISM (prismaticcoefficient): 0.672953209839946E+00
LCB (x - center of buoyancy): 0.520452247454729E+00
VCB (z - center of buoyancy): -0.224590866591310E-01
S (wetted surface area): 0.188230772251725E+00
V (displacement): 0.460251275140632E-02

- Resistance coefficients (force/(0.5*density*Sref*U2))**

CW (Wave resist. coeff. press. int.): 0.141699858836424E-02
CWTWC (Wave resist. coeff. wave cut) : 0.735864762819877E-03

Sref(Wetted surface at zero speed) : 0.180393621334547E+00

- Sinkage and Trim calculation

CZSINK (coefficient of sinking force) : -0.340750827260419E-01

CMTRIM (coefficient of trim moment) : -0.122892503467420E-03
XCOF (center of flotation) : 0.561565316415410E+00
BML (metacentric radius, long.) : 0.193411291120042E+01
TRIMAN (trim angle in degree) : -0.412734941330616E-01
ZSINK (draft change at Lpp/2) : -0.255313197952535E-02
ZSINKF (draft change at XCOF) : -0.250878288876394E-02
ZSINKB (draft change at bow) : -0.291331116273759E-02
ZSINKS (draft change at stern) : -0.219295279631311E-02

- Convergence test :
- Max wave change = -0.3108E-02 at panel no : 1736
- Max wave elevation = 0.1041E-01 at panel no : 1232

- Max dyn. BC residual = -.254210E-03 at panel no : 1715
- Max tot. BC residual = 0.101186E+00 at panel no : 1715

- Norm dyn. BC residual = 0.864641E-05
- Norm tot. BC residual = 0.168659E-02

- Convergence test:
- Change of sinkage= 0.3262E-03
- Change of trim angle = 0.1030E+00

==

Case no 1 : Flow Angle = 0.0 Fn = 0.316 Iteration no 3

==

- Iterations
IT (iterations): 3

- Hull data, non-dimensionalized by Lpp

LPP (length): 0.100000000000000E+01
B (breadth): 0.140135116323039E+00
T (draught): 0.498536256039459E-01
WPA (water plane area): 0.120925466597029E+00
CWPA (water plane area coefficient) : 0.862920513929372E+00
CB (blockcoefficient): 0.652184646369482E+00
CPRISM (prismaticcoefficient): 0.669917800441087E+00
LCB (x - center of buoyancy): 0.517175074466747E+00
VCB (z - center of buoyancy): -0.224322639892750E-01
S (wetted surface area): 0.186345178825311E+00
V (displacement): 0.455632082680483E-02

- Resistance coefficients (force/(0.5*density*Sref*U2))**

CW (Wave resist. coeff. press. int.): 0.148481367573202E-02
CWTWC (Wave resist. coeff. wave cut) : 0.758852560410153E-03

Sref(Wetted surface at zero speed) : 0.180393621334547E+00

- Sinkage and Trim calculation
CZSINK (coefficient of sinking force) : -0.346519652893618E-01
CMTRIM (coefficient of trim moment) : -0.113019239576753E-03
XCOF (center of flotation) : 0.554393317663329E+00
BML (metacentric radius, long.) : 0.188785802317795E+01
TRIMAN (trim angle in degree) : -0.390479728125196E-01
ZSINK (draft change at Lpp/2): -0.261799526202180E-02
ZSINKF (draft change at XCOF): -0.258092536250476E-02
ZSINKB (draft change at bow): -0.295875310792565E-02
ZSINKS (draft change at stern) : -0.227723741611795E-02

- Convergence test:
- Max wave change = -0.1338E-02 at panel no : 1360
- Max wave elevation = 0.1122E-01 at panel no : 1232
- Max dyn. BC residual = -.505244E-04 at panel no : 1275
- Max tot. BC residual = -.261185E-01 at panel no : 1232
- Norm dyn. BC residual = 0.156606E-05
- Norm tot. BC residual = 0.714496E-03

- Convergence test:
- Change of sinkage= 0.7214E-04
- Change of trim angle = 0.2226E-02

==

Case no 1: Flow Angle = 0.0Fn= 0.316 Iteration no 4

==

- Iterations
IT (iterations) : 4
- Hull data, non-dimensionalized by Lpp

LPP (length): 0.100000000000000E+01
B (breadth): 0.140129880267848E+00
T (draught): 0.499000516549314E-01
WPA (water plane area): 0.121305878209647E+00
CWPA (water plane area coefficient) : 0.865667464910269E+00

CB (blockcoefficient): 0.652527061824723E+00
CPRISM (prismaticcoefficient): 0.669955482882519E+00
LCB (x - center of buoyancy): 0.517464011549378E+00

VCB (z - center of buoyancy): -0.224674394685698E-01
S (wetted surface area): 0.186813750706007E+00
V (displacement): 0.456278782159841E-02

- Resistance coefficients (force/(0.5*density*Sref*U2))**

CW (Wave resist. coeff. press. int.): 0.144156100515801E-02
CWTWC (Wave resist. coeff. wave cut) : 0.791323700601579E-03
Sref(Wetted surface at zero speed) : 0.180393621334547E+00

- Sinkage and Trim calculation

CZSINK (coefficient of sinking force) : -0.346649940668877E-01
CMTRIM (coefficient of trim moment) : -0.134285193782480E-03
XCOF (center of flotation) : 0.555194027751557E+00
BML (metacentric radius, long.) : 0.190784290051757E+01
TRIMAN (trim angle in degree) : -0.462310597878070E-01
ZSINK (draft change at Lpp/2) : -0.261833420496505E-02
ZSINKF (draft change at XCOF) : -0.257379901548693E-02
ZSINKB (draft change at bow) : -0.302177630995684E-02
ZSINKS (draft change at stern) : -0.221489209997326E-02

- Convergence test:

- Max wave change = -0.6346E-03 at panel no : 1360
- Max wave elevation = 0.1179E-01 at panel no : 1232
- Max dyn. BC residual = -.134394E-04 at panel no : 1275
- Max tot. BC residual = -.141256E-01 at panel no : 1232
- Norm dyn. BC residual = 0.358378E-06
- Norm tot. BC residual = 0.368470E-03

- Convergence test:

- Change of sinkage = 0.7126E-05
- Change of trim angle = 0.7183E-02

==

Case no 1: Flow Angle = 0.0Fn= 0.316 Iteration no 5

==

- Iterations

IT (iterations) : 5

- Hull data, non-dimensionalized by Lpp

LPP (length): 0.100000000000000E+01
B (breadth): 0.140121586758761E+00
T (draught): 0.499598983041474E-01
WPA (water plane area): 0.121305705782640E+00

CWPA (water plane area coefficient) : 0.865717471437748E+00
CB (blockcoefficient): 0.651461473608020E+00
CPRISM (prismaticcoefficient): 0.669480602978887E+00
LCB (x - center of buoyancy) : 0.517296963257234E+00
VCB (z - center of buoyancy): -0.224774885672839E-01
S (wetted surface area): 0.186807764126835E+00
V (displacement): 0.456053013390664E-02

- Resistance coefficients (force/(0.5*density*Sref*U2))**
CW (Wave resist. coeff. press. int.): 0.143610498437740E-02
CWTWC (Wave resist. coeff. wave cut) : 0.811739921598838E-03
Sref(Wetted surface at zero speed) : 0.180393621334547E+00

- Sinkage and Trim calculation
CZSINK (coefficient of sinking force) : -0.346509733306132E-01
CMTRIM (coefficient of trim moment) : -0.138977791063726E-03
XCOF (center of flotation) : 0.554806969999404E+00
BML (metacentric radius, long.) : 0.191034544257115E+01
TRIMAN (trim angle in degree) : -0.478819347943342E-01
ZSINK (draft change at Lpp/2) : -0.261856370698128E-02
ZSINKF (draft change at XCOF): -0.257276166386243E-02
ZSINKB (draft change at bow) : -0.303641241417446E-02
ZSINKS (draft change at stern) : -0.220071499978810E-02

- Convergence test:
- Max wave change = -0.3352E-03 at panel no : 1360
- Max wave elevation = 0.1212E-01 at panel no : 1232
- Max dyn. BC residual = -.376496E-05 at panel no : 1275
- Max tot. BC residual = -.918508E-02 at panel no : 1275
- Norm dyn. BC residual = 0.102047E-06
- Norm tot. BC residual = 0.189196E-03

- Convergence test:
- Change of sinkage = 0.1037E-05
- Change of trim angle = 0.1651E-02

==
Case no 1: Flow Angle = 0.0Fn= 0.316 Iteration no 6
==

- Iterations
IT (iterations): 6

- Hull data, non-dimensionalized by Lpp

LPP (length): 0.100000000000000E+01
B (breadth): 0.140114159714654E+00
T (draught): 0.499738042421955E-01
WPA (water plane area): 0.121317926843685E+00
CWPA (water plane area coefficient) : 0.865850582773018E+00
CB (blockcoefficient): 0.651191544452357E+00
CPRISM (prismaticcoefficient): 0.668436704607811E+00
LCB (x - center of buoyancy): 0.517284832871141E+00
VCB (z - center of buoyancy) : -0.224819697693943E-01
S (wetted surface area): 0.186822202733476E+00
V (displacement): 0.455966767198542E-02

- Resistance coefficients (force/(0.5*density*Sref*U2))**
CW (Wave resist. coeff. press. int) : 0.143301351438979E-02
CWTWC (Wave resist. coeff. wave cut) : 0.822525549787831E-03
Sref(Wetted surface at zero speed) : 0.180393621334547E+00

- Sinkage and Trim calculation
CZSINK (coefficient of sinking force) : -0.346501932392414E-01
CMTRIM (coefficient of trim moment) : -0.139581853859185E-03
XCOF (center of flotation) : 0.554647794101839E+00
BML (metacentric radius, long.) : 0.191193715525727E+01
TRIMAN (trim angle in degree) : -0.480885084665902E-01
ZSINK (draft change at Lpp/2): -0.261831062718136E-02
ZSINKF (draft change at XCOF): -0.257244458029833E-02
ZSINKB (draft change at bow) : -0.303796202973895E-02
ZSINKS (draft change at stern) : -0.219865922462378E-02

- Convergence test:
- Max wave change = -0.1684E-03 at panel no : 1360
- Max wave elevation = 0.1226E-01 at panel no : 1232
- Max dyn. BC residual = -.994209E-06 at panel no : 1275
- Max tot. BC residual = -.585421E-02 at panel no : 1275
- Norm dyn. BC residual = 0.274149E-07
- Norm tot. BC residual = 0.997836E-04

- Convergence test:
- Change of sinkage= 0.3171E-06
- Change of trim angle = 0.2066E-03

===

Case no 1: Flow Angle = 0.0Fn= 0.316 Iteration no 7

==

- Iterations

IT (iterations): 7

- Hull data, non-dimensionalized by Lpp

LPP (length): 0.100000000000000E+01
B (breadth): 0.140111369015991E+00
T (draught): 0.499752624894490E-01
WPA (water plane area): 0.121317252624959E+00
CWPA (water plane area coefficient) : 0.865863016520188E+00
CB (blockcoefficient): 0.651132019976398E+00
CPRISM (prismaticcoefficient): 0.667933270301271E+00
LCB (x - center of buoyancy): 0.517295350979396E+00
VCB (z - center of buoyancy): -0.224837108672085E-01
S (wetted surface area): 0.186822080089800E+00
V (displacement): 0.455929310865840E-02

- Resistance coefficients (force/ (0.5*density*Sref*U2))**

CW (Wave resist. coeff. press. int.): 0.143251017609904E-02
CWTWC (Wave resist. coeff. wave cut) : 0.828067750368835E-03
Sref(Wetted surface at zero speed) : 0.180393621334547E+00

- Sinkage and Trim calculation

CZSINK (coefficient of sinking force) : -0.346510204540302E-01
CMTRIM (coefficient of trim moment) : -0.139208766790662E-03
XCOF (center of flotation) : 0.554558644230214E+00
BML (metacentric radius, long) : 0.191238593380193E+01
TRIMAN (trim angle in degree) : -0.479629136728625E-01
ZSINK (draft change at Lpp/2): -0.261819191799503E-02
ZSINKF (draft change at XCOF): -0.257252028972571E-02
ZSINKB (draft change at bow) : -0.303674729921566E-02
ZSINKS (draft change at stern): -0.219963653677440E-02

- Convergence test:

- Max wave change = 0.8250E-04 at panel no : 1552
- Max wave elevation = 0.1231E-01 at panel no : 1232

- Max dyn. BC residual = -.243567E-06 at panel no : 1318

- Max tot. BC residual = -.321473E-02 at panel no : 1275

- Norm dyn. BC residual= 0.650106E-08
- Norm tot. BC residual = 0.513405E-04

- Convergence test:
- Change of sinkage = 0.7571E-07
- Change of trim angle = 0.1256E-03

==

Case no 1: Flow Angle = 0.0Fn = 0.316 Iteration no 8

==

- Iterations

IT (iterations): 8

- Hull data, non-dimensionalized by Lpp

LPP (length): 0.100000000000000E+01
B (breadth): 0.140110980879361E+00
T (draught): 0.499741033100662E-01
WPA (water plane area): 0.121314107958227E+00
CWPA (water plane area coefficient) : 0.865842971027957E+00
CB (blockcoefficient): 0.651129640953513E+00
CPRISM (prismaticcoefficient): 0.667677787189118E+00
LCB (x - center of buoyancy) : 0.517306574487829E+00
VCB (z - center of buoyancy): -0.224843864699480E-01
S (wetted surface area): 0.186820560095018E+00
V (displacement) : 0.455915806797160E-02

- Resistance coefficients (force/ (0.5*density*Sref*U2))**

CW (Wave resist. coeff. press. int.): 0.143263583646553E-02
CWTWC (Wave resist. coeff. wave cut) : 0.830511342263437E-03
Sref(Wetted surface at zero speed) : 0.180393621334547E+00

- Sinkage and Trim calculation

CZSINK (coefficient of sinking force) : -0.346520543543946E-01
CMTRIM (coefficient of trim moment) : -0.138753001516939E-03
XCOF (center of flotation) : 0.554506706584443E+00
BML (metacentric radius, long.) : 0.191243357966734E+01
TRIMAN (trim angle in degree) : -0.478092755884594E-01
ZSINK (draft change at Lpp/2) : -0.261814572489894E-02
ZSINKF (draft change at XCOF) : -0.257266373340391E-02
ZSINKB (draft change at bow): -0.303536036090492E-02
ZSINKS (draft change at stern) : -0.220093108889295E-02

- Convergence test:
- Max wave change = 0.3868E-04 at panel no : 1552
- Max wave elevation = 0.1233E-01 at panel no : 1232
- Max dyn. BC residual = -.533194E-07 at panel no : 1318

- Max tot. BC residual = 0.162602E-02   at panel no   : 1295
- Norm dyn. BC residual = 0.131326E-08
- Norm tot. BC residual = 0.253025E-04

- Convergence test :
- Change of sinkage=   0.1434E-06
- Change of trim angle   =   0.1536E-03

****** Convergence achieved after8 iterations ******

==

SHIPFLOW-XBOUND VERSION 5.1.00 2016-07-25 AT 10:53:13

==

Licensed under the SHIPFLOW EDUCATIONAL LICENSE AGREEMENT
--- To be used only in academic education ---
- COMMANDS AND KEYWORDS FOR XBOUND
Both input and default values are printed

- CONTROL
save
file = XBLIMIT

- INICON
sgro =   1
turb
poin =   1
girt =   0.00000E+00
t11   =   1.00000E-04
h12   =   1.40411E+00
beta =   0.00000E+00

- RESISTANCE
xl1   =   5.00000E-02
xl2   =   9.00000E-01

- ROUGHNESS
h   =   0.00000E+00

c = 0.00000E+00

- TRACE

sgro = 1
grou = 1
stat = 100
stre = 10
ista = 10
idis = 1
s1 = 5.00000E-02
ds1 = 1.00000E-02
sn = 9.00000E-01
dsn = 0.00000E+00
jdis = 0
p1 = 5.00000E-02
dp1 = 0.00000E+00
pn = 9.50000E-01
dpn = 0.00000E+00

- Sinkage and Trim calculation

XCOF (center of flotation) : 0.5545067E+00
TRIMAN (trim angle in degrees) : -0.4780928E-01
ZSINKF (draft change at XCOF) : -0.2572664E-02
ZSINK (draft change at Lpp/2) : -0.2618146E-02
ZSINKB (draft change at bow) : -0.3035360E-02
ZSINKS (draft change at stern) : -0.2200931E-02

- Resistance coefficients (force/(0.5*density*Sref*U2))**

CW (Wave resist. coeff): 0.1432636E-02
Sref(Wetted surface at zero speed) : 0.1803936E+00

- Total skin friction coefficient:

CF (Total skin friction coefficient) : 3.108E-03
AREA (Area for normalization) : 8.432E-02

==

SHIPFLOW-XCHAP VERSION 5.1.00 2016-07-25 AT 10:53:16

==

Licensed under the SHIPFLOW EDUCATIONAL LICENSE AGREEMENT
--- To be used only in academic education ---

INDATA SECTION

- CONTROL

rest

maxi = 50
cfl = 1.00000E+00
limi
sche = FROMM
rela = ADI
disc = 0.00000E+00
conv = 1.00000E-06
refi = 1.00000E+00
easm
stre

- FRAME

imax = 0
jmax = 0
kmax = 0
xste = 1.50000E+00
zsli = 0.00000E+00

*** XGRID STARTED BY XCHAP**

- Coordinate transformation

Sinkage and trim will be taken from the XPDB-file,
sinkage : -2.57266E-03
trim : 0.000 + -0.048 (initial + correction)
xcof : 0.555

- COMMANDS AND KEYWORDS FOR XGRID

Both input and default values are printed

- OUTPUT

Interpolated grid -> XVGRID-file
Coarse grid -> XGPOST-file

- OFFSET

h1gr = main
ogrp = aft
abgr = boss
fbgr = bulb

- SIZE

ksim = 76 (default)
etam = 30
aeta = 0 (default)
ueta = 0 (default)
zeta = 40
habo = 0.00000E+00 (default)
hund = 0.00000E+00 (default)

- COARSE
ksic = 76.0 (default)
zeta = 40.0 (default)
fatt = 1.00000E+00 (default)

- XDISTR
xsta = 5.00000E-01
NM = 25 (default)
xapu = 9.00000E-01 (default)
NA = 30
xapd = 9.80000E-01 (default)
NW = 20
xend = 1.50000E+00

- RADIUS
radi = 2.50000E-01
cent = 0.00000E+00 (default)
rsti = 0.00000E+00 (default)

- YPLUS
This card was not found.
No wall laws assumed
ytar = 8.30000E-01 (default)
yexp = 1.00000E+00 (default)

- SKIN

The "skin" thickness at the keel is defined by:

x	**thickness**
0.90000	2.31901E-06
1.2000	2.31901E-06

The "skin" thickness at the waterline is defined by:

x	**thickness**
0.90000	2.31901E-06
1.0000	2.31901E-06

- SINGUL
The singul(keel) card was not found.
The default rule for monohull is used
The singul(water) card was not found.
The default line that follows the centre of the grid will be used.

- ETASMOOTH
This card was not found.
The eta-boundary smoothing has been turned off.
time = 1.00000E+00 (default)
zeta = 8.0 (default)

- POISSON
This card was not found.
The poisson solver has been turned on.
maxi = 60 (default)
ycri = 1.00000E-09 (default)
zcri = 1.00000E-09 (default)
orfy = 1.00000E+00 (default)
orfz = 1.00000E+00 (default)

- NEUMANN
This card was not found.
The Neumann b.c. at the eta-boundaries has been turned off.
neuw = 20 (default)
neuh = 1 (default)
neum = 40 (default)

- IMPROVE
impw = 4 (default)
imph = 1 (default)
impm = 40 (default)
angs = 1.00000E-03 (default)
conf = 16.0 (default)

- FEEDBACK
No feedback card was found, default values will be used.

---END OF ECHO
- Estimated memory requirements for XGRID
memory in integer words : 19334446
available memory (SHIPFLOWMEM) : 200000000
- Estimated memory requirements for XGRID
memory in integer words : 20416838
available memory (SHIPFLOWMEM) : 200000000

- Poisson solver iteration history:
max change max change

iter.	of y	of z
1	1.69135E-03	1.76526E-03
2	8.10469E-04	8.31021E-04
3	5.97280E-04	6.67581E-04
4	4.97897E-04	5.65528E-04
5	4.39171E-04	5.04695E-04
6	5.40689E-04	4.87169E-04
7	7.22730E-04	6.02091E-04
8	7.94035E-04	6.83398E-04
9	7.95466E-04	7.12819E-04
10	7.63385E-04	7.10016E-04
11	7.16946E-04	7.06414E-04
12	6.70989E-04	6.88212E-04
13	6.21189E-04	6.62980E-04
14	5.66326E-04	6.44163E-04
15	5.07409E-04	6.26488E-04
16	4.50124E-04	6.08570E-04
17	4.01449E-04	5.93188E-04
18	3.59294E-04	5.79627E-04
19	3.15358E-04	5.68557E-04
20	3.06428E-04	5.61762E-04
21	3.88537E-04	5.55552E-04
22	4.70237E-04	5.49201E-04
23	5.52094E-04	5.42018E-04
24	6.13573E-04	5.33236E-04
25	6.71124E-04	5.29564E-04
26	6.88139E-04	5.25216E-04
27	6.74796E-04	5.15866E-04
28	6.63320E-04	5.07530E-04
29	6.28631E-04	5.07746E-04
30	5.73533E-04	5.01816E-04
31	4.62139E-04	4.85286E-04
32	3.51055E-04	4.58526E-04
33	3.10486E-04	4.27399E-04
34	2.49701E-04	3.90886E-04
35	1.81295E-04	3.68850E-04
36	1.58553E-04	3.52533E-04
37	1.62576E-04	3.39451E-04
38	1.59732E-04	3.25670E-04
39	1.58332E-04	3.14820E-04
40	1.51616E-04	3.04920E-04
41	1.41234E-04	2.94720E-04
42	1.34541E-04	2.86851E-04

43	1.25257E-04	2.79557E-04
44	1.14743E-04	2.72093E-04
45	1.08312E-04	2.65993E-04
46	1.05603E-04	2.61015E-04
47	1.02997E-04	2.55848E-04
48	1.00463E-04	2.50574E-04
49	9.79924E-05	2.45274E-04
50	9.56846E-05	2.40210E-04
51	9.34694E-05	2.35679E-04
52	9.12989E-05	2.31152E-04
53	8.91744E-05	2.26669E-04
54	8.70972E-05	2.22259E-04
55	8.51285E-05	2.17950E-04
56	8.32487E-05	2.13758E-04
57	8.14103E-05	2.09699E-04
58	7.96137E-05	2.05780E-04
59	7.78861E-05	2.02006E-04
60	7.62409E-05	1.98374E-04

- Maximum number 60 (= maxit) iterations reached.

- Calculation of inlet profiles:

Reading XBDB file: selfprop_XBDB
created: 2016-07-25 at 10:53:14
text card: Self Propulsion KCS
number of data points: 1000
xl1 = 5.000E-02 (xl2 = 9.000E-01)
Reynolds number: 1.000E+07
Data interpolated from section: 1

- MAXIMUM TOTAL WAKE VARIATION, PROPELLER: KP505
WVAR (maximum total wake variation) : 0.997497
WRAD (maximum found at radius) : 0.434783
- MEAN WAKE FRACTION, PROPELLER: KP505
Wn (Mean wake fraction for KP505) : 0.2919458

- EXTRAPOLATION TO FULL SCALE ACCORDING TO ITTC78

CTS (Ship drag coefficient): 0.00394386
RS (Ship drag [kN]) : 4344.25
PE (Ship effective power [MW]): 65.1967

- PROPULSIVE FACTORS, PROPELLER: KP505

KT (Thrustcoefficient): 0.201385
KQ (Torquecoefficient): 0.0267428
JV (Advance ratio) : 0.655682
CT (Prop thrust coefficient): 5.21151

From resistance test
CTMR (CT model from resistance test): 0.00636314

From self-propulsion simulation
CTOW (Non-dimensional towing force): 0.00108572
CTMS (CT model from self prop. test): 0.00612472
t(Thrust deduction fraction) : 0.0473155

From open water test
JTM (JTM): 0.505482
KQO (KQ0): 0.0262297
ETAO (Propellerefficiency): 0.617675
WTM (Effective mean wake): 0.229075
ETAR (Relativerelativeefficiency): 0.980813
ETAH (Hullefficiency): 1.35852
ETAD (Propulsiveefficiency): 0.823022
Re_min(Minblade Re) : 883313
Re_max(Max blade Re) : 942171
WTS (Effective mean wake ship) : 0.124851
Kt/J^2 (Propeller load) : 0.3759
JTS (Advance ratio ship scale) : 0.872822
KTS (Thrust coefficient ship) : 0.286367
KQS (Torque coefficient ship) : 0.0100092
NS (Propeller speed ship scale [rpm]) : 114.286
TS (Thrust ship scale [kN]) : 4147.98
QS (Torque ship scale [kNm]) : 1167.76
PD (Delivered power ship scale [MW]) : 13.9758
etaDS (Total efficiency ship scale) : 4.66499
eta0S (Propeller efficiency ship scale) : 3.97438
etaHS (Hull efficiency ship scale) : 1.19673

OVERLAPPING GRID SECTION
No of frames : 3
No of grids : 3
No of points : 238862
No of interpolation cells : 0
No of discretization cells: 280788
No of outside cells : 7232
Total no of cells : 288020

Standard deviation for forces in XCHAP
(Displayed in percent of average force)
std(CPV)= : 12.09 %
std(CF)= : 0.36 %
Datapoints: 4

- Resistance:

CF	(Frictional resist. coeff.)	: 2.951E-03
CPV	(Viscous pres. resist. coeff.)	: 1.589E-03
CV	(Viscous resist. coeff.)	: 4.540E-03
CW	(Wave resist. coeff.)	: 1.433E-03
CT	(Total resist. coeff.)	: 5.972E-03
K	(Form factor)	: 0.513
S	(Wetted surface / L**2)	: 0.1804

SHIPFLOW started: 2016-07-25 at 10:51:24, ended: 2016-07-25 at 10:54:30